Geological development, gold mineralization and exploration methods in the late Archean Hattu schist belt, Ilomantsi, eastern Finland
Edited by Pekka A. Nurmi and Peter Sorjonen-Ward
Geological Survey of Finland, Special Paper 17,147-184, 1993.

# PETROGENESIS OF THE LATE ARCHEAN HATTU SCHIST BELT, ILOMANTSI, EASTERN FINLAND: GEOCHEMISTRY AND SR, ND ISOTOPIC COMPOSITION

by
Hugh O'Brien, Hannu Huhma and Peter Sorjonen-Ward

**O'Brien, H. E., Huhma, H. and Sorjonen-Ward, P. 1993.** Petrogenesis of the Late Archean Hattu schist belt, Ilomantsi, eastern Finland: Geochemistry and Sr, Nd isotopic composition. *Geological Survey of Finland, Special Paper 17*, 147-184, 28 figures, 3 tables and 1 appendix.

The 2750 Ma Late Archean Hattu schist belt in eastern Finland consists of supracrustal rocks dominated by sediments, with lesser amounts of komatiites, tholeiitic basalts and calc-alkaline rocks all intruded by typical Archean tonalite-trondhjemite-granodiorite series (TTG) rocks. Metamorphic conditions following accretion of the schist belt reached upper greenschist, lower amphibolite conditions with maximum temperatures estimated at 550 ± 50 °C.

The Hattu schist belt volcanics can be divided into komatiites, tholeiites, low-Ti tholeiites that show some characteristics of calc-alkaline basalts, and andesites/dacites. Crystal fractionation models suggest the tholeiites were dominated by olivine + chromite ± clinopyroxene ± plagioclase removal and the low-Ti tholeiites by clinopyroxene + olivine + magnetite removal. Several members of the low-Ti tholeiite group may be parental magmas to the andesites and dacites whereas the tholeiite fractionation trend projects away from the more evolved volcanics. REE profiles of the Hattu schist belt basalts are mostly typical of Archean basalts and discriminant diagrams suggest that these basalts are either island arc- or continental arc-derived. Negative Ta, Nb and Ti anomalies in the andesites and dacites suggest they are also arc-related magmas.

The TTG series granitoids intruding to the Hattu schist belt show a relatively small range in composition. Feldspar porphyry dikes that are found throughout the belt can only be distinguished from the plutonic rocks by the absence of negative Eu anomalies. This suggests plagioclase accumulation in the plutons subsequent to intrusion.

Metagraywackes in the Hattu schist belt are mostly andesitic to dacitic in composition although some basaltic andesite compositions apparently reflect a large amount of locally derived basaltic detritus. The metagraywackes with < 65 weight % $SiO_2$ overlap in composition with the volcanics whereas a large group of samples with greater than 65 weight % $SiO_2$ have no intrusive or volcanic equivalents in terms of $TiO_2$, $Fe_2O_3$, MgO or Cr, Ni, V, Sc. Rather than calling on a missing felsic component rich in compatible elements, we suggest some sedimentary process enriched these elements in the sedimentary sequence, which we suspect was mostly locally derived.

Sr isotopes on the Kuittila tonalite give a poorly constrained isochron of 2789 ± 290 Ma with a $Sr_i$ = 0.70146 ± 0.0009. Nd isotopes from 14 samples of the tonalite intrusives give $\varepsilon_{Nd}$(2750 Ma) of +0.9 to +2.1 and $T_{DM}$ model ages ca. 2800 Ma. In contrast, 3 Silvevaara Granodiorite samples have lower $\varepsilon_{Nd}$(2750) from -0.4 to -2.1 and older $T_{DM}$ ages near 3.0 Ga. Nd data from the volcanics include an amphibolite from Tiittalanvaara with an $\varepsilon_{Nd}$(2750) of

+1.3, close to what is expected for model mantle, whereas a pillow basalt from Poikopää gives an $\varepsilon_{Nd}(2750)$ -6 which could represent Proterozoic Sm/Nd resetting. Other volcanic samples include a meta-andesite with a low $\varepsilon_{Nd}(2750)$ of -2.4 and a metadacite with an $\varepsilon_{Nd}(2750)$ of +1.7. Nd isotopic data on 3 metagraywackes give $\varepsilon_{Nd}(2750\ Ma)$ values slightly more negative than the intrusives (-0.6 to +1.2). However, taken as a whole, the bulk of the isotopic data argue against a significant older crustal component in the source of the Hattu schist belt magmas or metagraywackes.

Key words (GeoRef Thesaurus, AGI): greenstone, gold, komatiite, tholeiite, tonalite, radiogenic isotopes, Hattu, Finland

*Hugh O'Brien*, Hannu Huhma, Peter Sorjonen-Ward, Geological Survey of Finland, FIN-02150 Espoo, Finland*
*present address: *Department of Geological Sciences, AJ-20, University of Washington, Seattle, WA, 98195 USA*

## INTRODUCTION

The Archean Hattu schist belt represents the sediment-dominated, easterly, N-S trending arm of the Ilomantsi Greenstone Belt (Fig. 1). It is from this belt that Archean gold mineralization from Fennoscandia was first reported (Salminen and Hartikainen, 1986; Nurmi et al., 1988). Because of similarities in age, lithologies and mineralization type with Archean gold provinces in Canada and Australia, an exploration and research program at the Geological Survey of Finland was initiated in 1986.

A considerable portion of the research effort of this project has been oriented towards understanding the structural and lithologic controls and physicochemical processes important in the precipitation of the Hattu schist belt gold mineralization. Most of the contributions in this volume address these topics and include, for example, modeling of mass transfer related to hydrothermal alteration of the rocks in the Hattu schist belt (Bornhorst and Rasilainen,1993, this volume). The purpose of the present paper is instead to characterize host rocks unaffected by the mineralizing hydrothermal fluids and is complementary to Sorjonen-Ward (1993, this volume) which describes, in detail, the Hattu schist belt stratigraphy, rock types and map unit field relationships. Our goal here is to describe the magmatic evolution, sediment provenance and geochemical signatures relevant to identifying sources of the schist belt rocks and through isotopic analysis determine if crust significantly older than 2.75 Ga was important.

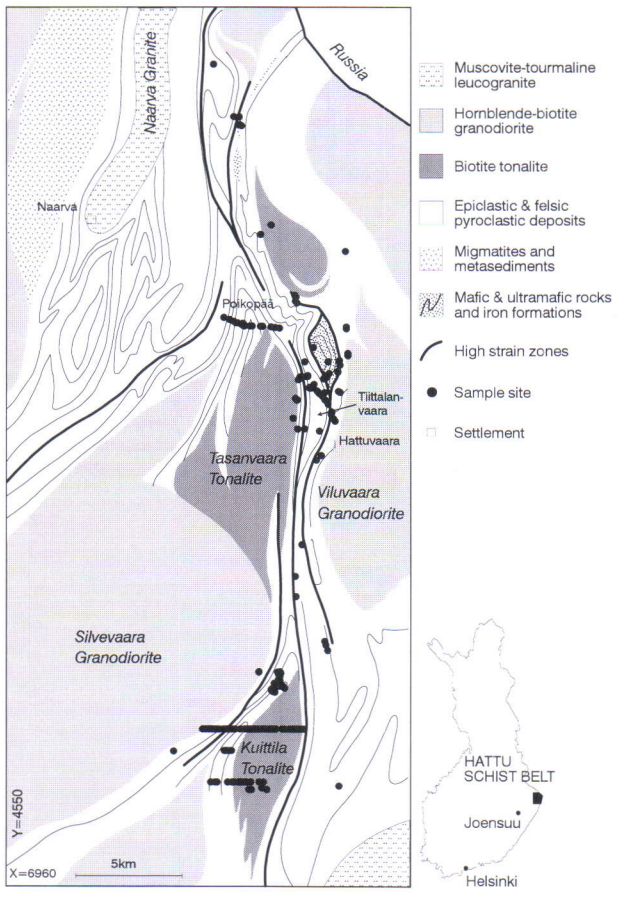


Fig. 1. Geological sketch map of the Late Archean Hattu schist belt showing sample locations.

## GENERAL GEOLOGY

### Supracrustal lithostratigraphy and volcanism

Lithologies of the Hattu schist belt are dominated by felsic volcanics, volcanogenic sediments and thick graywacke sequences. Tholeiitic and komatiitic flows are generally restricted to a few horizons within this sedimentary package and intermediate volcanic and volcaniclastic material are not abundant. No depositional substrate to the sequence has been identified, although it is possible that mafic rocks in the southeast of the study area represent basement.

Stratigraphic sequences are discussed in detail in Sorjonen-Ward (1993, this volume). In brief, the northern Hattu schist belt sequence begins with feldspathic graywackes of turbidite origin and coarse-clastic deposits of the Sivakkojoki Formation intercalated with sporadic tholeiitic basalt flows and porphyritic andesite. The succeeding Hosko and Kuljunki Formations contain turbidites in their lower parts but consist predominantly of coarse-clastic deposits with some felsic pyroclastics. Near Hattuvaara a persistent but thin mafic horizon marks the base of the conglomerate-dominated Tiittalanvaara Formation which passes upwards via Fe-rich chemogenic sediments into the mafic and ultramafic Pampalo Formation. In this formation, massive tholeiitic flows and breccias, and komatiite flows with rare relict cumulus features and brecciated flow tops are overlain by a thick, poorly exposed and undifferentiated sequence of graywackes.

In the southern part of the schist belt, turbiditic sediments appear to overlie the low rank banded iron formations of the Ukkolanvaara Formation. The Ruukinpohja Formation, not sampled for this study, may represent the lowest exposed unit in the schist belt and comprises thick massive and pillowed mafic lavas abruptly overlain by feldspathic clastic deposits and turbidites.

### Intrusive granitoids and associated porphyry dikes

Granitoids intruding the Hattu schist belt can be classified independently of geochemistry, using a combination of mineralogy, texture, geophysical signatures and isotopic age data. No evidence has been found to indicate that any of the presently studied granitoids predate deformation of the Hattu schist belt sediments, nor has it been possible to establish relative intrusive relationships, because granitoids form discrete plutons in contact with schist belt rocks rather than each other.

The Silvevaara Granodiorite is the largest pluton intruding the Hattu schist belt, and effectively defines its western margin. It has a strong magnetic signature compared to other granitoids, probably due to the presence of magnetite. The granodiorite commonly contains hornblende, and in a few places pyroxene, within a medium-grained groundmass interstitial to tabular and weakly oriented K-feldspar phenocrysts. Ion-probe single-grain zircon studies (Sorjonen-Ward and Claoué-Long 1993) indicate the presence of xenocrystic zircons up to 3.19 Ga, although most define a chord intercepting the concordia at 2757±4 Ma, which is interpreted as the age of emplacement of the pluton. No chemical analyses of this intrusion are available at present, but the results of Sm-Nd isotopic studies will be presented and discussed below. Plagioclase porphyritic dikes, whose origin and interpretation is contentious, due to anomalously old ages (Vaasjoki et al., 1993, this volume), intrude country rocks close to the western margin of the Silvevaara Granodiorite, but it is not clear whether they are consanguinous.

The Kuittila Tonalite (= Tonalite 1) and Tasanvaara Tonalite (= Tonalite 2) are both medium-grained foliated biotite tonalites containing very few enclaves of any kind, and belong to a group of lenticular intrusions that can be traced along the entire Hattu schist belt. Both plutons appear to have been intruded during active regional deformation in similar structural settings and have similar U-Pb zircon isotopic ages. The Tasanvaara Tonalite age is more precise, at 2748±6 Ma, compared to 2745±11 Ma for the Kuittila Tonalite (Vaasjoki et al., 1993, this volume). Therefore, on the basis of field characteristics and petrography, some chemical similarity between the two intrusions might be anticipated. Numerous porphyritic tonalite dikes containing phenocrysts of quartz and oscilliatory zoned plagioclase occur along the western margin of the Kuittila Tonalite, although mutual intrusive relations have not been established. One of these dikes does however reveal an age of 2756±6 Ma which, at a 2 confidence level, overlaps with the age of the tonalite. The central part of the Kuittila Tonalite is a finer grained and more leucocratic trondhjemitic lithology but because of poor exposure it is difficult to establish whether this is a gradational or sharp contact. The Viluvaara Granodiorite (= Tonalite 3) forms the eastern boundary of the central segment of the Hattu schist belt and is characteristically medium-grained, with tabular

K-feldspar phenocrysts up to 3-4 cm in size, except at the margin, where K-feldpsar phenocrysts are lacking and the rock resembles the Kuittila and Tasanvaara tonalites.

The Naarva Leucogranite is a tourmaline-rich two-mica granite forming a discrete elongate pluton along the northwestern margin of the schist belt. It varies from aplitic to pegmatitic, with tourmaline rosettes up to 20 cm across and commonly displays lithological banding due to variations in both grain size and tourmaline abundance. In many places this layering is folded with a geometry similar to that in country-rock sediments, while enclaves record evidence of earlier deformation. Therefore, although no U-Pb isotopic data are available yet, the intrusion is clearly syntectonic.

## Age of Hattu Schist Belt

Detailed descriptions of all of the U-Pb zircon ages measured from this belt are given in Vaasjoki et al. (1993, this volume). In brief, the supracrustal volcanic and metasedimentary rocks have U-Pb zircon ages from 2726 ± 14 Ma (a Tiittalanvaara conglomerate porphyry clast) to 2859 ± 50 Ma (a Poikopää crystal-lithic sediment). The latter apparently contains some older inherited zircon. Two other supracrustal rocks give ages of 2754 ± 6 Ma and 2744 ±6 Ma while a Hattuvaara metagraywacke has an age of 2761 ± 11 Ma. These data show that the bulk of the volcanic and intrusive activity occurred at approximately 2750 Ma; the isotopic data are unable to discriminate events with more precision.

## Metamorphic Conditions

Mineral assemblages in the Hattu schist belt rocks indicate prograde metamorphism reached upper greenschist, lower amphibolite facies. The metasediments are mostly mica schists containing quartz + plagioclase + potassium feldspar + sericite ± biotite ± chlorite ± tourmaline. Several samples contain andalusite pseudomorphs (now muscovite + kyanite) that possibly resulted from contact metamorphism associated with abundant tonalite-granodiorite intrusions. Staurolite is not common which may reflect a lack of aluminous compositions rather than a lack of sufficient temperature. Garnet occurs in more Fe-rich rocks and in some samples is particularly rich in Mn. The garnet is commonly associated with chlorite making it difficult to find suitable samples for biotite - garnet geothermometry. Temperatures calculated for seven samples with stable biotite - garnet grain boundaries give a range from 490 °C to 640 °C depending on the solution models used (Table 1). Removing outliers, and taking into account the high Mn is some garnets, our best estimates from these metagraywackes indicate a temperature peak of 550 ± 50 °C.

All of the basalt samples have been converted to hornblende + plagioclase assemblages rather than chlorite-epidote-actinolite, consistent with T 500 °C at 3-5 kb (Apted & Liou, 1983). Assemblage stability is very dependent on $CO_2$ activity however, so that at low $CO_2$, which may be present in unaltered parts of the schist belt, albite-actinolite hornblende

Table 1. Equilibration temperatures using garnet-biotite Fe/Mg partitioning from Hattu schist belt metagraywackes.

| Location | Sample Number | FS temp. °C | PL temp. °C | HS temp. °C |
|---|---|---|---|---|
| Korvilansuo | R326/67C | 484-536* | 553-585 | 539-595 |
| Muurinsuo | PSW-1919-9 | 490-508* | 557-568 | 550-572 |
| Muurinsuo | PSW-1919-8 | 481-506* | 551-567 | 535-566 |
| Iso Kivijärvi | PGW89-2119 | 485-551 | 553-593 | 526-595 |
| Kuljunki | PGW90-2513 | 501-548 | 563-591 | 557-612 |
| Enonsuo | PSW90-2522 | 560-631 | 598-638 | 564-636 |
| Pieni Kivijärvi | PGW88-2108 | 514-572* | 571-606 | 557-622 |

FS = Ferry and Spear, 1978; PL = Perchuck and Lavrenteva, 1983; HS = Hodges and Spear, 1982
*garnets with high Mn contents. These give low temperatures by the solution models of Ferry and Spear (1978) because of the lack of a Mn correction.

may be present in greenschist facies (Will et al., 1990). Only rarely do relict phenocrysts appear to be preserved in the basalts. In contrast, many of the more felsic volcanics contain zoned feldspar phenocrysts in a recrystallized biotite + feldspar ± quartz matrix (these samples tend to appear much less recrystallized in handsample than in thin section). The intrusive rocks have the least growth of metamorphic minerals, yet nearly all samples have polygonal, recrystallized textures.

## SAMPLING AND ANALYTICAL PROCEDURE

The Archean Hattu Schist belt rocks have been subjected to a metamorphic event reaching lower amphibolite facies, while isotopic evidence seems to indicate another metamorphic overprint in some areas ca. 1.8 Ga (Kontinen, et al., 1992; O'Brien et al., 1993, this volume). Additionally, large amounts of hydrothermal fluids associated with Au mineralization moved through major shear zones in the schist belt (Bornhorst and Rasilainen, 1993, this volume). This widespread hydrothermal activity caused retrogressive alteration characterized by chlorite-muscovite-biotite-albite-epidote-carbonate assemblages (Nurmi et al., 1993, this volume). For these reasons, caution must be used when interpreting geochemical data from these rocks. The Hattu schist belt samples were selected from a larger set of outcrop and drill-core samples and represent the extended type set of Bornhorst et al.(1993, this volume). Only samples from outside prospect areas (thus avoiding areas most affected by hydrothermal alteration) and samples that did not contain visible alteration or mineralization were used. Geochemical screens were then applied to this subset to remove obviously altered samples. Elements that act as markers of hydrothermal alteration in the Hattu schist belt include boron, tungsten, molybdenum, tellurium, silver and gold (Bornhorst and Rasilainen, 1993, this volume). All samples with anomalous values of these elements were excluded from diagrams and discussions. Furthermore, throughout the following discussions, our emphasis will be on the less mobile elements (e.g., transition elements like Ni & Cr, and major elements Fe, Ti, Al) to minimize the effects of hydrothermal alteration that seems to be present to some extent in nearly all of the Hattu schist belt samples.

Although a large data set was used in this study, 213 samples before geochemical screening, it is difficult to be absolutely sure that the sample population is proportional to the volume of each of the rock types in the Hattu schist belt. The *volcanics* sample population is dominated by mafic/ultramafic and felsic compositions. Intermediate volcanics are not abundant in the sample population and we believe they are relatively sparse in the stratigraphic section. *Metagraywackes* are abundant in the sample set reflecting their predominance in the field. Most of these are intermediate in composition between the mafic volcanics and the felsic volcanics/intrusives. The proportion of *intrusive* rocks in the sample set roughly correlates to their areal distribution in the field and are tonalite, granodiorite or trondhjemite in composition.

Major and trace compositions of the Hattu schist belt extended type samples are given in the appendix (available in spreadsheet format from the senior author). Samples are designated in most cases by their field sample number (e.g., HJO-88-32) or, in the case of the volcanics, a short label is used (e.g., V10) to allow clarity in the diagrams. Major and trace elements for the data set were analyzed by various analytical techniques at XRAL laboratories, Canada. Details of sample preparation methods, analytical techniques used for each element, analytical errors and appropriate detection limits are given in Bornhorst et al. (1993, this volume). Some obvious problems with the data set include rather large analytical errors for rare earth elements at low abundance levels. This limits the usefulness of these elements particularly for the komatiites.

Isotopic analyses of Sr and Nd were made at the Unit for Isotope Geology, Geological Survey of Finland. 150-300 mg of sample powder was dissolved in teflon-lined bombs using a HF - $HNO_3$ mixture. Following evaporation the samples were brought to dryness again as chloride salts, and redissolved in 1.5 N HCl. This solution was aliquoted for spiking by isotopic tracer solutions. In the older set of samples, the REE fraction was collected from the primary chromatography columns and Nd and Sm were separated in methanol-based solutions (Huhma, 1986). For the newer set of samples, Sr and Rb fractions were collected from the primary columns as well as the REE fraction. Nd and Sm were separated using dilute HCl in HDEHP teflon columns (Richard et al., 1976). The isotopic compositions of Sr (+ Rb in spiked samples) and Nd (+ Sm in spiked samples) were measured on a VG sector 54 thermal emission mass spectrometer at the Geological Survey of Finland. Relevant normalization factors and results from standards are given in Tables 2

and 3. The Rb and Sr isotope dilution concentration data presented here are preliminary because of difficulties with attaining absolutely complete sample dissolution and development of new isotope dilution spikes and mass spectrometer techniques. They are, nevertheless, considerably more accurate than the XRF values reported in the appendix.

## GEOCHEMISTRY OF VOLCANICS

### Major and compatible trace elements of volcanics

As an additional geochemical screen to discern altered volcanic type samples, the data are plotted in total alkali vs. $SiO_2$ (TAS, Fig. 2). The bulk of samples plot below the line demarcating typical calc-alkaline from alkaline rock types and cluster into two major groups, basalts and dacites. Even though all of the type samples were taken from nonprospect areas and no alteration is discernible in hand sample, each of the samples in Fig. 2 with high $K_2O + Na_2O$ is from the vicinity of a known alteration zone. We have therefore chosen to exclude all of the volcanic samples with unusually high $K_2O + Na_2O$, assuming that they represent altered magma compositions.

The least altered Hattu schist belt volcanics remaining after geochemical screening are plotted in $Al_2O_3$ - $FeO+Fe_2O_3+TiO_2$ - MgO (cation %, Fig. 3). The elements comprising this diagram are relatively immobile (Jensen, 1976), and therefore give a reasonably true picture of the magma compositions that formed these rocks. Using the original designations of Jensen (1976), three of the samples plot within the field for peridotitic komatiites, five plot within the field of komatiitic basalt and the remainder are tholeiitic and calc-alkaline series rocks. Three of the primitive samples (V8, V10, V11) plot very near the komatiite - tholeiite divider. These three samples represent the most primitive Hattu basalts and hence most likely parental magmas of any proposed Hattu schist belt volcanic series. Six of the other basalts are classified as Fe-tholeiites using the divisions of Fig. 3. The ten tholeiites with the highest combined Fe + Ti in Fig. 3 have higher $TiO_2$ contents at a given $Fe_2O_{3,tot}$ than the remaining basalts (Fig. 4). These higher $TiO_2$ contents are more typical of Archean tholeiitic basalts in general (Condie, 1990). Based on $TiO_2$ content, the basalts will be subdivided into tholeiites (ten samples) and low-Ti tholeiites (six samples) in subsequent discussions. Although there

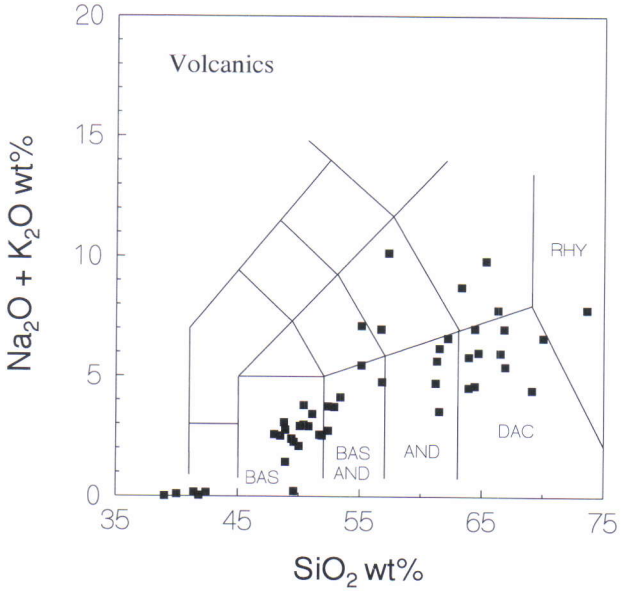


Fig. 2. Total alkali ($Na_2O + K_2O$) - $SiO_2$ for the Hattu schist belt volcanic rocks. The fields are those from Le Bas et al, 1986. BAS=low K basalt, AND=andesite, DAC=Dacite, RHY=rhyolite. Samples with unusually high $Na_2O + K_2O$ are not used in subsequent diagrams and discussions.

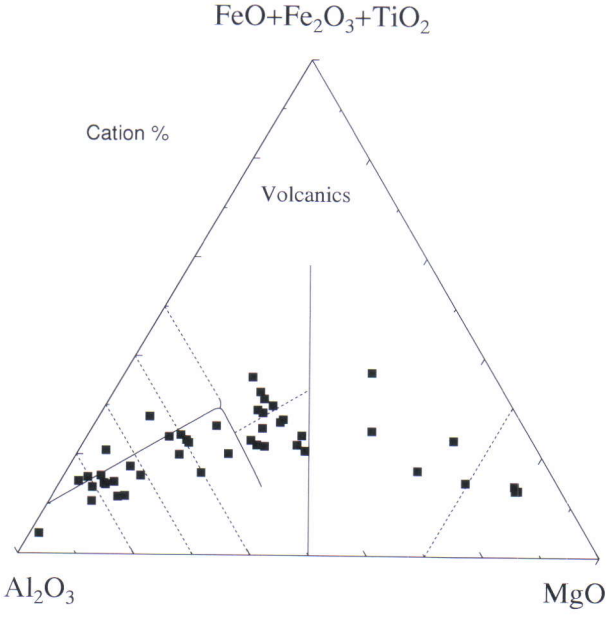


Fig. 3. $Al_2O_3$ - $FeO+Fe_2O_3+TiO_2$ - MgO diagram (after Jensen, 1976) for the Hattu schist belt volcanics. Abbreviations are as in Fig. 2.

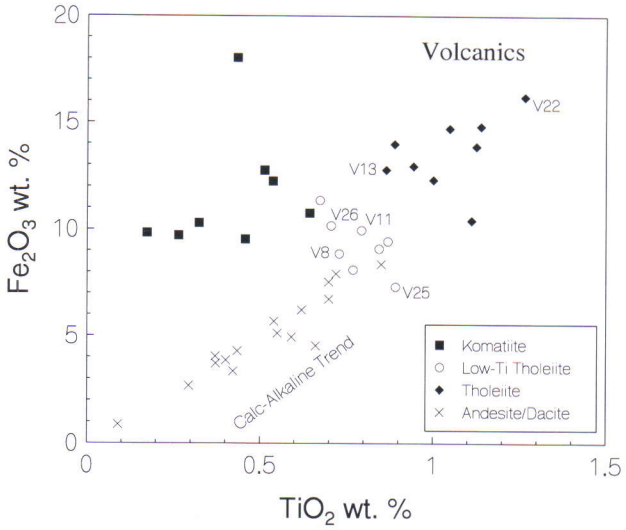


Fig. 4. $Fe_2O_3$ - $TiO_2$ diagram for the Hattu schist belt volcanics. The volcanics have been grouped into komatiites, tholeiites (with more typical Archean tholeiite $TiO_2$ contents), low-Ti tholeiites and andesites/dacites. Samples discussed in the text are labeled and the "V" label is given for each of the volcanic rocks in the appendix.

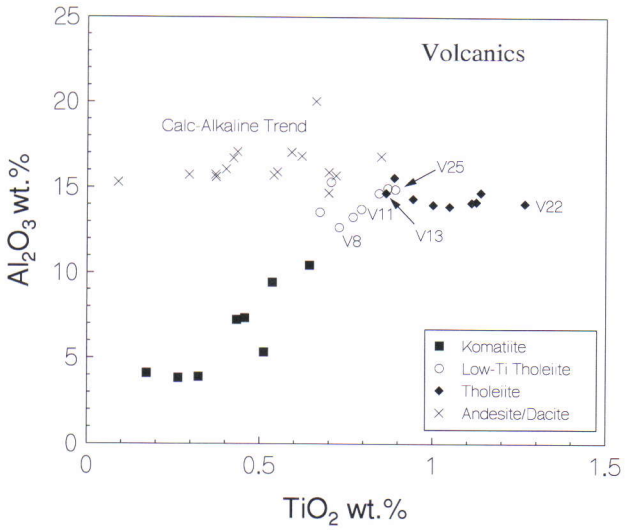


Fig. 5. $Al_2O_3$-$TiO_2$ diagram for the Hattu schist belt volcanics. The tholeiite fractionation path is from V13 to V22.

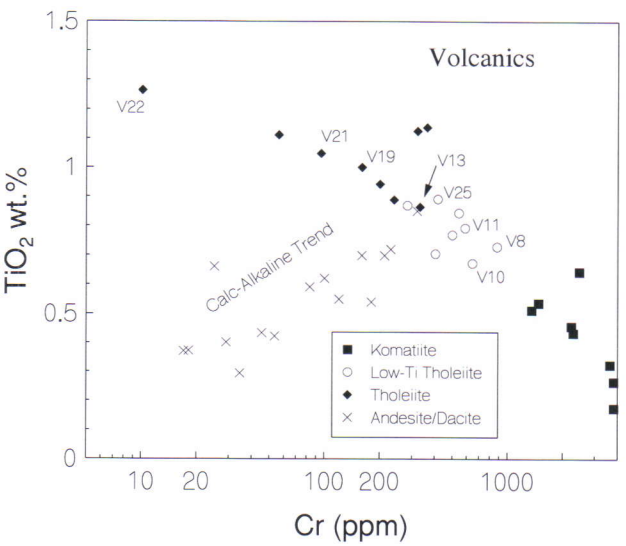


Fig. 6. $TiO_2$ - log Cr diagram for the Hattu schist belt volcanics. The tholeiite trend projects away from the calc-alkaline rocks whereas the low-Ti tholeiites plot at the Cr-rich end of the calc-alkaline trend.

is some scatter, the low-Ti tholeiites are positioned at the Fe-rich end of the calc-alkaline trend in Fig. 4 and plot with calc-alkaline basalts V25 and V26. Samples forming the remainder of the calc-alkaline trend in Fig. 4 are andesite to dacite in composition.

Given that these are five spatially related volcanic rock types (komatiite, tholeiite, low-Ti tholeiite, calc-alkaline basalt and andesite/rhyolite), fractional crystallization schemes can be tested to determine if these rock types are genetically related. For example, with increasing $TiO_2$ in the tholeiites, $Al_2O_3$ contents decrease very slightly (Fig. 5). This is consistent with the fractionation of small amounts of an aluminous mineral, the most likely in these magma compositions being plagioclase. Slight negative Eu anomalies in the samples which plot at the $TiO_2$-rich end of the tholeiite trend in Fig. 5 (e.g., V22) also suggest small amounts of plagioclase removal (see below). The low-Ti tholeiites are positioned at the mafic end of the calc-alkaline trend which extends to low $TiO_2$ contents at nearly constant $Al_2O_3$. This array is consistent with fractional crystallization of ilmenite or Ti-bearing magnetite without large amounts of plagioclase. Consequently, we would expect to see little or no negative Eu anomalies in the andesites and dacites, as indeed is the case (see below).

The tholeiites form a relatively well defined array in $TiO_2$ versus log Cr (Fig. 6) with a variation in Cr content from >350 ppm to <50 ppm. This continuous array with increasing $TiO_2$ and rapidly decreasing Cr content (note the log scale in Fig. 6) strongly suggests fractionation that does not involve the removal of magnetite or ilmenite. The separation of the tholeiites from the komatiites is clear in this diagram. However, the primitive basalts V8, V10 and V11 plot relatively close to the komatiite field and together with the remaining low-Ti tholeiites are positioned at the Cr-rich end of the calk-alkaline trend. The spread of andesite and dacite compositions in Fig. 6 is consistent with the fractional crystallization of both a Cr-bearing mineral (e.g., clinopyroxene) and as described above, ilmenite or magnetite.

Whereas the diagrams involving $TiO_2$ (Fig. 4-6) show the tholeiite fractionation trend extending away

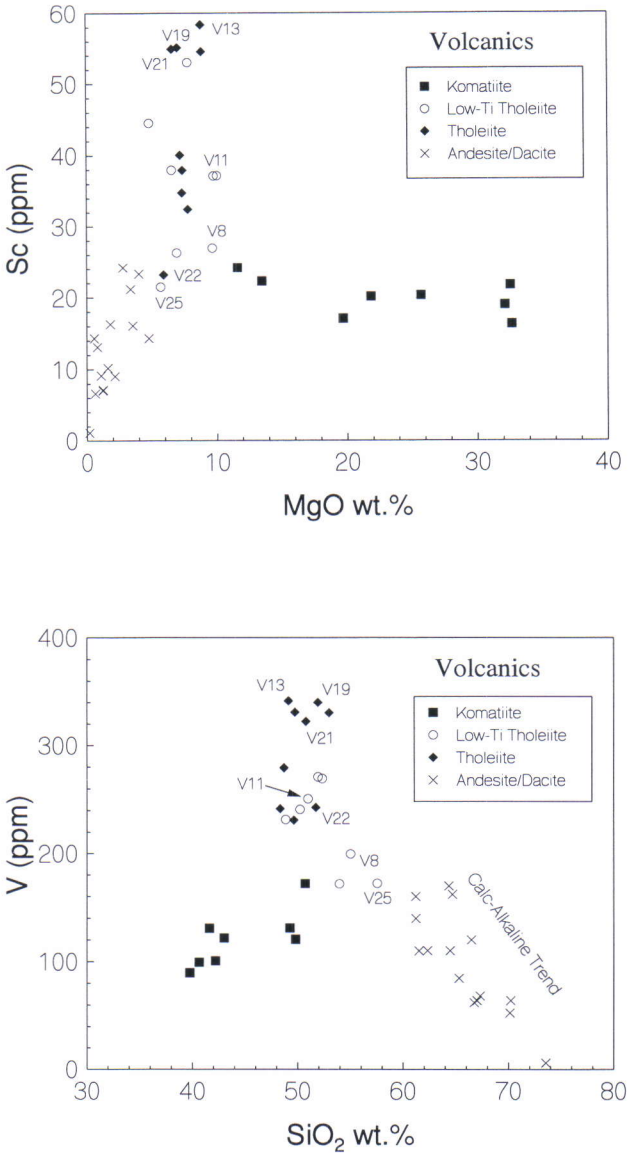


Fig. 7 a. V versus $SiO_2$ b. Sc versus MgO diagram for the Hattu schist belt volcanics.

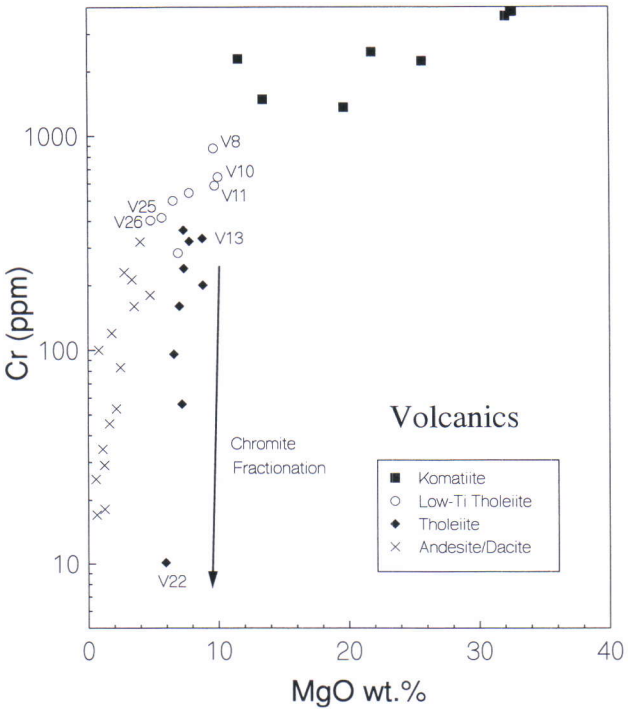


Fig. 8. Cr versus MgO wt.% for the Hattu schist belt volcanics. In this diagram the fractionation path of the tholeiites is distinct from the low-Ti tholeiites and appears to reflect the importance of chromite removal.

from the low-Ti tholeiites and calc-alkaline basalts, the elements V and Sc show the opposite (Figs. 7a & 7b). The least fractionated tholeiites (e.g., V13) have very high V and Sc, and both elements decrease toward the most evolved tholeiite (V22). All of this occurs with only slight variation in MgO and $SiO_2$ (Fig. 7). However, two tholeiites (V19 and V21) have high Sc and V contents even though they are relatively low in Cr (cf. Fig. 6). This requires that at least some Cr depletion in the tholeiites was not accompanied by Sc and V depletion and that the loss of a mineral such as chromite also played an important role in the tholeiites. Clinopyroxene fractionation alone or clinopyroxene + magnetite would produce a sympathetic loss of Cr, Sc and V like that seen in the andesites and dacites. As described above, significant magnetite fractionation in the tholeiites is unlikely based on $TiO_2$ contents.

The importance of chromite fractionation in the tholeiites is confirmed by Cr versus MgO (Fig. 8). Cr contents drop off to very low values even though MgO contents remain relatively high. In contrast, the less dramatic depletion of Cr relative to MgO in the low-Ti tholeiites suggests clinopyroxene fractionation control rather than chromite. Similar clinopyroxene-controlled fractionation trends would also describe the range of komatiite compositions in Cr - MgO (Fig. 8). The dacites have low Cr and MgO contents, as expected after considerable evolution and mafic mineral removal.

Fractional crystallization of olivine is the most likely mineral to have depleted Ni significantly over a small range in MgO in the tholeiites and low-Ti tholeiites. The komatiite Ni contents do not significantly decrease over 20 wt.% MgO further confirming the dominance of clinopyroxene fractionation and a lesser importance of olivine fractionation. The andesites and dacites are distinctly separated in Fig. 9. The andesites have Ni concentrations as high as many of the tholeiites and low-Ti tholeiites.

In summary the two tholeiite trends appear to have been dominated by somewhat different fractionating mineralogies. The tholeiites can be explained by olivine + chromite clinopyroxene plagioclase removal. The low-Ti tholeiite compositions are consistent with the removal of clinopyroxene + olivine +

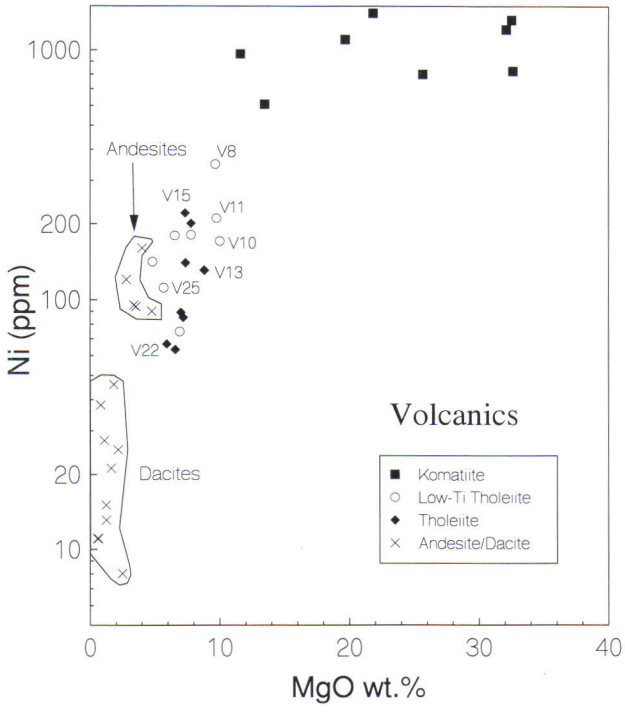


Fig. 9. Ni versus MgO wt.% for the Hattu schist belt volcanics. The tholeiites and low-Ti tholeiites show considerable overlap whereas in this diagram the andesites are clearly separated from the dacites.

magnetite without significant amounts of plagioclase. The possibility of a magma series in the Hattu schist belt is worth further testing. The data appear to be more consistent with andesite evolution from magmas like the more primitive low-Ti tholeiites (V8, V10, V11) than magmas like the calc-alkaline basalts.

## Incompatible trace elements of volcanics

The REE profiles of the Hattu schist belt komatiites are unusual when compared with other komatiite suites in the world. For example, the komatiites from Kuhmo, Suomussalmi and Tipasjärvi, 150 to 300 km north of the Hattu schist belt, show a range in overall REE enrichment, but all have flat or light rare earth element (LREE) depleted profiles (Jahn et al., 1980). In contrast, the few Hattu schist belt komatiites we have analyzed have LREE-enriched patterns (Fig. 10a). Although this could be an extremely important observation considering the importance placed on the worldwide extent of depleted mantle sources by Jahn et al. (1980), we believe instead that it is a function of modification of the more mobile trace elements in the Hattu schist belt komatiites. Concentrations of relatively mobile incompatible elements such as Cs, Rb and Ba (see Fig. 12a, below) have likewise been modified. Although a few samples apparently show relict primary volcanoclastic features (Sorjonen-Ward, 1993a, this volume) all are recrystallized as serpentinites or talc schists. In light of this evidence for alteration, we speculate that none of the analyzed Hattu schist belt komatiites represent original magma compositions in terms of rare earth and incompatible elements.

Rare earth element concentrations and profiles of the Hattu schist belt basaltic rocks are however, very similar to basalts from Kuhmo, Suomussalmi and Tipasjärvi. The REE profiles of these rocks have been divided into two panels in Fig. 10 (b and c) according to profile type. Tholeiites and low-Ti tholeiites with relatively flat REE profiles (Fig. 10b) are primitive with MgO ranging from 8.8 to 6.5 weight % in the tholeiites and 10 to 6.6 weight % in the low-Ti tholeiites. The low-Ti tholeiites have a tendency to show slight LREE enrichment although the profiles are not curved. The differences in LREE enrichment are better presented in $(La/Sm)_N$ - Sm (Fig. 11) which shows that although there is overlap, the low-Ti tholeiites have higher $(La/Sm)_N$ at a given $Sm_N$ (subscript N refers to chondrite normalized value).

Basalts with LREE-enriched patterns include tholeiites V15, V17 and V22 and low-Ti tholeiites V8 and V24, and calc-alkaline basalt V25 (Fig. 10c). The REE profiles and MgO contents of the three tholeiites are very similar to more evolved samples from the Tipasjärvi tholeiitic series reported by Jahn et al. (1980). We interpret the slight negative Eu anomalies in these three samples (Fig. 10c) to represent minor plagioclase fractionation rather than post-magmatic alteration as suggested for some Archean tholeiites (Sun and Nesbitt, 1977). The elevated LREE profiles of basalts V24 and V25 (Fig. 10c) cannot be the result of enrichment by fractional crystallization of large amounts of REE-poor mafic minerals because these two basalts have MgO contents (6.9 and 5.6 weight %, respectively) similar to several of the basalts with flat REE profiles. Low-Ti tholeiite V8 is even more primitive (9.7 weight %

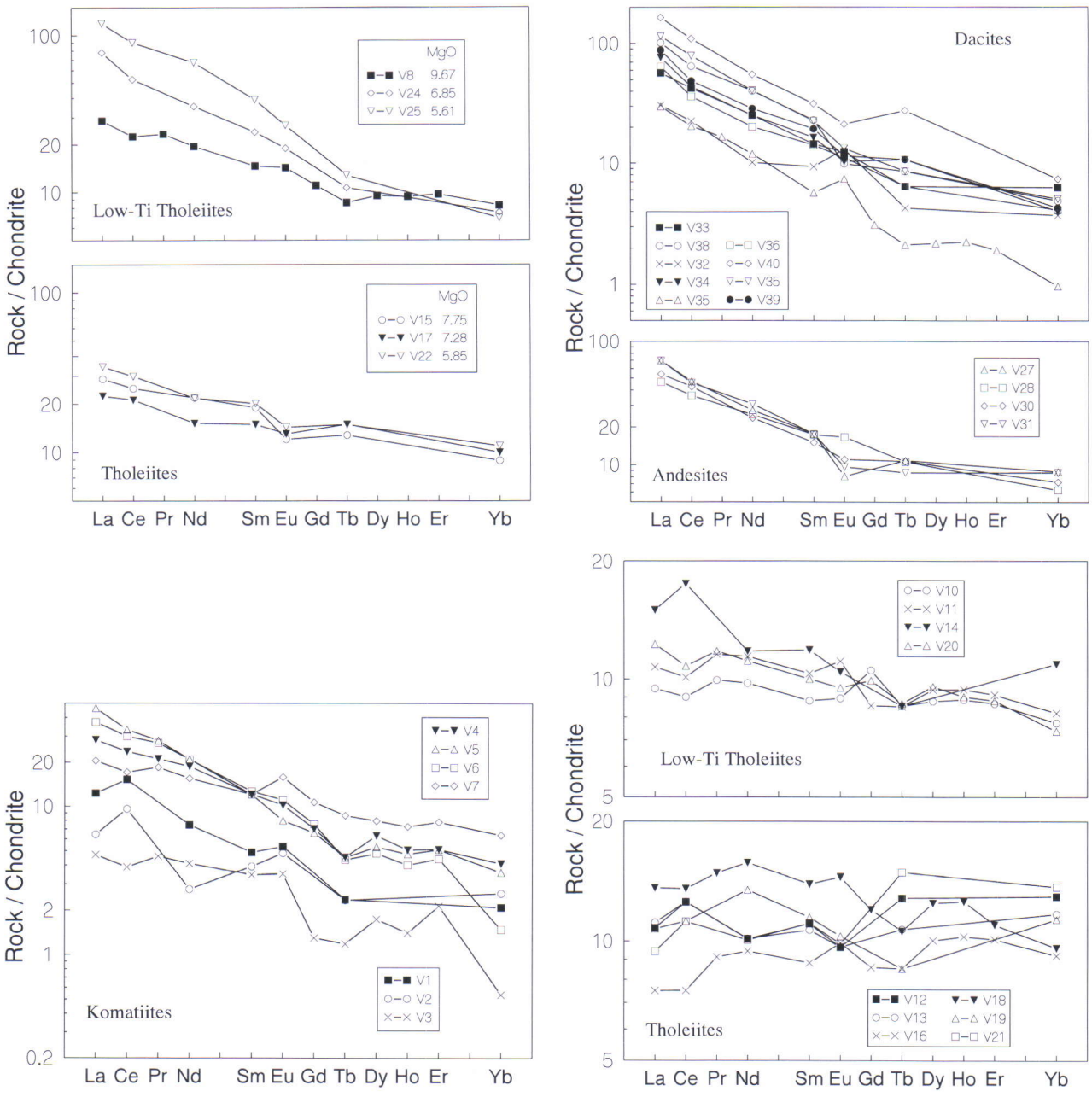


Fig. 10. Chondrite-normalized rare earth element (REE) diagrams for the Hattu schist belt volcanics. a. komatiites b. tholeiites and low-Ti tholeiites with flat REE patterns c. tholeiites and low-Ti tholeiites with enriched REE patterns d. intermediate e. evolved. Chondrite REE values from Boynton, 1984.

MgO) yet is LREE-enriched.

The andesites and dacites have strongly fractionated REE profiles (Fig. 10d) in accord with their evolved compositions. However, the bulk of the dacite samples (MgO from 1.25 to 0.58 wt.%) have REE concentrations no higher than those of basalts V24 and V25. This implies that either the dacites evolved from basaltic parents of a different composition than V24 and V25 or that a REE-rich phenocryst mineral, for example apatite, was important in their evolution. Only one Hattu schist belt andesite or dacite has HREE depletion characteristic of Archean granitoids and felsic volcanic rocks commonly seen in other Archean greenstone belts (e.g., Martin, 1986; Condie, 1992).

Average incompatible trace element compositions (mantle normalized) for each of the Hattu schist belt volcanic rock types are plotted in Fig. 12a. The average tholeiite and low-Ti tholeiite on this diagram exclude the enriched samples depicted in Fig. 10c. The two basalt groups and the komatiites show redistribution of the more mobile elements (e.g., Cs, Rb, Ba). Towards the right of Fig. 12a, considering less mobile elements, the two tholeiite groups are

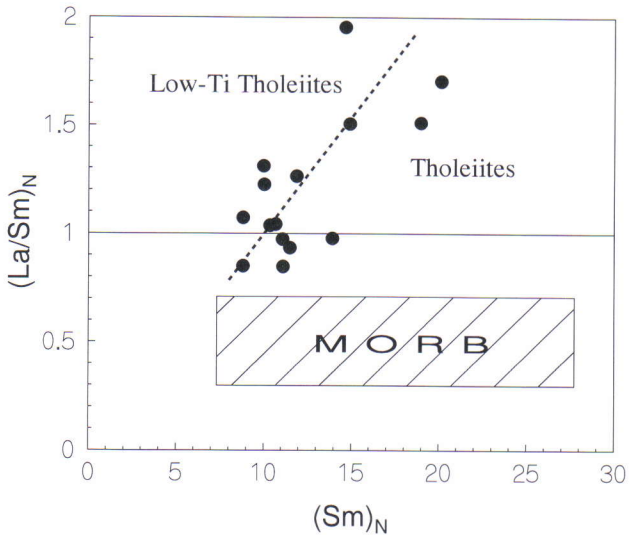


Fig. 11. La/Sm - Sm (chondrite normalized) for the Hattu schist belt tholeiites and low-Ti tholeiites compared to the field for MORB (Sun and Nesbitt, 1977).

very similar, although the low-Ti tholeiites are somewhat lower in Tb, Y, Yb, Lu and of course, Ti. As expected, the profiles of the intermediate and evolved rocks are elevated relative to the basalts except for large negative Ta, Nb and Ti anomalies and low Y, Yb and Lu. In Fig. 12b LREE-enriched, low-Ti tholeiites V8 and V24 and calc-alkaline basalt V25 are compared with average tholeiites and low-Ti tholeiites with flat-REE profiles. The enrichments in incompatible elements of basalts V24 and V25 are almost as high as those seen in the intermediate and evolved rocks.

## GEOCHEMISTRY OF INTRUSIVE ROCKS

### Major and incompatible trace elements of intrusive rocks

The Hattu schist belt intrusive samples come from three separate plutons, the Kuittila, Tasanvaara and Viluvaara plutons. The Kuittila and Tasanvaara plutons are dominated by tonalite, whereas the Viluvaara pluton is mostly granodioritic with only a rim of tonalite against the supracrustals (Fig. 1). To illustrate the geochemical similarity of these intrusive rocks to the volcanics, the intrusive samples are plotted in a total alkali vs. $SiO_2$ (TAS) diagram (Fig. 13). All but two samples plot below the line demarcating typical calc-alkaline from alkaline rock types. As in the case for the volcanics, these two samples have been removed from further discussion. The intrusives cluster in the dacite and rhyolite compositional fields, while the sample at low $SiO_2$ is a metagabbro (amphibolite) probably related to the basalts. Petrographically the bulk of the samples are tonalites, minor granodiorites and trondhjemites. In terms of normative feldspar composition (O'Connor, 1965), the bulk of the samples plot in the trondhjemite field (Fig. 14) and in the granodiorite field of the quartz-alkali feldspar-plagioclase diagram (Fig. 15; LeMaitre, 1989).

$K_2O$, $Na_2O$ and $Al_2O_3$ of the intrusive samples plotted against $SiO_2$ produce a cluster of data points without any obvious trends (Fig. 16a). Many of the least compatible trace elements, including Ba, Cs, Li, Pb, Rb, and Sr show a similar lack of correlation with $SiO_2$. In contrast, major elements, $TiO_2$, $Fe_2O_3$, MgO, CaO, $P_2O_5$ and compatible trace elements Co, Cr, Ni, Sc, V all decrease linearly with increasing $SiO_2$ from tonalite to granodiorite to trondhjemite (Fig. 16b,c). Hf, Zr and the light and middle rare earth elements also decrease with increasing $SiO_2$, most likely due to the fractional crystallization of zircon and apatite, respectively. The very low $P_2O_5$ contents of the most evolved rocks (Fig. 16c) suggests fractionation of a phosphate mineral (i. e., apatite and/or monazite).

Although the plots using $SiO_2$ (Fig. 16 a-c) can be used to distinguish different rock types, none differentiate the three plutons from each other. If, however, MgO is used on the abscissa as an index of fractionation, some coherent correlations emerge. Cr - MgO (Fig. 16d) and Ni - MgO (not shown) exhibit two relatively continuous trends, with the Kuittila tonalites comprising a distinctly higher Cr (and Ni) group. The Kuittila tonalites can be further subdivided into two groups separated at about 2 wt. % MgO, where there is a slight bend and gap in the Cr - MgO trend (Fig. 16d). The Tasanvaara and Viluvaara tonalites and the granodiorites and trondhjemites from Kuittila represent the lower Cr (and Ni) trend. Based on field relationships, it is apparent that the central trondhjemite body of the Kuittila pluton represents a separate intrusive phase. These data suggest the possibility that the Kuittila trondhjemites evolved from tonalitic magmas more closely allied to the Tasanvaara pluton compositions.

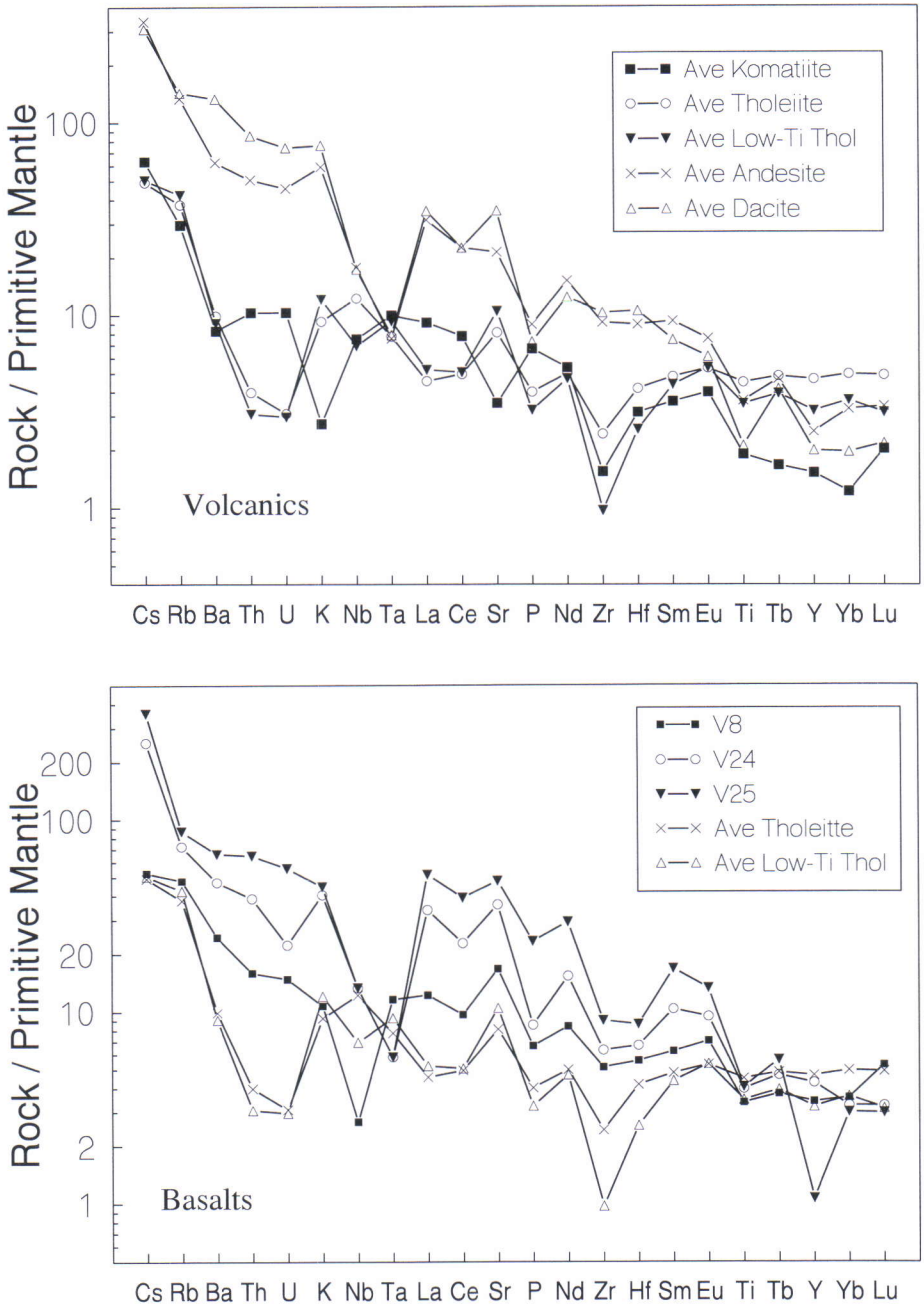


Fig. 12. Primitive mantle-normalized incompatible element diagrams for the Hattu schist belt volcanics. a. Comparison of komatiite, tholeiites (with flat REE patterns), intermediate and evolved volcanics. **b.** Comparison of tholeiites and low-Ti tholeiites with flat REE patterns and basalts 8, 24 and 25. Primitive mantle values are from McDonough et al., 1985.

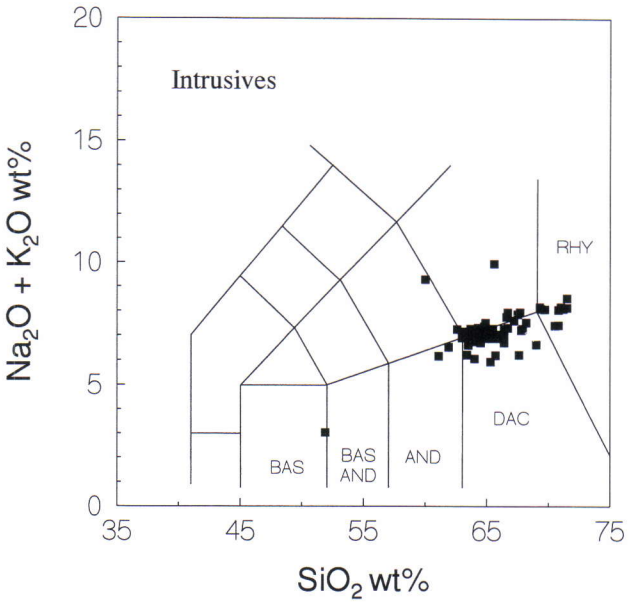


Fig. 13. Total alkali ($Na_2O + K_2O$) - $SiO_2$ for the Hattu schist belt intrusive rocks. The two samples with high ($Na_2O + K_2O$) are not used in the following discussions.

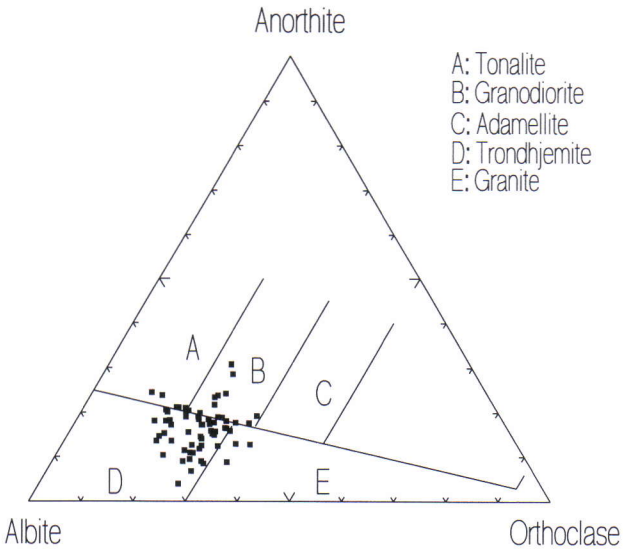


Fig. 14. Normative feldspar compositions of the Hattu schist belt intrusive rocks. After O'Connor, 1965.

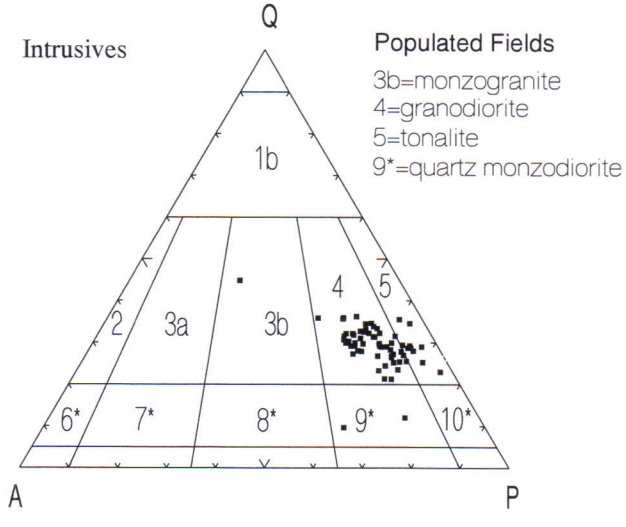


Fig. 15. Normative quartz (Q) - alkali feldspar (A) - plagioclase (P) compositions of the Hattu schist belt intrusive rocks. After LeMaitre (1989).

The feldspar porphyry dikes cover the entire compositional range of the intrusive rocks, but importantly do not lie significantly outside this range. One feldspar porphyry dike (P506/7.2, Fig. 16d) plots at the primitive end of the tonalite trend and may represent an initial Kuittila tonalite magma.

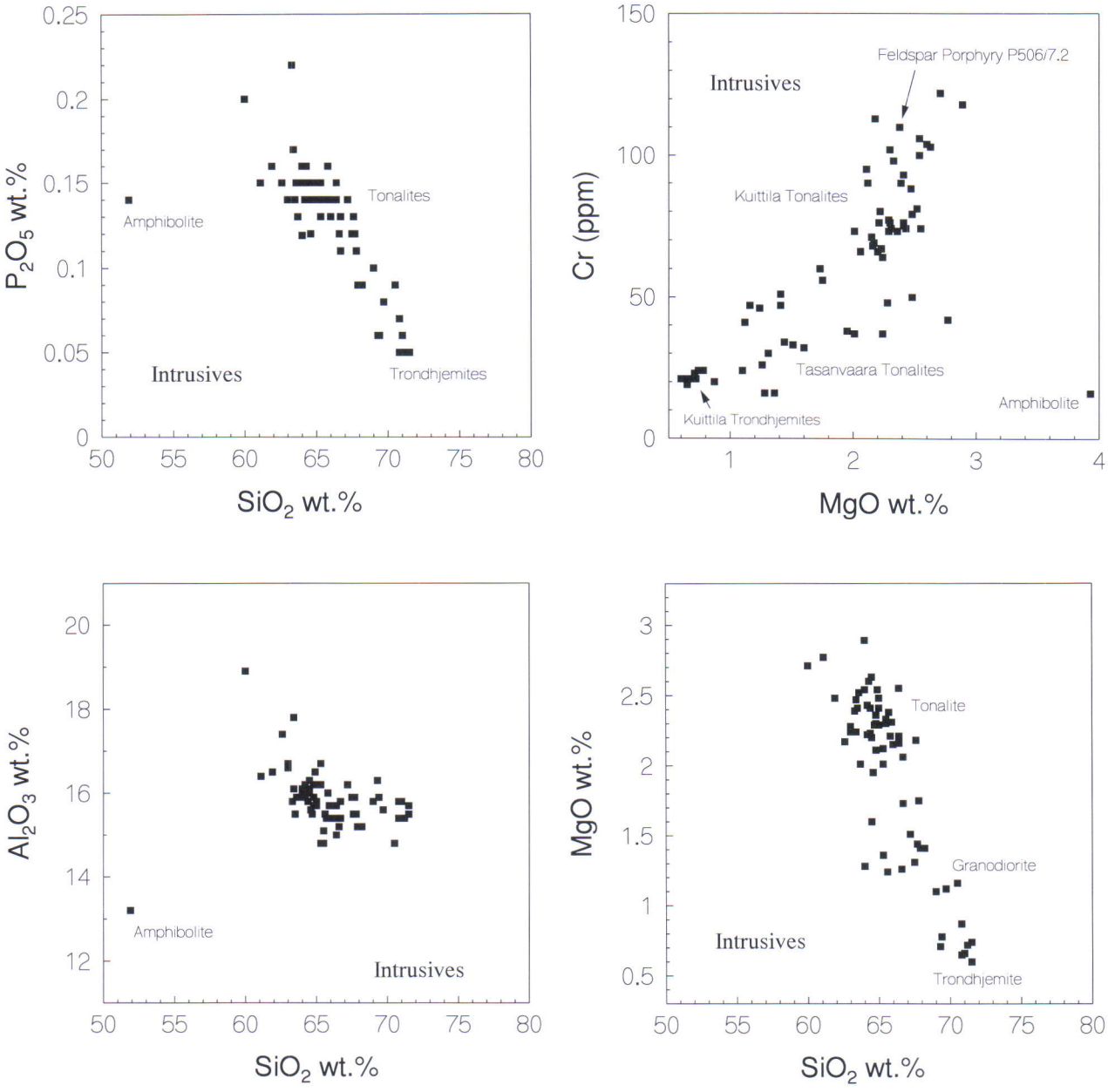


Fig. 16. Variation diagrams for Hattu schist belt intrusive rocks. a. $Al_2O_3$ - $SiO_2$ b. MgO - $SiO_2$ c. $P_2O_5$ - $SiO_2$ d. Cr - MgO.

## Incompatible trace elements of intrusive rocks

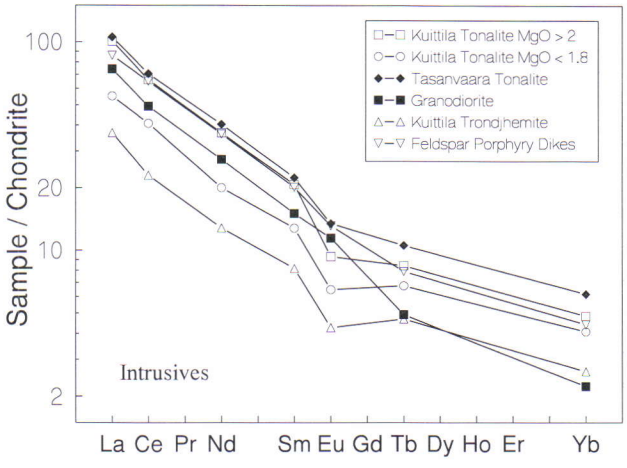


Fig. 17. Chondrite-normalized REE diagram for Hattu schist belt intrusive rock averages. The Kuittila tonalite samples have been divided into two types depending on MgO content.

Average Kuittila and Tasanvaara tonalites have similar REE profile shapes and concentrations if the most evolved tonalites are considered separately (Fig. 17). The Tasanvaara samples, however, have slightly higher HREE concentrations. REE concentrations in the Kuittila samples progressively decrease from tonalites to evolved tonalites to trondhjemites, yet essentially the same REE profile is maintained. All three of the Kuittila profiles exhibit a negative Eu anomaly, suggesting some loss of plagioclase before or during crystallization of the plutons. The granodiorites, on the other hand, have a steeper REE profile and do not have the negative Eu anomaly displayed by the tonalites.

The one distinction we can make between the feldspar porphyry dikes and the tonalites is that the dike rocks lack a negative Eu anomaly. This is reasonable if the feldspar porphyry dike rocks represent initial magma compositions unaffected by crystal accumulation effects and may indicate that most of the modification of the pluton rocks by crystal accumulation (crystal growth on walls, or crystal settling) occurred after pluton emplacement.

The incompatible trace elements to the left of La remain at essentially the same concentration throughout the range of Kuittila pluton sample compositions (Fig. 18, lower panel). An absence of enrichment of

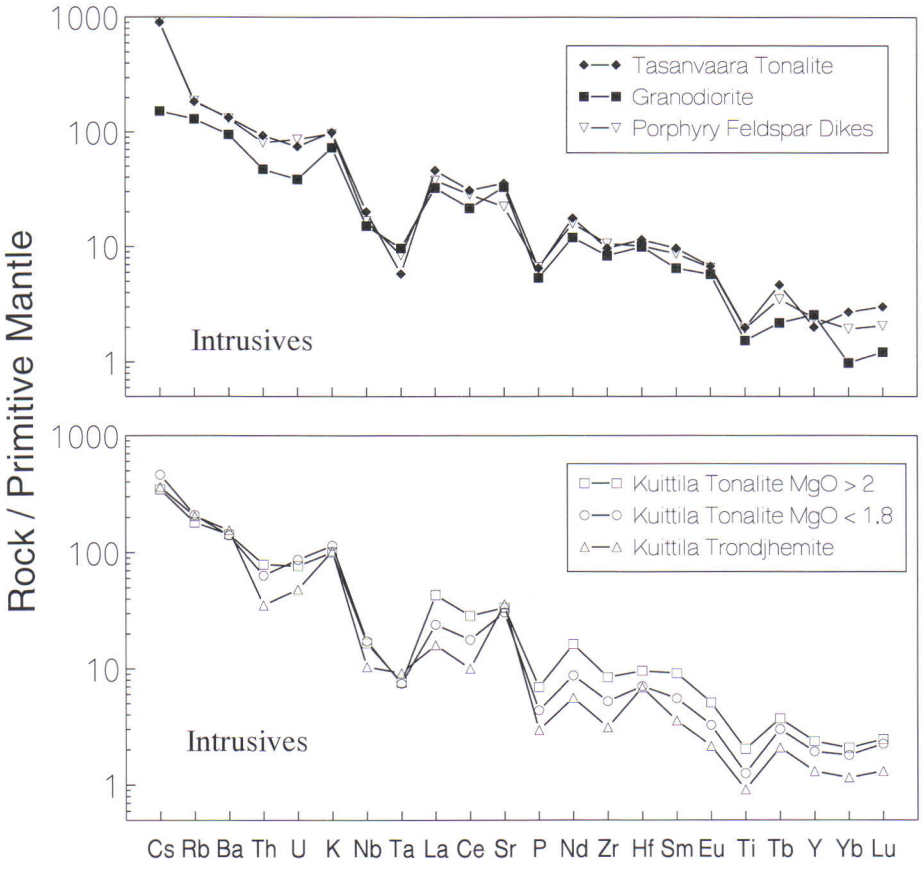


Fig. 18. Primitive mantle-normalized incompatible element diagram for Hattu schist belt intrusive rocks. Primitive mantle values are from McDonough et al., 1985.

these normally highly incompatible elements with increasing $SiO_2$ requires that appropriate minerals (e.g., Ba, Sr in alkali feldspar; Cs, Li, Rb in biotite or muscovite; Sr, U, Th, Pb in zircon and apatite) accumulated in sufficient quantities to maintain roughly constant concentrations in all daughter magmas. Incompatible elements to the right of La show decreasing concentration with decreasing MgO (except Sr, Fig. 18). The decrease in concentration is consistent with significant apatite and zircon fractional crystallization as suggested by the $P_2O_5$ data. Incompatible element concentrations of the porphyry dikes are quite similar to those in the tonalites (Fig. 18, top panel).

## MAGMA SOURCES AND TECTONIC SETTING

### Sr Isotopes

Whole rock Sr isotope work was carried out on 9 samples from the Kuittila tonalite pluton. Sr isotopic analyses have not been done, to any extent, at the Geological Survey of Finland for a number of years because of the early recognition of problems associated with resetting of this isotopic system during Proterozoic metamorphism in much of Finland (e.g., Wetherill et al., 1962).

Listed in Table 2 are the Sr, Rb concentrations, Sr isotopic compositions and calculated uniform reservoir (UR) model ages for one feldspar porphyry dike, three trondhjemite and five tonalite samples from the Kuittila pluton. Fig. 19 presents the Kuittila $^{87}Sr/^{86}Sr$ - $^{87}Rb/^{86}Sr$ data and an isochron calculated according to the method of York (1969) using the program ISOPLOT (Ludwig, 1988). The samples define an isochron of 2789 ± 290 Ma with an initial $^{87}Sr/^{86}Sr$ of 0.70146 ± 0.0009. The large error in the calculated age is due to the small spread in Rb/Sr, the probability of some real scatter in initial ratios, the possibility of some redistribution of Sr and Rb during upper greenschist to lower amphibolite metamorphism and the analytical difficulties mentioned above. Although imprecise, this age compares well with the 2750 Ma U-Pb zircon age from the pluton (Vaasjoki et al., 1993, this volume). Calculated $T_{UR}$ model ages from these Sr data (mean of 2863 Ma, median of 2984 Ma) compare favorably to Kuittila Nd $T_{DM}$ model

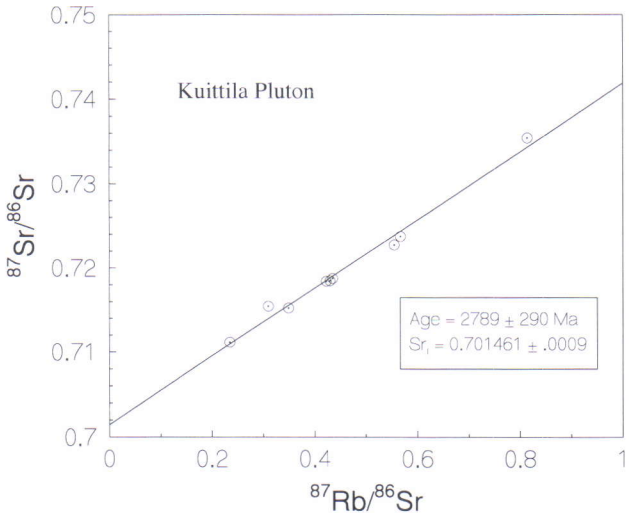


Fig. 19. Rb - Sr isochron for 9 Kuittila pluton whole-rock samples. Slope of the line gives an age of 2790 ± 290 Ma.

Table 2. Sr, Rb concentrations by isotope dilution and Sr isotopic compositions of samples from the Kuittila pluton, Hattu schist belt.

| Sample | Rocktype | Rb (ppm) | Sr (ppm) | $^{87}Rb/^{86}Sr$ | $^{87}Sr/^{86}Sr$ | $T_{UR}$* |
|---|---|---|---|---|---|---|
| P479/9.9 | Granodiorite | 74.23 | 916.5 | 0.23451 | 0.711135±7 | 2991 |
| P476/2.6 | Tonalite | 112.1 | 398.8 | 0.81420 | 0.735448±6 | 2914 |
| P560/7.2 | Tonalite | 81.9 | 765.8 | 0.30952 | 0.715450±7 | 3305 |
| P486/12.5 | Granodiorite | 85.8 | 571.3 | 0.43505 | 0.718758±7 | 2785 |
| P475/4.2 | Tonalite | 108.8 | 555.5 | 0.56708 | 0.723755±7 | 2739 |
| P506/7.2 | Feldspar Porph. | 54.9 | 455.9 | 0.34888 | 0.715237±7 | 2774 |
| P478/5.3 | Granodiorite | 108.1 | 564.2 | 0.55500 | 0.722744±6 | 2663 |
| P561/7.2 | Tonalite | 88.6 | 607.3 | 0.42238 | 0.718431±7 | 2822 |
| P544/7.8 | Tonalite | 88.8 | 598.2 | 0.42970 | 0.718483±7 | 2773 |

All isotopic ratios normalized to $^{86}Sr/^{88}Sr = 0.1194$. Measurements of $^{87}Sr/^{86}Sr$ on National Bureau of Standards SRM987 (n=33) during the period of sample analysis gave 0.710232±22 (2 $\sigma_m$). *$T_{UR}$ ages calculated using source $^{87}Rb/^{86}Sr = 0.0816$, $^{87}Sr/^{86}Sr = 0.7045$.

ages given in the next section. These Sr model ages do not allow a large amount of older crustal material in the source of the Kuittila tonalite magma. However, because Sr model ages are particularly difficult to interpret, we prefer to rely more on model ages calculated from Nd data.

## Nd isotopes

In addition to the 9 Kuittila samples described above, 5 other intrusive rocks from within or at the margin of the Hattu schist belt have been analyzed for Nd isotopic composition and Nd, Sm concentrations (Table 3). These samples include a felsic porphyry dike from Kivisuo, an additional Kuittila tonalite sample, a tonalite sample from the Tasanvaara pluton and 2 granodiorite samples from the Silvevaara pluton, intruded into the metasediments on the western edge of the Hattu schist belt. The small range in Sm/Nd of this set of 14 samples does not allow an isochron to be calculated. Instead, we must rely on the interpretation of Nd model ages and $\varepsilon_{Nd}$ calculated for 2750 Ma, the best U-Pb zircon age estimate for these plutons (Vaasjoki et al., 1993, this volume). Inherent in these calculated values is the possibility of open-system behavior of Nd and Sm. If Sm/Nd fractionation occurred within the scale of the whole rock samples, for example in the Proterozoic, then any calculated Archean $\varepsilon_{Nd}$ values are meaningless.

The range of $\varepsilon_{Nd}(2750)$ for all of the intrusive rocks from within the Hattu schist belt is small, from +0.9 to +2.1, and all have a $T_{DM}$ age close to 2.8 Ga. The three Silvevaara granodiorite samples have instead, lower $\varepsilon_{Nd}(2750)$ from -0.4 to -2.1 and older $T_{DM}$ ages near 3.0 Ga. A straightforward interpretation of $T_{DM}$ ages is that they represent the time at which large Sm/Nd fractionation occurred during crust extraction from the mantle, leaving behind a depleted mantle residuum. The similarity of intrusion and $T_{DM}$ ages of the Kuittila and Tasanvaara tonalites and the feldspar porphyry dikes strongly imply that there

Table 3. Nd, Sm concentrations by isotope dilution and Nd isotopic compositions of samples from the Hattu schist belt.

| Sample | Rocktype | Sm | Nd (ppm) | $^{147}Sm/^{144}Nd$ | $^{143}Nd/^{144}Nd$ | $\varepsilon_{Nd}(2750)$ | $T_{CHUR}$* | $T_{DM}$§ |
|---|---|---|---|---|---|---|---|---|
| P479/9.9 | Kuittila granodiorite | 1.29 | 6.47 | 0.1200 | 0.511269±07 | +0.5 | 2702 | 2892 |
| P476/2.6 | Kuittila tonalite | 2.75 | 14.70 | 0.1126 | 0.511204±15 | +1.8 | 2582 | 2773 |
| P560/7.2 | Kuittila tonalite | 4.17 | 24.49 | 0.1024 | 0.511046±10 | +2.3 | 2558 | 2734 |
| P486/12.5 | Kuittila granodiorite | 1.19 | 6.25 | 0.1142 | 0.511217±07 | +1.5 | 2608 | 2799 |
| P475/4.2 | Kuittila tonalite | 2.66 | 14.73 | 0.1086 | 0.511045±06 | +0.8 | 2675 | 2847 |
| P506/7.2 | Kuittila feld. porph. | 3.19 | 17.85 | 0.1075 | 0.511040±10 | +0.4 | 2710 | 2876 |
| P478/5.3 | Kuittila granodiorite | 3.61 | 20.58 | 0.1054 | 0.511035±15 | +1.1 | 2659 | 2827 |
| P561/7.2 | Kuittila tonalite | 2.89 | 16.34 | 0.1066 | 0.511062±12 | +1.2 | 2647 | 2820 |
| P544/7.8 | Kuittila tonalite | 4.37 | 26.19 | 0.1004 | 0.511063±05 | +3.4 | 2476 | 2659 |
| A1095 | Kivisuo feld. porph. | 3.14 | 18.62 | 0.1019 | 0.510982±10 | +1.2 | 2654 | 2818 |
| A285 | Kuittila tonalite | 4.09 | 24.02 | 0.1029 | 0.511019±10 | +1.6 | 2623 | 2795 |
| A1094 | Tasanvaara tonalite | 4.69 | 25.30 | 0.1120 | 0.511148±10 | +0.9 | 2672 | 2851 |
| A284 | Kelsimä granodiorite | 5.96 | 32.40 | 0.1111 | 0.511054±10 | -0.7 | 2810 | 2974 |
| A339 | Kelsimä granodiorite | 3.51 | 19.51 | 0.1088 | 0.510983±10 | -2.1 | 2931 | 3077 |
| A339b | Kelsimä granodiorite | 3.91 | 22.25 | 0.1064 | 0.510983±10 | -0.4 | 2783 | 2942 |
| M8603917 | Poikapää mafic lava | 3.21 | 9.79 | 0.1984 | 0.512305±22 | | | |
| | duplicate | 3.49 | 10.73 | 0.1964 | 0.512344±14 | | | |
| M8603967 | Tiittalanvaara amphib. | 1.63 | 4.49 | 0.2187 | 0.513108±10 | | | |
| A1038 | Poikapää meta-andesite | 3.67 | 16.94 | 0.1311 | 0.511331±10 | -2.4 | 3026 | 3201 |
| | duplicate | 3.87 | 17.72 | 0.1320 | | | | |
| A1039 | Poikapää metadacite | 3.07 | 18.30 | 0.1013 | 0.510996±11 | +1.7 | 2615 | 2786 |
| | duplicate | 3.15 | 18.80 | 0.1013 | | | | |
| A221 | Hattuvaara mica schist | 3.94 | 22.39 | 0.1063 | 0.511060±10 | +1.2 | 2652 | 2826 |
| S18 | Ukkolanvaara m. schist | 2.11 | 10.02 | 0.1276 | 0.511422±14 | +0.7 | 2676 | 2893 |
| | duplicate | 2.05 | 9.75 | 0.1274 | | | | |
| S20 | Leppärinne mica schist | 2.80 | 14.37 | 0.1176 | 0.511174±11 | -0.6 | 2811 | 2986 |

All isotopic ratios normalized to $^{146}Nd/^{144}Nd = 0.7219$. Measurements of $^{143}Nd/^{144}Nd$ on LaJolla (n=27) during the period of sample analysis gave 0.511851±11 (2 $\sigma_m$). *$T_{CHUR}$ ages calculated using source $^{147}Sm/^{144}Nd = 0.1967$, $^{143}Nd/^{144}Nd = 0.512638$. §$T_{DM}$ ages calculated using $\varepsilon_{Nd}(T)=0.25T^2-3T+8.5$.

was not a significant contribution of older crust in their sources. In contrast, the Silvevaara intrusion, which is not internal to the Hattu schist belt, apparently had a larger contribution of older crustal material in its genesis.

Two mafic Hattu schist belt volcanic rocks that could provide information on local mantle evolution have also been analyzed for Nd isotopes. An amphibolite from Tiittalanvaara has slightly depleted LREE and gives an $\varepsilon_{Nd}(2750)$ of +1.3, close to what is expected for model mantle. In contrast, a pillow basalt from Poikopää has $\varepsilon_{Nd}(2750)$ ca. -6 (average for two dissolutions). This rather odd value could represent Proterozoic Sm/Nd resetting, but clearly, further work is necessary on mafic samples from the schist belt.

The more evolved meta-andesite and crystal lithic sediment ("metadacite") (Table 3) from Poikopää are also problematic. The meta-andesite (U-Pb zircon age = 2754 Ma) has a low $\varepsilon_{Nd}(2750)$ of -2.4 whereas, the sediment (U-Pb zircon age = 2860 Ma) has an $\varepsilon_{Nd}(2750)$ of +1.7. If the older zircon age of the sediment represents incorporation of older crustal material, e.g. inherited older zircon cores, then it should have an $\varepsilon_{Nd}(2750)$ lower than that of the meta-andesite. The opposite is in fact the case, most likely the result of Proterozoic resetting of the Nd isotopic system.

## Trace element discriminants

Primitive-mantle normalized incompatible element patterns can be used as geochemical signatures characteristic to the particular tectonic regime in which a magma was formed. For example, mid-ocean ridge basalts (Wood, 1979) typically have curved, concave-down patterns with increasing concentrations towards the least incompatible elements (those elements to the right in Fig 12), indicative of partial melting of depleted mantle. However, it is important to note that caution is necessary when applying these diagrams to Archean rocks because of: 1. alteration and redistribution of the relatively mobile incompatible trace elements; 2. uncertainties whether present day distinctive trace element signatures are relevant to the Archean; 3. fractional crystallization in more evolved samples may influence incompatible trace element profiles.

Condie (1990) has shown that almost all Precambrian greenstone basalts have trace-element characteristics similar to those of modern subduction-related basalts and the elevated Cs, Rb and Ba in the Hattu schist belt tholeiites are, to some extent, consistent with this proposal. It is certain, even given the possibility of some incompatible trace element redistribution in these basalts, that they are unlike MORB. The distinctive Ta, Nb and Ti anomalies in basalts V24 and V25 (Fig. 12) align these two samples closely to subduction-produced basalts (e.g., Perfit et al, 1981).

The tholeiites appear to represent a fractionation series that is distinct from the other basalts and clearly projects away from the more evolved calc-

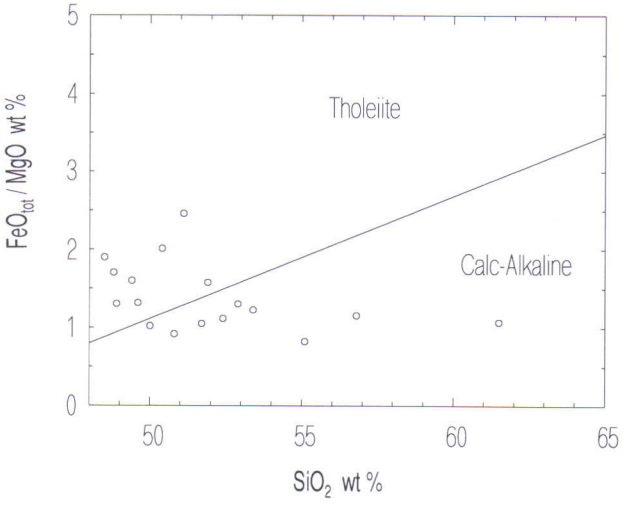


Fig. 20. $FeO_{tot}/MgO$ - $SiO_2$ for Hattu schist belt basalts. The basalts we have termed tholeiite plot appropriately in the tholeiite field whereas our low-Ti tholeiite group plots completely within the calc-alkaline basalt field of this diagram. After Miyashiro, 1974.

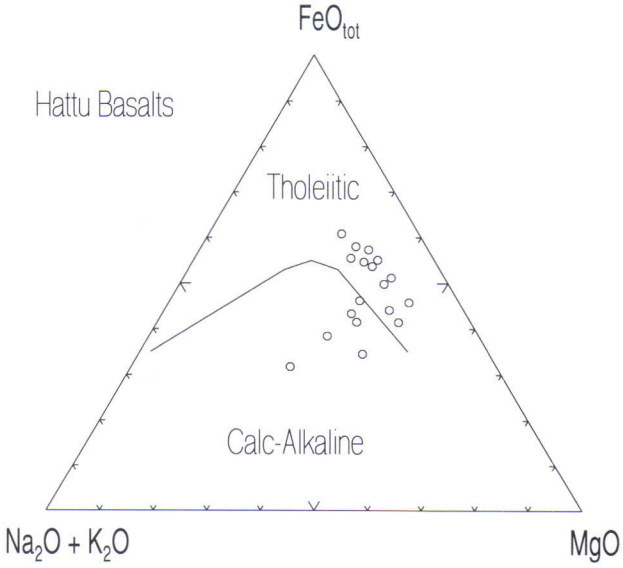


Fig. 21. $Na_2O + K_2O$ - $FeO_{tot}$ - MgO for Hattu schist belt basalts. Six of nine low Ti tholeiites plot within the calc-alkaline field of this diagram. After Irvine and Baragar, 1971.

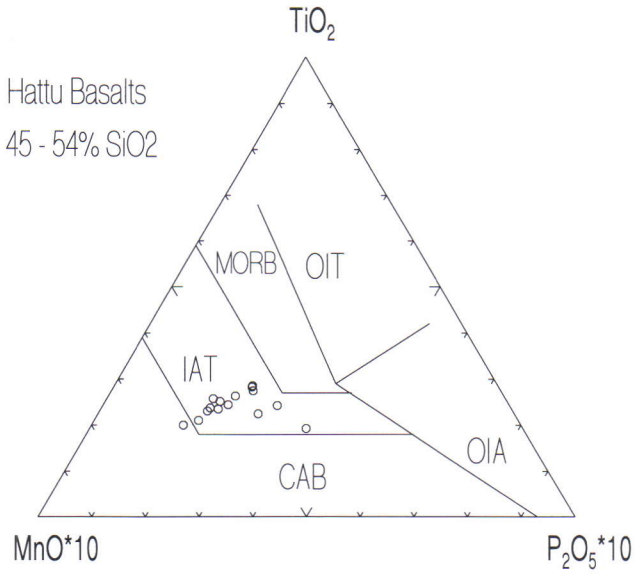


Fig. 22. MnO (x 10) - $TiO_2$ - $P_2O_5$ (x 10) tectonic discriminant diagram with the Hattu schist belt basalts containing 45 to 54 wt. % $SiO_2$ plotted. Abbreviations are: IAT = island arc tholeiite, CAB = calc-alkaline basalt, MORB = mid-ocean ridge basalt, OIT = ocean island tholeiite, OIA = ocean island alkaline basalt. After Mullen, 1983.

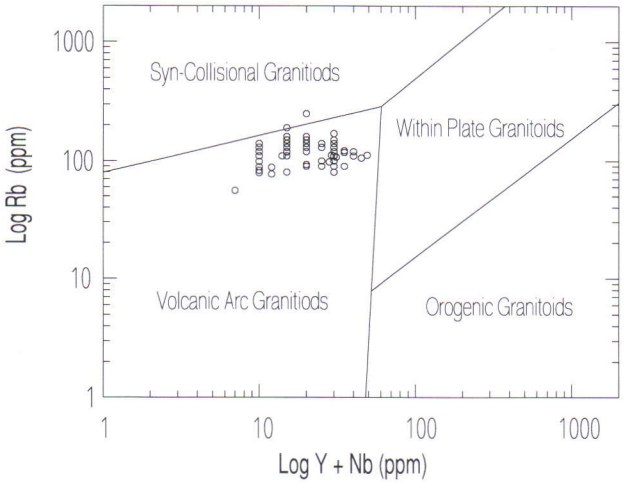


Fig. 23. Log Rb - log (Y + Nb) tectonic discriminant diagram with the Hattu schist belt intrusive rocks plotted. After Pearce et al., 1984.

alkaline rocks. On the other hand, several basalts, eg., V10, V11, and V8 have major and compatible trace element compositions that would be expected of parental magmas of the calc-alkaline series rocks. Several geochemical parameters suggest a calc-alkaline affinity for the low-Ti tholeiites. For example, all of the low-Ti tholeiites plot in the calc-alkaline field of FeO/MgO - $SiO_2$ (Fig. 20) and many in the calc-alkaline field of the familiar AFM diagram (Fig. 21). The tectonic discriminant plot of $TiO_2$ - MnO - $P_2O_5$, however, places all of the basalts except V25 in the island arc tholeiite field (Fig. 22). Condie (1990) has suggested that Archean greenstones are dominated by basalts typical of island arcs whereas Proterozoic greenstone belts have greater amounts of calc-alkaline basalts. The Hattu schist belt low-Ti tholeiites have characteristics of both island arc tholeiites and calc-alkaline basalts and together with the tholeiites are distinct from mid-ocean ridge and within plate basalts.

As expected, the profiles of the intermediate and evolved rocks are elevated relative to the basalts except for large negative Ta, Nb and Ti anomalies and low Y, Yb and Lu. The negative Ta, Nb and Ti anomalies are typical of subduction related magmas (e.g., Perfit et al, 1981) while the Y, Yb and Lu concentrations, although low, are not as depleted as is typical for Archean felsic volcanics (Condie, 1992).

The Hattu schist belt internal granitoids have compositions similar to granitoids formed in volcanic arc settings. For example, the discriminant log Rb - log (Y+Nb) shows that the Hattu schist belt tonalite and trondhjemite compositions are within the field for volcanic arc granitoids (Fig. 23). Our Nd isotopic data are also consistent with an island arc environment as the data indicate these granitoids were formed as juvenile additions to the crust at approximately 2.75 Ga. No evidence exists for significant contribution from older, previously stabilized crust. However, the Nd data cannot be used to resolve the issue as to whether these granitoids were extracted essentially direct from melting of oceanic crust or by fractional crystallization of mantle-derived basalts.

The Hattu tonalite-trondhjemite-granodiorite (TTG) rocks have REE profiles generally similar to those displayed by other Archean TTG suites (Martin, 1986) except for higher HREE than in typical Archean tonalites (Condie, 1992). Very low HREE and Y contents (1 to 4 times chondrites) in Archean tonalite magmas have been suggested to reflect melting of metamorphosed, subducting oceanic crust (eclogite) with large amounts of garnet and/or amphibole preferentially retaining the HREE and Y (Martin, 1986). Post-Archean tonalites, in contrast, are suggested to be products of fractional crystallization of basaltic magmas because of their distinctly higher HREE and Y contents (6 to 15 times chondrites). However, adakites are modern analogues to the Archean TTG, have low HREE and Y, and are apparently slab-derived tonalitic magmas (Defant and Drummond, 1990).

A number of samples from our data set plot well within the proposed Archean - Post-Archean tonalite HREE and Y gap. Felsic volcanic rocks from the Kuhmo greenstone belt, very similar to those described here, have an even wider range of HREE concentrations, from 1 to 15 times chondrites (Taipale, 1988). The significance of these Archean tonalitic magmas with intermediate depletion of HREE in

terms of their sources and the processes by which they were generated is unclear. Perhaps both partial melting of oceanic crust *and* fractional crystallization from basaltic parent magmas generated the Finnish greenstone belt tonalites. These data invite further scrutiny of models which propose to distinguish these processes based on extent of HREE (and Y) depletion.

## GEOCHEMISTRY OF METASEDIMENTS

### Major and compatible trace elements of sediments

As a tool to compare the metasediment and volcanic rock compositions, the metasediment samples from the Hattu schist belt extended type set are plotted in the total alkali vs. $SiO_2$ (TAS) diagram (Fig. 24). The metagraywackes cluster in the volcanic andesite and dacite fields, while the metasediments at low silica and $K_2O$ + $Na_2O$ are the Fe-formation samples. Although the latter, containing garnet - grunerite - magnetite assemblages, are very interesting mineralogically, they are nevertheless left out of further discussions in this paper and remain an area of future research.

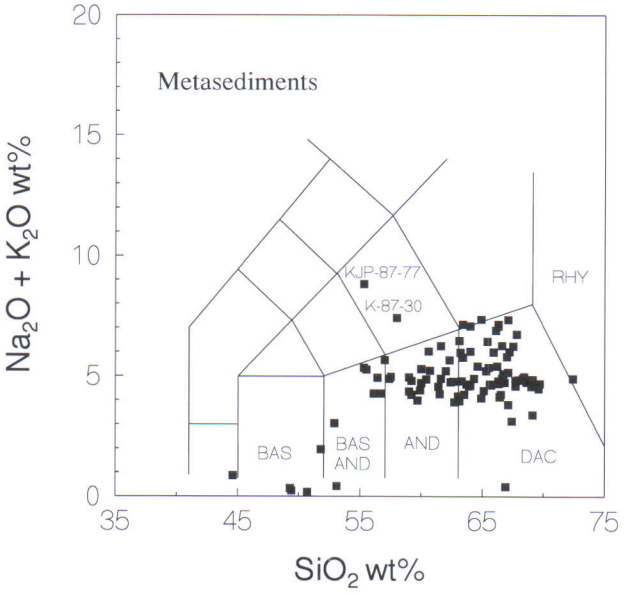


Fig. 24. Total alkali ($Na_2O$ + $K_2O$) - $SiO_2$ for Hattu schist belt metasedimentary rocks. The metasediments at low $SiO_2$ are the Fe-formation samples. The metagraywackes range from basaltic andesite to dacite in composition. Two labeled samples with high ($Na_2O + K_2O$) are discussed in the text.

In Fig. 25 data for the Hattu schist belt metagraywackes, volcanics and intrusives have been assembled for direct comparison. Because of similar geochemical behavior among many of the elements we will discuss, only $TiO_2$ - $SiO_2$ and Cr - $SiO_2$ are shown in Fig. 25, but each of these are representative of a group of elements.

The metagraywackes have similar compositions to the volcanic rocks including major elements $TiO_2$, $Fe_2O_3$ and MgO and compatible trace elements Cr, Ni, Sc, and V at $SiO_2$ between 65 and 56 wt. % (Fig.

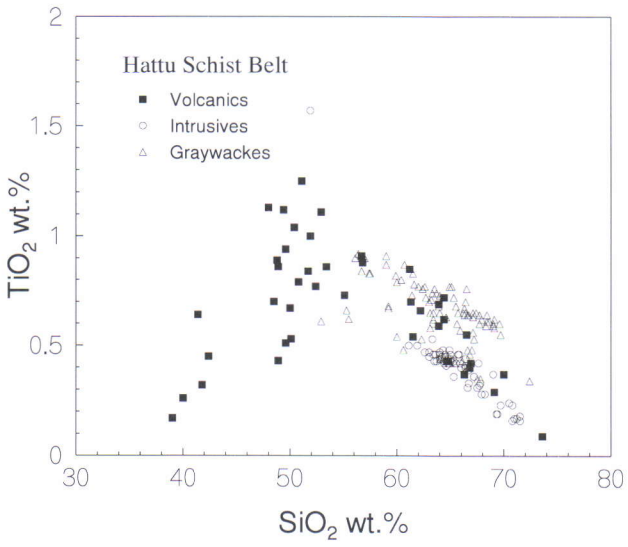


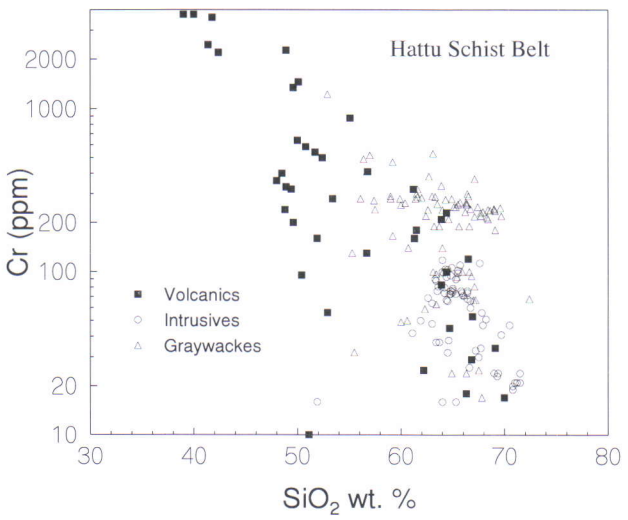


Fig. 25. a. $TiO_2$ versus $SiO_2$ b. Cr versus MgO diagram for Hattu schist belt metagraywackes. The large cluster of samples with > 65 wt. % $SiO_2$ have no Hattu schist belt volcanic or intrusive equivalents.

25 a, b). At 56 wt. % $SiO_2$ the metagraywacke field nearly intersects the compositional field of basalts. This is exemplified by sample HJO-86-118, the most primitive metasediment. It is not a true metagraywacke because it has 13 wt. % MgO, and probably represents very locally derived basaltic epiclastic material or reworked pyroclastics. Because the lowest $SiO_2$ metagraywackes are basaltic andesite in composition, the $TiO_2$ (and $Fe_2O_3$, MgO) - $SiO_2$ field for metagraywackes points directly towards the main group of basalts, and implies that the basalts represent one important source end member for the sediments. A few metagraywackes at low $SiO_2$ that plot towards the komatiites in $TiO_2$ (Fig. 25a; likewise for $Fe_2O_3$, MgO) and Cr (Fig. 25b; likewise for Ni, Sc, V) suggest some metagraywackes contain a component of komatiites.

At levels of $SiO_2$ greater than 65 wt %, the intrusive and felsic volcanic compositional fields converge and the fields for volcanics and metagraywackes diverge. Relative to the intrusives and felsic volcanics, nearly all of the metagraywackes with higher $SiO_2$ are enriched the major elements $TiO_2$, $Fe_2O_3$ and MgO and compatible trace elements Cr, Ni, Sc, and V in (Fig. 25 a, b). The sediments that formed these graywackes cannot be simple mixtures of basaltic and felsic volcanogenic material because no appropriate felsic end member exists. There are also a few metagraywackes that plot into the intrusive and felsic volcanic compositional field at levels of $SiO_2$ above 65 weight %. These metagraywackes, with MgO < 2 weight %, are indistinguishable from the intrusive and felsic volcanics. This strongly suggests these graywackes contain a large proportion of felsic volcanic material (?locally derived), or were even formed of felsic volcanogenic epiclastic material.

## Rare earth elements of metasediments

Of the total 54 metagraywacke samples analyzed for REE, 48 of these can be divided into groups with similar REE characteristics according to >3, between 2 and 3, and less than 2 weight % MgO. In Fig. 26, only the high and low MgO groups have been plotted for clarity but the samples intermediate in MgO content have intermediate REE characteristics. The higher MgO group has 35-77 times chondrites La, 7.8 - 11 times chondrites Yb, concave-up profiles and, on average, small negative Eu anomalies. Three outliers have relatively flat REE profiles (Fig. 26), basaltic sample HJO-86-118 (13 wt. % MgO) and two others HJO-86-115 and HJO-86-109 (4.5 and 3.8 wt. % MgO, respectively). These three samples clearly have a large component of basaltic material. The lower MgO group (< 2 weight % MgO) was

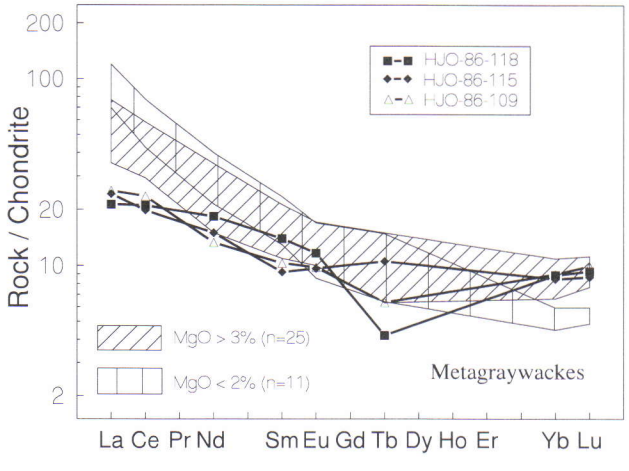


Fig. 26. Chondrite-normalized rare earth element (REE) diagrams for Hattu Schist Belt metagraywackes. Three metagraywackes have relatively flat-REE profiles and one sample is enriched in both LREE and HREE. The REE fields for the higher MgO and lower MgO metagraywacke groups pivot about the MREE. The intermediate MgO metagraywacke group (not shown) have intermediate REE profiles.

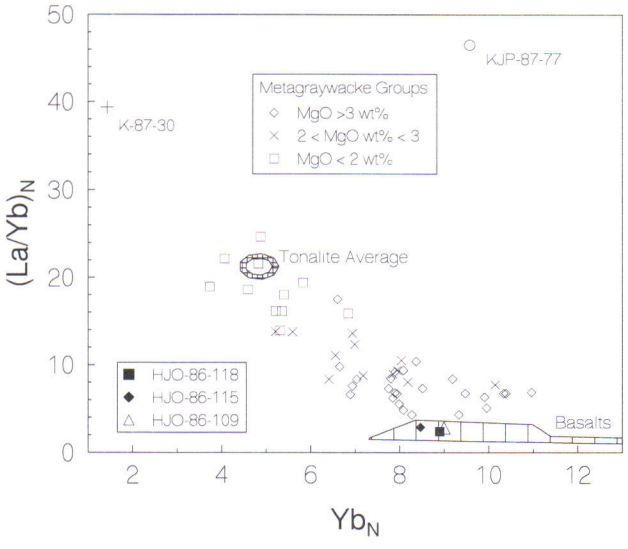


Fig. 27. La/Yb - Yb (chondrite normalized) for Hattu schist belt metagraywackes. All three metagraywacke groups are plotted in this diagram. Also plotted is the Kuittila tonalite average and the field for the Hattu schist belt basalts. Several samples with unique La/Yb or Yb (chondrite normalized) compositions are labeled and discussed in the text.

described above as containing a major felsic volcanic component and shows REE profiles very similar to the felsic volcanics and tonalites. These metagraywackes have 70 - 120 times chondrites La, 4.6 - 5.8 times chondrites Yb, less concave profiles than the higher MgO group and, on average, more pronounced negative Eu anomalies. Sample HJO-86-106 is one exception to the pattern in that it has elevated LREE and HREE.

A plot of $La/Yb_N$ - $Yb_N$ (Fig. 27) better displays the differences among the metagraywacke groups. The high and low MgO types are nearly completely separated on this diagram, whereas the intermediate group overlaps the end members considerably. The overall trend is one of increasing $(La/Yb)_N$ with decreasing $Yb_N$, a result of concomitant LREE enrichment and Yb depletion as indicated by the fields pivoting about the MREE in Fig. 26. The metagraywacke samples with < 2 weight % MgO have $La/Yb_N$ and $Yb_N$ values that cluster around the Hattu schist belt tonalite average (Fig. 27). The higher MgO metagraywackes have $Yb_N$ values similar to the Hattu schist belt basalts, with a tail extending off the main correlation trend to high $Yb_N$ (Fig. 27). The three samples with relatively flat REE profiles plot within the basalt field whereas the remainder have $(La/Yb)_N$ values two to five times those of the basalts. Dilution of basaltic detritus with LREE-enriched, low Yb material could explain the shift in $(La/Yb)_N$ of the higher MgO metagraywackes away from the basalt field even though they show a range in Yb concentrations essentially the same as that of the basalts.

The two samples with unique $(La/Yb)_N$ or $Yb_N$ values (Fig. 27) were also distinctive distinguished by their unusually high $K_2O + Na_2O$ in Fig. 19. Sample K-87-30 has a very similar REE profile to the granodiorites whereas sample KJP-87-77, which contains abundant garnet, shows extreme REE enrichment. None of the trace elements indicative of hydrothermal alteration are abnormally high in these two samples yet it is still likely they represent sediments affected by some type of alteration effect.

## Incompatible trace elements of metasediments

For the most part, incompatible trace elements of the metasediments can not be distinguished from those of the intermediate and felsic volcanics. In Fig. 28, using average values, the metagraywacke group with > 3 weight % MgO closely mimics the profile of the intermediate volcanics (open symbols plotting together) and likewise for the metagraywackes with < 2 weight MgO and the felsic volcanics (filled

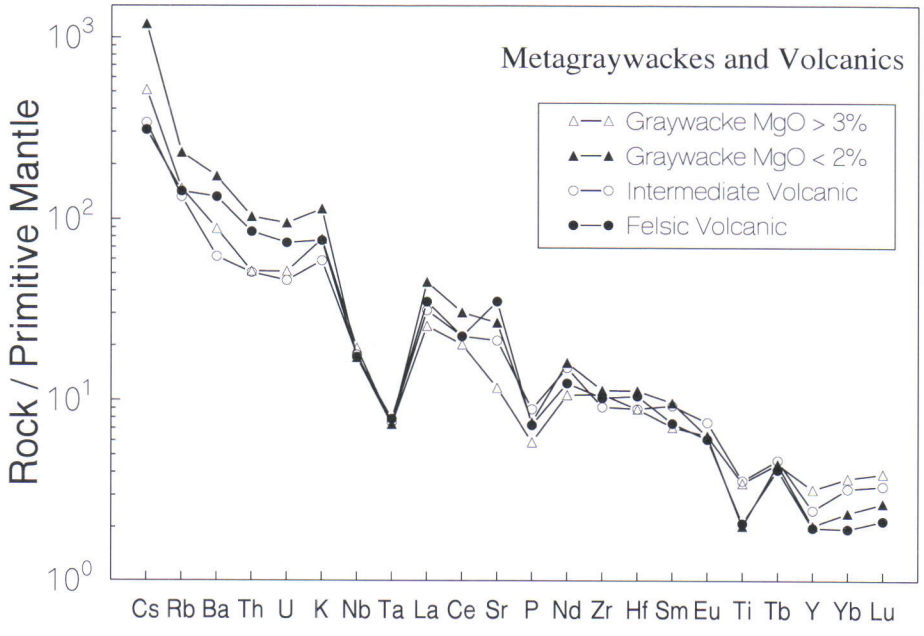


Fig. 28. Primitive mantle-normalized incompatible element diagrams for Hattu schist belt metagraywacke (triangles) and volcanic (circles) averages. The higher MgO metagraywacke average has a very similar profile to the intermediate volcanic average (open symbols plot together) and likewise for the low MgO metagraywacke and felsic volcanic averages. Primitive mantle values are from McDonough et al., 1985.

symbols plotting together). However, this is not true for all elements including, most notably, strontium. This is due to the fact that several intermediate and felsic volcanics have particularly high Sr contents, then when averaged, produce a Sr spike in the profiles.

Although not plotted in Fig. 28 for the sake of clarity, the metagraywackes with between 2 and 3 weight % MgO and $SiO_2$ > 65 weight % plot between the two metagraywacke end members and therefore have no incompatible trace element characteristics that could distinguish them from the intermediate to felsic volcanics. This is in contrast to our earlier observation that there are no volcanic equivalents to the these metagraywackes in terms of $TiO_2$, $Fe_2O_3$, MgO, Cr, Ni, Sc, and V contents. Additionally, we have suggested there is a significant basaltic component in the sediments that formed the metagraywackes with > 3 weight % MgO even though they have incompatible trace element concentrations significantly higher than those of the basalts (Fig. 12a). Several possible solutions to this problem are discussed below.

## Nd isotopes of Metasediments

The metasediments from within the Hattu schist belt have $\varepsilon_{Nd}(2750)$ from -0.6 to +1.2, not a very large range, but slightly lower than the range for the intrusives. These metasediments give model ages ($T_{DM}$) between 2986 to 2826 Ma. The younger model age comes from sample A221 (Table 3) from which zircon separates provide a U-Pb upper intercept age of 2761 ± 11 Ma. All of these data imply that the sediments that formed the metagraywackes and mica schists had a relatively newly formed crust as their major provenance. The igneous rocks of the Hattu schist belt seem the most likely source of these sediments.

## Sediment provenance

The major question to be answered about the metagraywackes is whether they are compositionally similar to the Hattu schist belt volcanic and intrusive rocks and therefore likely represent epiclastic material internally derived, or whether they represent mixtures with some detrital material from outside the belt. The enrichment of $TiO_2$, $Fe_2O_{3,tot}$ and MgO and compatible trace elements Cr, Ni, Sc, and V in the Hattu schist belt metagraywackes relative to the coexisting intrusive and extrusive igneous rocks, especially at levels of $SiO_2$ > 65 weight %, point to a compositional separation that is somewhat difficult to explain. Relatively high concentrations of these elements in Archean sediments is typical (Taylor and McClennan, 1985). Elevated Cr, Ni and MgO could represent a significant komatiite component as suggested for the South African metasediments (Wronkiewicz and Condie, 1987; 1989). However, as we have pointed out, the $TiO_2$, $Fe_2O_3$, V and Sc correlations with $SiO_2$ (Fig. 20) do not point toward a komatiite end member for the bulk of the Hattu schist belt metagraywackes. Rather, concentrations of these elements are consistent with basalts as one end-member the metagraywackes.

Although the mafic end-member can be explained by existing rocks, the felsic end-member is missing. It is possible that the bulk of the felsic volcanic material from the belt was not preserved, but rather eroded into the sedimentary column. Nevertheless, it is unlikely that such felsic igneous rocks formed by evolution along a normal calc-alkaline liquid-line-of-descent could have contained such high concentrations of transition metals. The Nd data presented above do not require any significant sedimentary detritus from outside the Hattu schist belt.

Instead of a missing felsic component, there is the possibly that some physical or chemical weathering process enhances the transition elements in the metagraywackes. Intense chemical weathering of ultramafic rocks that preferentially enhance Cr and Ni contents in Archean sediments has been suggested by Wronkiewicz and Condie (1989) and Wiggering and Beukes (1990). By this process, very small amounts of weathering products from komatiites could affect the sediment transition elements greatly, while having little dilutional effect on such elements as $SiO_2$. However, the low $TiO_2$, Sc and V contents of the ultramafic rocks we have analyzed cannot explain the high concentrations of these elements in the most of the Hattu schist belt metasedimentary rocks. One other possible solution is that during weathering of felsic volcanic rocks, magnetite and possibly other heavy minerals were preferentially removed to the sedimentary pile. This problem remains unsolved.

## SUMMARY AND CONCLUSIONS

The Late Archean Hattu schist belt is approximately 2750 Ma old based on zircon U-Pb analyses. Supracrustal rocks from the belt are dominated by sediments, with lesser amounts of komatiites, basalts and calc-alkaline rocks. Granitoids intruded into the belt are typical Archean tonalite-trondhjemite-granodiorite series rocks. Metamorphic conditions following accretion of the schist belt reached upper greenschist, lower amphibolite conditions. Our best maximum temperature estimate is 550 ± 50 °C based on garnet - biotite Fe/Mg geothermometry. This is higher than metamorphic grades from many other greenstone belts in Canada, South Africa and Western Australia, but similar to metamorphic grades in the Kuhmo greenstone belt 150 to 300 km to the north of this study area (Jahn et al, 1980; Piirainen, 1988).

The Hattu schist belt volcanics can be divided into komatiites, tholeiites, low-Ti tholeiites that show some characteristics of calc-alkaline basalts, and andesites/dacites. We have outlined a consistent crystal fractionation model for the basalts, in which the tholeiites were dominated by olivine + chromite ± clinopyroxene ± plagioclase removal and the low-Ti tholeiites by clinopyroxene + olivine + magnetite removal. Several members of the low-Ti tholeiite group have compositions that could represent parental magmas to the andesites and dacites whereas the tholeiite fractionation trend projects away from the more evolved volcanics. Trace elements of the komatiites have been modified, probably as a consequence of hydrothermal alterations and/or metamorphism. The REE profiles of the Hattu schist belt basalts are mostly typical of Archean basalts, although several samples show considerable LREE-enrichment. Discriminant diagrams suggest that the basalts are either island arc- or continental arc-derived. The andesites and dacites have negative Ta, Nb and Ti anomalies characteristic of arc magmas.

The TTG series granitoids internal to the Hattu schist belt show a relatively small range in composition, but the three main tonalite plutons can be distinguished from each other by compatible trace elements with MgO as an index of fractionation. Feldspar porphyry dikes, found throughout the belt, can only be distinguished chemically from the plutonic rocks by the absence of a negative Eu anomaly. This may be the result of plagioclase accumulation in the plutons subsequent to intrusion and suggests the dike-rocks may be close to initial tonalite magma compositions.

Metagraywackes in the Hattu schist belt are mostly andesitic to dacitic in composition although some basaltic andesite compositions apparently reflect a large amount of locally derived basaltic detritus or tuffaceous material. The metagraywackes with < 65 weight % $SiO_2$ overlap in composition with the volcanics whereas a large group of samples with greater than 65 weight % $SiO_2$ have no intrusive or volcanic equivalents in terms of $TiO_2$, $Fe_2O_3$, MgO or Cr, Ni, V, Sc. In contrast, none of the metagraywackes have incompatible trace elements (including REE profiles) distinct from the volcanics and intrusives. Rather than invoking a missing felsic component rich in compatible elements, we suggest some sedimentary process enriched these elements in the sedimentary sequence, which we suspect was mostly locally derived.

Sr isotopes on the Kuittila tonalite give a poorly constrained isochron of 2789 ± 290 Ma with a $Sr_i$ = 0.70146 ± 0.0009. Nd isotopes of the intrusives give $\varepsilon_{Nd}$(2750 Ma) of 0.9 to 2.1 and $T_{DM}$ model ages ca. 2800 Ma. Nd data from the volcanics are sparse and give conflicting results in some cases. The metagraywacke $\varepsilon_{Nd}$(2750 Ma) values are slightly more negative than the intrusives and volcanics (-0.6 to +1.2). However, none of these isotopic data (except possibly the Poikopää basalt) suggest a significant older crustal component in the source of the Hattu schist belt magmas or metagraywackes.

## ACKNOWLEDGMENTS

We would like to thank T. Bornhorst for reviewing this paper.

## REFERENCES

**Apted M.J. & Liou J.G., 1983.** Phase relations among greenschist, epidote-amphibolite, and amphibolite in a basaltic system. American Journal of Science 283-A. 328-354.

**Boynton W.V., 1984.** Cosmochemistry of the rare earth element: Meteorite studies. In P. Henderson (Editor), Rare Earth Element Geochemistry, p. 63-114. Elsevier, Amsterdam.

**Bornhorst, T.J.& Rasilainen K., 1993.** Mass transfer during hydrothermal alteration associated with Au mineralization within the late Archean Hattu schist belt, Ilomantsi, eastern Finland. In P.A. Nurmi & P. Sorjonen-Ward (Editors), Geological development, gold mineralization and exploration methods in the late Archean Hattu schist belt, Ilomantsi, eastern Finland. Geol. Surv. Finland, Spec. Paper 17, 273-289.

**Bornhorst, T.J., Rasilainen K. & Nurmi, P.A., 1993.** Geochemical character of lithologic units in the late Archean Hattu schist belt, Ilomantsi, eastern Finland. In P.A. Nurmi & P. Sorjonen-Ward (Editors), Geological development, gold mineralization and exploration methods in the late Archean Hattu schist belt, Ilomantsi, eastern Finland. Geol. Surv. Finland, Spec. Paper 17, 133-145.

**Condie, K.C., 1990.** Geochemical characteristics of Precambrian basaltic greenstones. In R.P. Hall & D.J. Hughes (Editors), Early Precambrian Basic Magmatism, p. 40-55. Blackie & Son Ltd., Glasgow.

**Condie, K.C., 1992.** Evolutionary changes at the Archean-Proterozoic boundary. In J.E. Glover and S.E. Ho (Editors), Archean Gold Deposits, Univ. of W. Australia Pub. 22, 177-189.

**Defant, M.J. & Drummond, M.S., 1990.** Derivation of some modern arc magmas by melting of young subducted lithosphere. Nature 347, 662-665.

**Ferry & Spear, 1978.** Experimental calibration of the partitioning of Fe and Mg between biotite and garnet. Contr. Min. Petr. 66, 113-117.

**Hodges & Spear, 1982.** Geothermometry, beobarometry and the $Al_2SiO_5$ triple point at Mt. Moosilauke, New hampshire. Am. Min. 67, 1118-1134.

**Huhma, H., 1986.** Sm-Nd, U-Pb and Pb-Pb isotopic evidence for the origin of the Early Proterozoic Svecokarelian crust in Finland. Geol. Surv. Finland, Bull. 337, 48pp.

**Irvine, T.N. & Barager, W.R.A., 1971.** A guide to the chemical classification of the common volcanic rocks, Can. J. Earth Sci. 8, 523-548.

**Jahn, B., Auvray, B., Blais, S. Capdevila, R. Cornichet, J. Vidal, F. & Hameurt, J., 1980.** Trace element geochemistry and petrogenesis of Finnish greenstone belts. J. Petrol. 21, 201-244.

**Jensen, L.S., 1976.** A new cation plot for classifying subalkalic volcanic rocks, Ont. Dept. Mines Misc. Pap. 66, 22p.

**Kontinen, A., Paavola, J. & Lukkarinen, H., 1992.** K-Ar ages of hornblende and biotite from Late Archaean rocks of eastern Finland - interpretation and discussion of tectonic implications. Geol. Surv. Finland, Bull. 365, 31pp.

**Le Bas, M.J., Le Maitre, R.W., Streckeisen, A. & Zanetin, A., 1986.** A chemical classification of volcanic rocks based on the total alkali-silica diagram. J. Petrol. 27, 745-750.

**LeMaitre, R.W., (ed.), 1989.** A Classification of Igneous Rocks and Glossary of Terms, Blackwell, Oxford, 193 p.

**Ludwig, K.R., 1988.** ISOPLOT - A plotting and regression program for radiogenic-isotope data, for IBM-PC compatible computers, ver 2.12. U. S. Geol. Surv. Open-File Rep. 88-557, 32p.

**Martin, H., 1986.** Effect of a steeper Archean geothermal gradient on geochemistry of subduction-zone magmas. Geology 14, 753-756.

**McDonough, W. F., McCulloch, M. T. & Sun, S. S., 1985.** Isotopic and geochemical systematics in Tertiary-Recent basalts from southeastern Australia and implications for the evolution of the subcontinental lithosphere. Geochim. Cosmochim. Acta 49, 2051-2067.

**Miyashiro, A., 1974.** Volcanic rock series in island arcs and active continental margins. Am. J. Sci. 274, 321-355.

**Mullen, E.D., 1983.** $MnO/TiO_2/P_2O_5$: a minor element discriminant for basaltic rocks of oceanic environments and its implications for petrogenesis. Earth Planet. Sci. Lett. 62, 53-62.

**Nurmi, P.A., Hartikainen, A., Damsten, M. & Rasilainen, K., 1988.** Geochemical exploration for Archean gold deposits in the Ilomantsi greenstone belt, eastern Finland. Bicentennial Gold '88, Extended Abstracts, Poster Program 1, Geological Society of Australia Inc. Abstracts 23, 559-561.

**O'Brien, H.E., Nurmi, P. A & Karhu, J.A., 1993.** Oyxgen, hydrogen and strontium isotopic compositions of gold mineralization in the late Archean Hattu schist belt, Ilomantsi, eastern Finland. In P.A. Nurmi & P. Sorjonen-Ward (Editors), Geological development, gold mineralization and exploration methods in the late Archean Hattu schist belt, Ilomantsi, eastern Finland. Geol. Surv. Finland, Spec. Paper 17, 291-306.

**O'Connor, J.T., 1965.** A classification for quartz-rich igneous rocks based on feldspar ratio. U. S. Geol. Surv. Prof. Pap. 525B, 79-84.

**Pearce J.A., Harris, N.B.W. & Tindle, A.G.,** 1984. Trace element discrimination diagrams for the tectonic interpretation of granitic rocks. J. Petrol. 25, 956-983.

**Perchuk & Lavrenteva, 1983.** Adv. in Phys. Geochem. 3, 199-239.

**Perfit, M.R., Gust, D.A., Bence, A.E., Arculus, R.J. & Taylor, S.R., 1981.** Chemical characteristics of island-arc basalts: implications for their mantle sources. Chem. Geol. 30, 227-256.

**Piirainen, T., 1988.** The geology of the Archean greenstone-granitoid terrain in Kuhmo, eastern Finland. Geol. Surv. Finland. Spec. Pap. 4, 39-51.

**Richard, P., Shimizu, N. & Allégre, C.J., 1976.** $^{143}Nd/^{146}Nd$, A natural trace: An application to oceanic basalts. Earth. Planet. Sci. Lett. 31, 209-278.

**Salminen, R. & Hartikainen, A., 1986.** Tracing of gold, molybdenum and tungsten mineralization by use of a step by step geochemical till study in Ilomantsi, eastern Finland. In Prospecting in Areas of Glaciated Terrain 1986. Inst. Min. Metall., London, 210-209.

**Sorjonen-Ward, P. 1993.** An overview of structural evolution and lithic units within and intruding the late Archean Hattu schist belt, Ilomantsi, eastern Finland. In P.A. Nurmi & P. Sorjonen-Ward (Editors), Geological development, gold mineralization and exploration methods in the late Archean Hattu schist belt, Ilomantsi, eastern Finland. Geol. Surv. Finland, Spec. Paper 17, 9-102.

**Sorjonen-Ward, P.G. and Claoué-Long, J., 1993.** A preliminary note on ion probe results for zircons from the Silvevaara granodiorite, Ilomantsi, Eastern Finland. Current Research 1992. Geol. Surv. Finland, Spec. Paper 18, 25-29.

**Sun, S.S. & Nesbitt, R.W., 1977.** Chemical heterogeneity of the Archean mantle, composition of the bulk earth and mantle evolution. Earth Planet. Sci. Letters 35,429-448.

**Taipale, K., 1988.** Volcanism in the Archean Kuhmo greenstone belt, eastern Finland. Geol. Surv. Finland. Spec. Pap. 4, 151-160.

**Taylor, S.R. & McLennan, S.M., 1985.** The Continental Crust: Its Composition and Evolution. Blackwell, Oxford, 312p.

**Vaasjoki, M., Sorjonen-Ward, P. & Lavikainen, S., 1993.** U-Pb age determinations and sulfide Pb-Pb characteristics from the late Archean Hattu schist belt, Ilomantsi, eastern Finland. In P.A. Nurmi & P. Sorjonen-Ward (Editors), Geological development, gold mineralization and exploration methods in the late Archean Hattu schist belt, Ilomantsi, eastern Finland. Geol. Surv. Finland, Spec. Paper 17, 103-131.

**Wetherill, G.W., Kouvo, O., Tilton, G.R. & Gast, P.W., 1962.** Age measurements on rocks from the Finnish Precambrian. J. Geol. 70, 73-88.

**Wiggering, H. & Beukes, N.J., 1990.** Petrography and geochemistry of a 2000-2200-Ma-old hematitic paleo-alteration profile on Ongeluk basalt of the Transvaal Supergroup, Griqualand West, South Africa. Precam. Res. 46, 241-258.

**Will, T.M., Powell, R., Holland, T. and Guiraud, M., 1990.** Calculated greenschist facies mineral equilibria in the system CaO-Feo-Mgo-Al203-SiO2-CO2-H2O. Contrib. Mineral. Petrol. 104, 353-368.

**Wood, D.A., 1979.** A variably veined suboceanic mantle - genetic significance for mid-ocean ridge basalts from geochemical evidence. Geology 7, 499-503.

**Wronkiewicz, D.J. & Condie, K.C., 1987.** Geochemistry of Archean shales from the Witwatersrand Supergroup, South Africa: source-area weathering, provenance and tectonic setting. Geochim. Cosmochim. Acta 51, 2401-2416.

**Wronkiewicz, D.J. & Condie, K.C., 1989.** Geochemistry of sediments from the Pongola Supergroup, South Africa: evidence for a 3 Ga continental craton. Geochim. Cosmochim. Acta 53, 1537-1549.

**York, D., 1969.** Least squares fitting of a straight line with correlated errors. Earth Planet. Sci. Letters 5, 320-324.

Volcanics

| Sample | HJO-86-30 | HJO-86-32 | KJP-87-80.2 | KJP-87-80.1 | KJP-87-14.2 | KJP-87-16 | HJO-87-79.1 | HJO-87-79.2 | KJP-87-99 | HJO-87-90 | KJP-87-38 | HJO-86-117 | HJO-86-116 | PAN-86-11 | PAN-86-6 | KJP-87-97 | PAN-86-5 | KJP-87-13.2 | PAN-86-17 | KJP-87-13.1 |
|---|---|---|---|---|---|---|---|---|---|---|---|---|---|---|---|---|---|---|---|---|
| | V1 | V2 | V3 | V4 | V5 | V6 | V7 | V8 | V9 | V10 | V11 | V12 | V13 | V14 | V15 | V16 | V17 | V18 | V19 | V20 |
| Rocktype | UM | UM | UM | UM | UM | UM | UM | MAF | MAF | MAF | MAF | MAF | MAF | MAF | MAF | MAF | MAF | MAF | MAF | MAF |
| SiO2 | 40.0 | 41.8 | 39.0 | 42.4 | 41.4 | 49.6 | 50.1 | 55.1 | 48.9 | 50.0 | 50.8 | 49.6 | 48.9 | 51.7 | 49.4 | 48.8 | 48.0 | 52.9 | 51.9 | 52.4 |
| TiO2 | 0.26 | 0.32 | 0.17 | 0.45 | 0.64 | 0.51 | 0.53 | 0.73 | 0.43 | 0.67 | 0.79 | 0.94 | 0.86 | 0.84 | 1.12 | 0.89 | 1.13 | 1.11 | 1 | 0.77 |
| Al2O3 | 3.78 | 3.87 | 4.03 | 7.23 | 10.4 | 5.32 | 9.33 | 12.7 | 7.18 | 13.5 | 13.7 | 14.3 | 14.6 | 14.6 | 14.1 | 15.6 | 14.6 | 14.1 | 14 | 13.3 |
| Fe2O3 | 9.56 | 10.2 | 9.65 | 9.4 | 10.7 | 12.7 | 12.1 | 8.87 | 17.9 | 11.3 | 9.92 | 12.9 | 12.7 | 9.05 | 13.8 | 14 | 14.7 | 10.4 | 12.3 | 8.12 |
| MnO | 0.12 | 0.1 | 0.16 | 0.18 | 0.2 | 0.26 | 0.22 | 0.18 | 0.43 | 0.19 | 0.15 | 0.2 | 0.2 | 0.18 | 0.2 | 0.21 | 0.24 | 0.18 | 0.16 | 0.19 |
| MgO | 32.0 | 31.8 | 32.0 | 25.3 | 21.7 | 19.6 | 13.3 | 9.67 | 11.5 | 9.96 | 9.71 | 8.81 | 8.76 | 7.75 | 7.75 | 7.38 | 7.28 | 7.18 | 7.01 | 6.55 |
| CaO | 1.77 | 1.07 | 2.36 | 6.57 | 7.78 | 8.57 | 7.82 | 5.63 | 10.3 | 10.9 | 10.9 | 9.44 | 9.32 | 11.9 | 9.89 | 9.3 | 9.99 | 9.87 | 10.2 | 12.5 |
| Na2O | 0.07 | 0.01 | 0.02 | 0.14 | 0.16 | 0.21 | 2.48 | 5.16 | 1.20 | 1.97 | 2.42 | 2.08 | 2.52 | 1.97 | 2.05 | 2.78 | 2.15 | 3.51 | 2.21 | 3.59 |
| K2O | 0.02 | 0.04 | 0.00 | 0.03 | 0.01 | 0.01 | 0.44 | 0.31 | 0.24 | 0.12 | 0.49 | 0.18 | 0.24 | 0.59 | 0.34 | 0.29 | 0.43 | 0.21 | 0.32 | 0.15 |
| P2O5 | 0.15 | 0.12 | 0.08 | 0.20 | 0.21 | 0.07 | 0.16 | 0.14 | 0.15 | 0.06 | 0.07 | 0.08 | 0.08 | 0.08 | 0.15 | 0.08 | 0.15 | 0.10 | 0.09 | 0.07 |
| LOI | 10.8 | 9.9 | 10.8 | 6.9 | 6.5 | 3.0 | 2.5 | 1.9 | 1.5 | 1.1 | 0.9 | 1.4 | 1.5 | 1.1 | 0.9 | 1.1 | 0.9 | 0.5 | 0.9 | 2.7 |
| Total | 98.53 | 99.18 | 98.27 | 98.75 | 99.67 | 99.85 | 99.02 | 100.34 | 99.70 | 99.75 | 99.80 | 99.92 | 99.72 | 99.74 | 99.73 | 100.41 | 99.52 | 100.03 | 100.12 | 100.34 |
| CO2 | 2.36 | 0.52 | 1.15 | 0.02 | 1.03 | 0.04 | 0.01 | 0.01 | 0.01 | 0.55 | 0.01 | 0.02 | 0.14 | 0.01 | 0.01 | 0.01 | 0.01 | 0.01 | 0.01 | 2.84 |
| B (ppm) | 5 | 5 | 20 | 20 | 5 | 5 | 10 | 10 | 450 | 10 | 20 | 5 | 5 | 10 | 5 | 20 | 180 | 10 | 5 | 20 |
| Ba | 20 | 110 | 14 | 12 | 43 | 19 | 176 | 166 | 139 | 29 | 80 | 70 | 50 | 110 | 150 | 44 | 140 | 81 | 80 | 40 |
| Ce | 11 | 7 | 2.8 | 17.8 | 25.1 | 23.5 | 13.5 | 17.9 | 14.8 | 7.2 | 8.1 | 10 | 10 | 14 | 20 | 6 | 17 | 10.9 | 9 | 8.5 |
| Co | 88 | 82 | 73 | 43 | 65 | 64 | 37 | 34 | 53 | 44 | 36 | 51 | 49 | 49 | 47 | 38 | 50 | 33 | 45 | 35 |
| Cr | 3740 | 3600 | 3740 | 2200 | 2450 | 1350 | 1460 | 877 | 2270 | 640 | 584 | 200 | 330 | 540 | 320 | 240 | 360 | 56 | 160 | 500 |
| Cs | 1.9 | 2.5 | 0.5 | 0.5 | 0.5 | 0.5 | 2 | 1 | 1 | 0.5 | 1 | 0.1 | 0.1 | 0.5 | 1.3 | 1 | 5.5 | 0.5 | 0.1 | 0.5 |
| Cu | 58 | 0.25 | 11 | 9 | 0.25 | 52 | 1 | 2 | 16 | 55 | 87 | 97 | 98 | 57 | 33 | 36 | 0.25 | 250 | 130 | 40 |
| Dy | . | . | 0.5 | 1.9 | 1.6 | 1.5 | 2.5 | 3 | 2.3 | 2.8 | 3 | . | . | . | . | 3.2 | . | 4 | . | 3 |
| Er | . | . | 0.4 | 1 | 1 | 0.9 | 1.6 | 2 | 1.4 | 1.8 | 1.9 | . | . | . | . | 2.1 | . | 2.3 | . | 1.8 |
| Eu | 0.35 | 0.32 | 0.23 | 0.7 | 0.55 | 0.79 | 1.14 | 1.03 | 0.75 | 0.65 | 0.81 | 0.7 | 0.7 | 0.76 | 0.88 | 0.72 | 0.95 | 1.06 | 0.75 | 0.68 |
| Gd | . | . | 0.3 | 1.7 | 1.6 | 1.9 | 2.7 | 2.8 | 2 | 2.7 | 2.2 | . | . | . | . | 2.2 | . | 3.1 | . | 2.5 |
| Hf | 0.5 | 0.4 | 0.5 | 0.5 | 2 | 2 | 2 | 2 | 2 | 0.5 | 0.5 | 1.7 | 1.8 | 1.6 | 2 | 0.5 | 2.1 | 0.5 | 2.3 | 0.5 |
| Ho | . | . | 0.09 | 0.34 | 0.32 | 0.28 | 0.51 | 0.66 | 0.48 | 0.63 | 0.67 | . | . | . | . | 0.73 | . | 0.9 | . | 0.63 |
| La | 3.4 | 1.8 | 1.3 | 8.2 | 13.4 | 11.2 | 6.2 | 8.7 | 6.8 | 2.9 | 3.3 | 3.3 | 3.4 | 4.6 | 8.8 | 2.3 | 6.9 | 4.2 | 3.3 | 3.7 |
| Li | 6 | 7 | 0.5 | 0.5 | 35 | 14 | 16 | 8 | 0.5 | 0.5 | 14 | 22 | 26 | 22 | 20 | 6 | 18 | 12 | 24 | 0.5 |
| Lu | 0.07 | 0.08 | 0.025 | 0.025 | 0.19 | 0.24 | 0.42 | 0.39 | 0.41 | 0.14 | 0.21 | 0.41 | 0.38 | 0.35 | 0.21 | 0.25 | 0.34 | 0.23 | 0.41 | 0.15 |
| Nb | 20 | 10 | 0.5 | 1 | 2 | 4 | 2 | 2 | 2 | 2 | 2 | 10 | 20 | 10 | 20 | 2 | 20 | 3 | 10 | 2 |
| Nd | 4 | 1.5 | 2.2 | 10.5 | 11.8 | 12.2 | 9.1 | 11.5 | 8.1 | 5.8 | 6.8 | 6 | 6 | 7 | 13 | 5.6 | 9 | 9.4 | 8 | 6.5 |
| Ni | 1300 | 1200 | 810 | 790 | 1400 | 1100 | 600 | 350 | 960 | 170 | 210 | 130 | 130 | 180 | 200 | 140 | 220 | 85 | 89 | 180 |
| Pb | 1 | 6 | 1 | 1 | 1 | 1 | 1 | 1 | 1 | 1 | 1 | 12 | 1 | 1 | 1 | 1 | 1 | 1 | 1 | 1 |
| Pr | . | . | 0.5 | 2.4 | 3.2 | 3.2 | 2.2 | 2.8 | 2.1 | 1.2 | 1.4 | . | . | . | . | 1.1 | . | 1.8 | . | 1.4 |
| Rb | 10 | 5 | 20 | 15 | 25 | 27 | 41 | 33 | 31 | 32 | 40 | 20 | 20 | 20 | 10 | 41 | 30 | 35 | 20 | 24 |
| S% | 0.13 | 0.005 | 0.025 | 0.025 | 0.025 | 0.025 | 0.025 | 0.025 | 0.025 | 0.025 | 0.025 | 0.005 | 0.005 | 0.14 | 0.005 | 0.025 | 0.005 | 0.16 | 0.05 | 0.025 |
| Sc | 21.4 | 18.8 | 16 | 20 | 20 | 17 | 22 | 27 | 24 | 37 | 37 | 54.4 | 58.1 | 52.8 | 32.3 | 38 | 34.5 | 40 | 55.1 | 38 |
| Sm | 0.85 | 0.69 | 0.6 | 2.2 | 2.2 | 2.4 | 2.3 | 2.8 | 1.9 | 1.7 | 2 | 2.13 | 2.05 | 2.29 | 3.66 | 1.7 | 2.88 | 2.7 | 2.22 | 1.9 |
| Sr | 130 | 70 | 44 | 107 | 27 | 45 | 157 | 396 | 67 | 103 | 160 | 90 | 200 | 240 | 340 | 293 | 310 | 229 | 110 | 346 |
| Ta | 0.25 | 0.25 | 0.5 | 0.5 | 0.5 | 0.5 | 0.5 | 0.5 | 0.5 | 0.5 | 0.5 | 0.25 | 0.25 | 0.25 | 0.25 | 0.5 | 0.25 | 0.5 | 0.25 | 0.5 |
| Tb | 0.1 | 0.1 | 0.05 | 0.2 | 0.2 | 0.2 | 0.4 | 0.4 | 0.4 | 0.4 | 0.4 | 0.6 | 0.5 | 0.4 | 0.6 | 0.4 | 0.7 | 0.5 | 0.4 | 0.4 |
| Th | 0.2 | 0.1 | 0.25 | 1 | 1.4 | 1.8 | 1.6 | 1.4 | 1.3 | 0.25 | 0.25 | 0.3 | 0.5 | 0.3 | 2.5 | 0.25 | 2.5 | 0.25 | 0.4 | 0.25 |
| U | 0.3 | 0.2 | 0.05 | 0.1 | 0.4 | 0.5 | 0.4 | 0.4 | 0.5 | 0.05 | 0.05 | 0.05 | 0.05 | 0.2 | 0.05 | 0.05 | 0.6 | 0.1 | 0.2 | 0.05 |
| V | 98 | 100 | 88 | 120 | 130 | 120 | 170 | 200 | 130 | 240 | 250 | 330 | 340 | 270 | 230 | 280 | 240 | 330 | 340 | 270 |
| Y | 5 | 5 | 2 | 9 | 8 | 7 | 14 | 16 | 13 | 16 | 17 | 30 | 20 | 20 | 20 | 19 | 10 | 22 | 20 | 17 |
| Yb | 0.39 | 0.49 | 0.1 | 0.8 | 0.7 | 0.3 | 1.3 | 1.7 | 1.2 | 1.6 | 1.7 | 2.67 | 2.41 | 2.26 | 1.85 | 1.9 | 2.08 | 2 | 2.35 | 1.5 |
| Zn | 97 | 71 | 77 | 81 | 170 | 140 | 110 | 86 | 98 | 83 | 81 | 120 | 110 | 91 | 140 | 120 | 160 | 78 | 130 | 66 |
| Zr | 5 | 5 | 1 | 13 | 39 | 5 | 52 | 57 | 44 | 6 | 10 | 40 | 30 | 30 | 60 | 6 | 60 | 15 | 30 | 3 |
| X | 6988.84 | 6988.46 | 6990.97 | 6990.97 | 6997.14 | 6997.54 | 6982.21 | 6982.21 | 6985.6 | 6986.3 | 6987.29 | 6983.54 | 6983.64 | 6987.2 | 6987.4 | 6985.14 | 6987.4 | 6997.13 | 6984.11 | 6997.13 |
| Y | 563.72 | 563.83 | 566.13 | 566.13 | 561.08 | 561.08 | 564.9 | 564.9 | 564.2 | 564.61 | 566.18 | 565.31 | 565.26 | 566.18 | 561.26 | 565.78 | 561.27 | 561.14 | 565.88 | 561.14 |

Appen. Cont.

Volcanics

| Sample | PAN-86-20 | PAN-86-23 | HJO-86-23 | HJO-86-21 | HJO-86-20 | HJO-86-22 | PAN-86-9 | PAN-86-3 | PAN-86-33 | P535/33. | KJP-87-12.1 | PAN-86-4 | HJO-87-122.2 | KJP-87-60 | P403/15 | HJO-86-107 | PAN-86-7 | HJO-86-28 | HJO-86-121 | PAN-86-2 |
|---|---|---|---|---|---|---|---|---|---|---|---|---|---|---|---|---|---|---|---|---|
| | V21 | V22 | V23 | | | | V24 | V25 | V26 | V27 | | V28 | V29 | | V30 | | | | | |
| Rocktype | MAF | MAF | MAF | MAF | MAF | MAF | ITUF | PLILA | ITUF | IAGL | IVULK | PLITUF | PLPF | IVULK | HLTUF | HAGL | PLHTUF | PLPF2 | HLTUF | HLTUF |
| SiO2 | 50.4 | 51.1 | 61.5 | 50.4 | 52.4 | 61.5 | 53.4 | 56.8 | 48.5 | 61.2 | 55.1 | 61.3 | 63.9 | 56.7 | 63.9 | 64.4 | 66.9 | 65.3 | 66.5 | 64.7 |
| TiO2 | 1.04 | 1.25 | 0.54 | 2 | 1.73 | 1.06 | 0.86 | 0.88 | 0.7 | 0.85 | 0.74 | 0.7 | 0.59 | 0.91 | 0.69 | 0.72 | 0.42 | 0.29 | 0.55 | 0.43 |
| Al2O3 | 13.8 | 13.9 | 15.7 | 12.4 | 12 | 11.2 | 14.8 | 14.7 | 15.2 | 16.8 | 17 | 15.9 | 17 | 16.2 | 14.5 | 15.7 | 16.6 | 16 | 15.9 | 16.9 |
| Fe2O3 | 14.6 | 16 | 5.68 | 20.5 | 21.9 | 15.9 | 9.34 | 7.21 | 10.1 | 8.37 | 9.12 | 6.74 | 4.93 | 9.36 | 7.44 | 7.93 | 3.33 | 3.21 | 5.12 | 4.25 |
| MnO | 0.22 | 0.21 | 0.08 | 0.26 | 0.28 | 0.2 | 0.18 | 0.13 | 0.22 | 0.09 | 0.12 | 0.11 | 0.08 | 0.13 | 0.08 | 0.08 | 0.04 | 0.05 | 0.07 | 0.06 |
| MgO | 6.53 | 5.85 | 4.77 | 3.75 | 2.37 | 1.07 | 6.85 | 5.61 | 4.78 | 4.02 | 3.55 | 3.55 | 2.48 | 1.74 | 3.34 | 2.80 | 2.15 | 1.85 | 1.82 | 1.61 |
| CaO | 9.11 | 6.85 | 3.12 | 5.81 | 6.4 | 4.19 | 8.41 | 7.41 | 16.1 | 1.28 | 4.98 | 5.51 | 4.01 | 4.52 | 2.9 | 1.22 | 3.44 | 2.14 | 3.05 | 3.99 |
| Na2O | 2.62 | 3.16 | 6.09 | 3.50 | 2.44 | 3.33 | 2.97 | 3.49 | 2.13 | 1.29 | 4.10 | 5.07 | 4.35 | 4.31 | 2.68 | 2.73 | 3.90 | 5.97 | 4.07 | 3.80 |
| K2O | 0.36 | 0.26 | 0.10 | 0.29 | 0.29 | 0.22 | 1.16 | 1.28 | 0.39 | 3.44 | 3.01 | 0.59 | 1.47 | 2.67 | 1.85 | 1.87 | 1.51 | 3.85 | 1.91 | 2.20 |
| P2O5 | 0.08 | 0.12 | 0.17 | 0.13 | 0.20 | 0.33 | 0.18 | 0.49 | 0.06 | 0.12 | 0.35 | 0.16 | 0.17 | 0.53 | 0.09 | 0.09 | 0.15 | 0.16 | 0.10 | 0.17 |
| LOI | 0.7 | 0.3 | 2.3 | 0.2 | 0.4 | 1.2 | 1.0 | 0.9 | 1.3 | 2.6 | 1.6 | 0.6 | 0.9 | 2.2 | 1.4 | 2.6 | 1.0 | 0.9 | 1.0 | 1.0 |
| Total | 99.46 | 99.01 | 100.06 | 99.20 | 100.40 | 100.16 | 99.15 | 98.85 | 99.49 | 100.08 | 99.69 | 100.25 | 99.83 | 99.23 | 98.86 | 100.16 | 99.44 | 99.75 | 100.09 | 99.11 |
| CO2 | 0.01 | 0.04 | 0.80 | 0.07 | 0.15 | 0.21 | 0.01 | 0.01 | 0.03 | 0.01 | 1.88 | 0.01 | 0.01 | 1.36 | 0.02 | 0.01 | 0.01 | 0.34 | 0.60 | 0.07 |
| B (ppm) | 5 | 5 | 5 | 50 | 40 | 230 | 5 | 5 | 5 | 110 | 10 | 10 | 5 | 50 | 5 | 80 | 360 | 5 | 30 | 60 |
| Ba | 80 | 90 | 70 | 70 | 100 | 90 | 320 | 450 | 50 | 470 | 978 | 280 | 516 | 1080 | 480 | 540 | 1160 | 2260 | 460 | 810 |
| Ce | 9 | 24 | 15 | 13 | 31 | 38 | 42 | 72 | 9 | 37 | 81 | 29 | . | 98.8 | 34 | 36 | 18 | 31 | 34 | 35 |
| Co | 49 | 61 | 15 | 55 | 38 | 13 | 35 | 26 | 48 | 33 | 18 | 27 | 8 | 22 | 29 | 49 | 10 | 8.3 | 20 | 12 |
| Cr | 95 | 10 | 180 | 7.8 | 0.25 | 6.7 | 280 | 410 | 400 | 320 | 98 | 160 | 83 | 130 | 210 | 230 | 53 | 78 | 120 | 45 |
| Cs | 3.8 | 1.4 | 1.3 | 1.5 | 0.1 | 0.1 | 4.8 | 6.8 | 2.3 | 12.7 | 18 | 2 | . | 14 | 6.3 | 5.8 | 5.8 | 5.1 | 9.5 | 2.4 |
| Cu | 29 | 260 | 0.25 | 3 | 34 | 0.25 | 12 | 6.5 | 36 | 42 | 66 | 17 | 11 | 95 | 59 | 70 | 6 | 6.5 | 38 | 17 |
| Dy | . | . | . | . | . | . | . | . | . | . | 3.7 | . | . | 4.3 | . | . | . | . | . | . |
| Er | . | . | . | . | . | . | . | . | . | . | 1.9 | . | . | 2 | . | . | . | . | . | . |
| Eu | 0.72 | 1.05 | 0.54 | 1.45 | 1.9 | 0.96 | 1.38 | 1.94 | 1 | 0.58 | 2.51 | 1.22 | . | 2.71 | 0.8 | 0.69 | 0.95 | 0.58 | 0.9 | 0.75 |
| Gd | . | . | . | . | . | . | . | . | . | . | 5.3 | . | . | 6.2 | . | . | . | . | . | . |
| Hf | 2.2 | 3 | 3.4 | 2.8 | 6.5 | 8.3 | 2.4 | 3.1 | 1.5 | 4 | 5 | 3 | . | 5 | 2.9 | 3.9 | 3.5 | 4 | 3.2 | 4.1 |
| Ho | . | . | . | . | . | . | . | . | . | . | 0.68 | . | . | 0.82 | . | . | . | . | . | . |
| La | 2.9 | 10.6 | 7.6 | 4.2 | 8.4 | 10.8 | 23.9 | 36.6 | 4 | 21 | 39.3 | 14.3 | . | 50.2 | 16.5 | 21 | 9.4 | 16.5 | 17.5 | 23.5 |
| Li | 16 | 16 | 16 | 18 | 16 | 18 | 30 | 28 | 6 | 58 | 100 | 18 | 48 | 12 | 62 | 50 | 26 | 16 | 56 | 30 |
| Lu | 0.49 | 0.39 | 0.18 | 0.65 | 1.12 | 1.57 | 0.24 | 0.22 | 0.31 | 0.33 | 0.2 | 0.17 | . | 0.15 | 0.23 | 0.31 | 0.14 | 0.13 | 0.22 | 0.13 |
| Nb | 10 | 10 | 10 | 30 | 30 | 30 | 10 | 10 | 10 | 10 | 6 | 20 | 15 | 8 | 20 | 10 | 20 | 10 | 20 | 5 |
| Nd | 6 | 13 | 8 | 8 | 16 | 24 | 21 | 40 | 6 | 16 | 43.5 | 15 | . | 51.4 | 14 | 18 | 6 | 14 | 15 | 15 |
| Ni | 63 | 66 | 90 | 5 | 2 | 4 | 74 | 110 | 140 | 160 | 32 | 94 | 8 | 28 | 94 | 120 | 25 | 23 | 46 | 21 |
| Pb | 6 | 1 | 1 | 1 | 1 | 1 | 8 | 16 | 1 | 20 | 1 | 8 | 7 | 20 | 12 | 8 | 20 | 12 | 6 | 24 |
| Pr | . | . | . | . | . | . | . | . | . | . | 10.7 | . | . | 13.2 | . | . | . | . | . | . |
| Rb | 20 | 10 | 5 | 50 | 30 | 10 | 50 | 60 | 30 | 190 | 111 | 40 | 69 | 100 | 100 | 110 | 80 | 130 | 100 | 110 |
| S% | 0.005 | 0.18 | 0.02 | 0.02 | 0.08 | 0.02 | 0.02 | 0.005 | 0.09 | 0.46 | 1.08 | 0.005 | 0.02 | 0.025 | 0.29 | 0.5 | 0.005 | 0.04 | 0.21 | 0.09 |
| Sc | 54.5 | 22.9 | 14.3 | 55.2 | 49.2 | 31.4 | 26 | 21.2 | 44.2 | 23.3 | 16 | 16.1 | . | 18 | 20.9 | 24.2 | 9 | 7.3 | 16.3 | 10.1 |
| Sm | 2.15 | 3.91 | 2.01 | 3.41 | 5.62 | 8.6 | 4.65 | 7.53 | 1.92 | 3.35 | 7.7 | 3.37 | . | 9.1 | 2.89 | 3.34 | 1.8 | 2.99 | 2.78 | 3.16 |
| Sr | 230 | 150 | 90 | 50 | 60 | 60 | 850 | 1130 | 390 | 130 | 825 | 450 | 729 | 1070 | 250 | 220 | 980 | 2170 | 680 | 1020 |
| Ta | 0.25 | 0.25 | 1 | 0.9 | 0.9 | 0.7 | 0.25 | 0.25 | 0.25 | 0.7 | 1 | 0.25 | . | 1 | 0.25 | 0.25 | 0.25 | 0.8 | 0.25 | 0.25 |
| Tb | 0.7 | 0.7 | 0.1 | 0.7 | 1.5 | 2 | 0.5 | 0.6 | 0.5 | 0.5 | 0.7 | 0.5 | . | 0.8 | 0.5 | 0.4 | 0.2 | 0.2 | 0.3 | 0.5 |
| Th | 0.4 | 0.7 | 1.9 | 0.2 | 0.7 | 1.1 | 3.4 | 5.7 | 0.3 | 5.3 | 7.7 | 4.5 | . | 9.7 | 3.8 | 4 | 8.9 | 3.4 | 4.6 | 9.2 |
| U | 0.05 | 0.2 | 0.05 | 0.05 | 0.05 | 0.6 | 0.6 | 1.5 | 0.05 | 1.6 | 1.9 | 0.9 | . | 1.6 | 1.3 | 1.5 | 2 | 2 | 1.5 | 1.4 |
| V | 320 | 240 | 110 | 310 | 56 | 12 | 170 | 170 | 230 | 160 | 160 | 140 | . | 150 | 160 | 170 | 68 | 54 | 120 | 84 |
| Y | 20 | 20 | 5 | 20 | 50 | 90 | 20 | 5 | 5 | 20 | 18 | 5 | 5 | 20 | 10 | 10 | 10 | 10 | 10 | 5 |
| Yb | 2.84 | 2.29 | 1.02 | 3.7 | 6.31 | 9.24 | 1.55 | 1.43 | 1.59 | 1.8 | 1.7 | 1.3 | . | 1.5 | 1.5 | 1.77 | 0.77 | 0.75 | 1.3 | 0.83 |
| Zn | 130 | 170 | 72 | 140 | 240 | 97 | 150 | 110 | 81 | 170 | 100 | 96 | 83 | 91 | 160 | 140 | 84 | 76 | 120 | 100 |
| Zr | 40 | 70 | 90 | 100 | 160 | 270 | 70 | 100 | 5 | 130 | 137 | 90 | 104 | 160 | 100 | 120 | 120 | 80 | 120 | 110 |
| X | 6985.66 | 6985.6 | 6984.93 | 6984.84 | 6985.04 | 6984.78 | 6987.47 | 6987.35 | 6966.58 | 6965.06 | 6997.1 | 6987.41 | 6969.55 | 7000.1 | 6987.65 | 6984.32 | 6987.41 | 6988.75 | 6982.82 | 6987.38 |
| Y | 565.85 | 565.31 | 565.18 | 565.22 | 565.36 | 565.09 | 561.25 | 561.28 | 557.97 | 561.05 | 561.19 | 561.28 | 562.632 | 559.87 | 560.624 | 564.5 | 561.25 | 563.78 | 565.58 | 561.28 |

| | Volcanics | | | | | | | | | Intrusives | | | | | | | | | |
|---|---|---|---|---|---|---|---|---|---|---|---|---|---|---|---|---|---|---|---|
| Sample | P415/4.5 | HJO-86-101 | KJP-87-12.2 | HJO-87-56 | KJP-87-14.1 | HJO-86-105 | PAN-86-1 | PAN-86-14 | PAN-86-8 | PAN-86-21 | PAN-87-31 | P506/7.2 | P502/4.4 | P503/6.5 | HJO-87-107 | P426/6.5 | PAN-87-30 | KJP-87-27 | HJO-87-136.2 |
| Rocktype | PLHVUL | PLHVUL | HVUL | HVUL | HVUL | PLHVUL | PLHTUF | HAGL | HVUL | KVAFB | QPLPF | QPLPF1 | QPLPF1 | QPLPF1 | QPLPF | QPLPF2 | QPLPF | QPLPF | TON1 |
| SiO2 | 66.3 | 66.8 | 57.3 | 69.1 | 63.3 | 64.4 | 70.0 | 62.2 | 73.6 | 51.9 | 63.4 | 65.7 | 65.3 | 65.3 | 64.5 | 65.3 | 64.0 | 65.6 | 64.0 |
| TiO2 | 0.37 | 0.4 | 0.57 | 0.29 | 0.54 | 0.62 | 0.37 | 0.66 | 0.09 | 1.57 | 0.6 | 0.46 | 0.43 | 0.43 | 0.46 | 0.36 | 0.44 | 0.26 | 0.47 |
| Al2O3 | 15.5 | 16 | 18.4 | 15.5 | 16.9 | 16.8 | 15.7 | 20 | 15.3 | 13.2 | 17.8 | 15.4 | 16.2 | 16.7 | 16.3 | 14.8 | 16 | 15.5 | 16.1 |
| Fe2O3 | 3.68 | 3.85 | 4.85 | 2.64 | 3.57 | 6.21 | 4.03 | 4.53 | 0.87 | 16.5 | 4.46 | 4.37 | 4.04 | 3.73 | 3.74 | 6.34 | 3.29 | 2.87 | 5.33 |
| MnO | 0.11 | 0.05 | 0.08 | 0.05 | 0.035 | 0.1 | 0.13 | 0.06 | 0.04 | 0.24 | 0.052 | 0.08 | 0.07 | 0.06 | 0.057 | 0.45 | 0.044 | 0.049 | 0.09 |
| MgO | 1.25 | 1.23 | 1.18 | 1.09 | 1.00 | 0.82 | 0.65 | 0.58 | 0.20 | 3.93 | 2.47 | 2.38 | 2.12 | 2.01 | 1.60 | 1.36 | 1.28 | 1.24 | 2.89 |
| CaO | 2.77 | 3.17 | 4.12 | 4.7 | 2.77 | 2.88 | 0.72 | 4.38 | 1.46 | 7.14 | 3.76 | 3.07 | 2.94 | 3.14 | 3.11 | 3.11 | 3.42 | 1.97 | 2.99 |
| Na2O | 4.11 | 4.79 | 7.10 | 3.50 | 5.78 | 4.97 | 3.56 | 4.38 | 6.14 | 2.77 | 5.20 | 4.45 | 4.90 | 5.40 | 5.07 | 0.42 | 4.78 | 6.28 | 4.61 |
| K2O | 3.67 | 2.20 | 3.04 | 0.93 | 2.95 | 2.03 | 3.06 | 2.23 | 1.66 | 0.26 | 1.73 | 1.75 | 1.99 | 1.85 | 2.15 | 5.53 | 1.29 | 3.67 | 2.39 |
| P2O5 | 0.14 | 0.15 | 0.29 | 0.07 | 0.22 | 0.23 | 0.15 | 0.22 | 0.03 | 0.14 | 0.17 | 0.14 | 0.14 | 0.13 | 0.15 | 0.15 | 0.12 | 0.14 | 0.16 |
| LOI | 1.5 | 1.1 | 2.8 | 0.7 | 1.9 | 0.9 | 1.5 | 0.6 | 0.7 | 1.2 | 0.8 | 1.3 | 1.0 | 1.3 | 1.2 | 1.4 | 4.2 | 1.1 | 0.8 |
| Total | 99.44 | 99.72 | 99.70 | 98.57 | 98.92 | 99.99 | 99.84 | 99.86 | 100.09 | 98.88 | 100.41 | 99.11 | 99.13 | 100.06 | 98.30 | 99.21 | 98.82 | 98.66 | 99.80 |
| CO2 | 0.79 | 0.01 | 2.52 | 0.01 | 0.98 | 0.15 | 0.01 | 0.02 | 0.02 | 0.01 | 0.01 | 0.30 | 0.26 | 0.29 | 0.31 | 0.02 | 0.01 | 0.08 | 0.19 |
| B (ppm) | 5 | 30 | 5 | 70 | 60 | 40 | 5 | 20 | 20 | 5 | 20 | 10 | 20 | 50 | 50 | 5 | 20 | 20 | 51 |
| Ba | 1420 | 1020 | 1180 | 449 | 1350 | 740 | 730 | 1340 | 950 | 50 | 772 | 730 | 680 | 590 | 1200 | 1590 | 446 | 2430 | 910 |
| Ce | 63 | 29 | 101 | 16.4 | 75.2 | 52 | 39 | 88 | 10 | 16 | 37 | 42 | 49 | 50 | 51.3 | 69 | 21.8 | 25.8 | . |
| Co | 7.5 | 7.7 | 5 | 6 | 4 | 13 | 7.7 | 11 | 1.1 | 38 | 14 | 14 | 12 | 11 | 9 | 6.1 | 7 | 6 | 24 |
| Cr | 18 | 29 | 26 | 34 | 4 | 100 | 17 | 25 | 2.5 | 16 | 88 | 110 | 90 | 73 | 32 | 16 | 16 | 46 | 118 |
| Cs | 4.7 | 7.4 | 10 | 4 | 8 | 8.4 | 3 | 7.5 | 1.4 | 2 | 7 | 6.1 | 6.9 | 8.2 | 7 | 48 | 5 | 2 | . |
| Cu | 57 | 11 | 5 | 14 | 6 | 11 | 5.5 | 1 | 1.5 | 170 | 16 | 55 | 24 | 34 | 22 | 6.5 | 8 | 21 | 9 |
| Dy | . | . | 2.7 | 0.7 | 1.6 | . | . | . | . | . | 1.8 | . | . | . | 2.2 | . | 1.2 | 1.3 | . |
| Er | . | . | 1.2 | 0.4 | 0.7 | . | . | . | . | . | 0.8 | . | . | . | 1.1 | . | 0.5 | 0.6 | . |
| Eu | 0.96 | 0.81 | 2.55 | 0.54 | 2 | 0.72 | 0.83 | 1.55 | 0.59 | 1.32 | 1.57 | 0.7 | 0.98 | 0.99 | 2.09 | 1.18 | 0.89 | 1.4 | . |
| Gd | . | . | 4.9 | 0.8 | 3.2 | . | . | . | . | . | 2.6 | . | . | . | 3.6 | . | 1.3 | 1.7 | . |
| Hf | 3.7 | 4.3 | 6 | 2 | 4 | 5.7 | 3.1 | 4.5 | 2.2 | 3.9 | 3 | 4 | 3.4 | 3.4 | 4 | 3.8 | 3 | 4 | . |
| Ho | . | . | 0.49 | 0.16 | 0.26 | . | . | . | . | . | 0.3 | . | . | . | 0.28 | . | 0.19 | 0.22 | . |
| La | 35 | 19.7 | 49.5 | 9.2 | 37.4 | 31.1 | 26.9 | 50.6 | 5.9 | 5.4 | 16.7 | 20.9 | 24.3 | 26 | 25.6 | 35.5 | 10.7 | 12.3 | . |
| Li | 26 | 28 | 28 | 16 | 50 | 24 | 22 | 22 | 16 | 22 | 84 | 40 | 40 | 34 | 41 | 110 | 26 | 0.5 | 45 |
| Lu | 0.2 | 0.15 | 0.07 | 0.025 | 0.025 | 0.19 | 0.15 | 0.24 | 0.04 | 0.76 | 0.025 | 0.13 | 0.15 | 0.14 | 0.32 | 0.19 | 0.025 | 0.025 | . |
| Nb | 20 | 10 | 7 | 2 | 5 | 10 | 10 | 20 | 10 | 30 | 2 | 10 | 10 | 20 | 4 | 10 | 1 | 5 | 20 |
| Nd | 24 | 12 | 52.6 | 7.1 | 38.3 | 24 | 17 | 33 | 6 | 10 | 22.9 | 17 | 21 | 20 | 28.8 | 29 | 10.8 | 13.4 | . |
| Ni | 13 | 15 | 8 | 27 | 6 | 38 | 11 | 11 | 3 | 16 | 81 | 59 | 43 | 35 | 19 | 11 | 16 | 17 | 51 |
| Pb | 40 | 20 | 4 | 1 | 1 | 12 | 16 | 12 | 16 | 1 | 1 | 24 | 20 | 12 | 20 | 64 | 1 | 12 | 9 |
| Pr | . | . | 13 | 2 | 10.2 | . | . | . | . | . | 5.3 | . | . | . | 7.3 | . | 2.9 | 3.4 | . |
| Rb | 150 | 80 | 110 | 54 | 118 | 110 | 110 | 90 | 50 | 5 | 83 | 80 | 90 | 100 | 77 | 250 | 56 | 88 | 106 |
| S% | 0.23 | 0.3 | 0.025 | 0.025 | 0.025 | 0.005 | 0.28 | 0.02 | 0.08 | 0.89 | 0.26 | 0.55 | 0.21 | 0.49 | 0.025 | 0.78 | 0.025 | 0.025 | 0.01 |
| Sc | 7.1 | 7 | 8 | 9 | 4 | 13.1 | 6.6 | 14.3 | 1.1 | 56.3 | 11 | 8.5 | 9.5 | 8.8 | 9 | 6.8 | 6 | 5 | . |
| Sm | 4.35 | 2.72 | 8.6 | 1.1 | 6.1 | 4.43 | 3.72 | 6.11 | 1.55 | 3.67 | 4.1 | 3.02 | 3.88 | 3.6 | 6.2 | 5.17 | 1.9 | 2.6 | . |
| Sr | 540 | 890 | 1200 | 401 | 1020 | 1200 | 360 | 1390 | 490 | 170 | 631 | 560 | 670 | 590 | 982 | 290 | 547 | 1880 | 755 |
| Ta | 0.25 | 0.25 | 1 | 0.5 | 0.5 | 0.8 | 0.25 | 0.25 | 0.25 | 0.7 | 0.5 | 0.7 | 0.25 | 0.25 | 0.5 | 0.25 | 0.5 | 0.5 | . |
| Tb | 0.4 | 0.3 | 0.6 | 0.1 | 0.3 | 0.4 | 0.5 | 1.3 | 0.2 | 1.2 | 0.3 | 0.3 | 0.5 | 0.3 | 0.4 | 0.4 | 0.2 | 0.2 | . |
| Th | 9.5 | 8.7 | 9.3 | 1.3 | 5.9 | 6.4 | 8 | 11 | 2.1 | 0.7 | 1.9 | 6.1 | 5.8 | 6.4 | 6.3 | 10 | 1.3 | 3.1 | . |
| U | 3.1 | 2.8 | 2.2 | 0.4 | 1.4 | 1.3 | 2.5 | 3 | 2.1 | 0.05 | 0.6 | 2.2 | 2.4 | 2.2 | 2.4 | 2.5 | 0.5 | 2 | . |
| V | 62 | 64 | 58 | 52 | 46 | 110 | 64 | 110 | 6 | 420 | 84 | 70 | 72 | 70 | 70 | 68 | 58 | 52 | . |
| Y | 10 | 10 | 13 | 4 | 8 | 5 | 10 | 20 | 5 | 40 | 8 | 20 | 10 | 5 | 8 | 10 | 6 | 7 | 25 |
| Yb | 1.04 | 0.85 | 0.7 | 0.2 | 0.2 | 1.01 | 0.88 | 1.53 | 0.3 | 4.53 | 0.5 | 0.76 | 0.9 | 0.87 | 0.7 | 1.16 | 0.3 | 0.4 | . |
| Zn | 91 | 70 | 98 | 50 | 91 | 120 | 93 | 73 | 73 | 220 | 100 | 100 | 60 | 52 | 90 | 210 | 66 | 54 | 79 |
| Zr | 130 | 90 | 153 | 79 | 112 | 140 | 120 | 120 | 30 | 100 | 100 | 120 | 90 | 100 | 88 | 160 | 65 | 102 | 96 |
| X | 6987.36 | 6984.74 | 6997.1 | 6982.32 | 6997.14 | 6984.9 | 6987.34 | 6983.76 | 6987.46 | 6985.44 | 6975.14 | 6966.6 | 6966.6 | 6966.6 | 6976.68 | 6987.316 | 6974.15 | 6988.55 | 6969.516 |
| Y | 561.336 | 563.89 | 561.19 | 564.2 | 561.1 | 564.27 | 561.32 | 563.84 | 561.26 | 565.88 | 563.75 | 560.53 | 560.73 | 560.68 | 564.06 | 562.2 | 563.78 | 563.76 | 562.738 |

Appen. Cont.

| | Intrusives | | | | | | | | | | | | | | | | | | | |
|---|---|---|---|---|---|---|---|---|---|---|---|---|---|---|---|---|---|---|---|---|
| Sample | HJO-86-102 | HJO-87-138 | HJO-87-126.2 | HJO-87-137 | P492/12. | HJO-87-125.1 | HJO-87-144 | P538/7.7 | P550/3.7 | P425/10. | P471/5.8 | HJO-87-139.1 | P490/9.5 | P494/11. | KJP-87-18 | P495/10. | HJO-87-219 | P544/7.8 | HJO-87-216 | P552/5 |
| Rocktype | TON2 | TON1 | TON1 | TON1 | TON1 | TON1 | TON1 | TON1 | TON1 | TON2 | TON1 | TON1 | TON1 | TON1 | TON1 | TON1 | TON1 | TON1 | TON1 | TON1 |
| SiO2 | 61.1 | 60.0 | 64.5 | 64.3 | 66.4 | 64.0 | 64.9 | 63.6 | 65.0 | 61.9 | 64.2 | 64.4 | 65.0 | 63.5 | 63.3 | 64.8 | 65.5 | 65.9 | 65.5 | 64.8 |
| TiO2 | 0.5 | 0.57 | 0.46 | 0.48 | 0.44 | 0.46 | 0.48 | 0.46 | 0.46 | 0.5 | 0.44 | 0.43 | 0.43 | 0.43 | 0.53 | 0.43 | 0.42 | 0.42 | 0.42 | 0.44 |
| Al2O3 | 16.4 | 18.9 | 16 | 16.1 | 15.4 | 15.9 | 16.5 | 15.9 | 15.7 | 16.5 | 15.9 | 15.8 | 15.8 | 15.5 | 15.8 | 15.7 | 15.1 | 15.7 | 14.8 | 16.2 |
| Fe2O3 | 5.9 | 5.48 | 4.86 | 5.11 | 4.52 | 4.82 | 4.68 | 4.71 | 4.29 | 5.98 | 4.54 | 4.73 | 4.6 | 4.43 | 5.22 | 4.71 | 4.11 | 4.49 | 4.4 | 4.56 |
| MnO | 0.1 | 0.07 | 0.09 | 0.14 | 0.06 | 0.09 | 0.06 | 0.08 | 0.08 | 0.12 | 0.08 | 0.09 | 0.08 | 0.08 | 0.08 | 0.08 | 0.07 | 0.09 | 0.08 | 0.07 |
| MgO | 2.77 | 2.71 | 2.63 | 2.60 | 2.55 | 2.54 | 2.54 | 2.52 | 2.48 | 2.48 | 2.43 | 2.41 | 2.41 | 2.41 | 2.39 | 2.36 | 2.33 | 2.31 | 2.30 | 2.30 |
| CaO | 5.28 | 1.98 | 3.58 | 2.54 | 1.77 | 3.55 | 2.06 | 3.9 | 3.89 | 4.61 | 3.95 | 3.38 | 3.09 | 3.78 | 4.11 | 3.03 | 3.06 | 2.69 | 3.52 | 3.03 |
| Na2O | 3.47 | 5.71 | 4.59 | 4.45 | 4.34 | 4.17 | 4.53 | 4.01 | 4.74 | 3.61 | 3.95 | 4.53 | 3.98 | 3.85 | 4.21 | 4.59 | 3.86 | 3.94 | 4.04 | 4.02 |
| K2O | 2.70 | 3.58 | 2.34 | 2.86 | 2.93 | 3.03 | 2.99 | 2.79 | 2.15 | 2.92 | 2.81 | 2.77 | 2.98 | 2.76 | 2.95 | 2.59 | 3.42 | 2.95 | 3.02 | 3.36 |
| P2O5 | 0.15 | 0.20 | 0.15 | 0.16 | 0.15 | 0.15 | 0.15 | 0.15 | 0.15 | 0.16 | 0.14 | 0.14 | 0.15 | 0.14 | 0.22 | 0.14 | 0.14 | 0.14 | 0.14 | 0.14 |
| LOI | 1.2 | 1.1 | 0.9 | 1.0 | 0.9 | 1.3 | 1.0 | 1.9 | 1.0 | 1.2 | 1.4 | 1.1 | 1.2 | 2.1 | 1.1 | 1.5 | 2.1 | 1.6 | 1.5 | 1.2 |
| Total | 99.53 | 100.28 | 100.13 | 99.74 | 99.49 | 100.02 | 99.89 | 99.97 | 99.94 | 99.94 | 99.83 | 99.76 | 99.75 | 98.96 | 99.89 | 99.90 | 100.09 | 100.25 | 99.69 | 100.08 |
| CO2 | 0.74 | 0.01 | 0.53 | 0.02 | 0.01 | 0.81 | 0.01 | 1.23 | 0.62 | 0.02 | 0.44 | 0.54 | 0.36 | 1.37 | 0.22 | 0.66 | 1.48 | 0.48 | 1.18 | 0.56 |
| B (ppm) | 5 | 5 | 5 | 5 | 5 | 11 | 5 | 5 | 5 | 5 | 5 | 5 | 5 | 5 | 30 | 5 | 19 | 5 | 5 | 5 |
| Ba | 890 | 1200 | 726 | 977 | 810 | 1040 | 1000 | 710 | 1140 | 970 | 900 | 980 | 1060 | 840 | 1050 | 780 | 938 | 970 | 978 | 1090 |
| Ce | 51 | . | . | . | 56 | . | . | 58 | 57 | 57 | 58 | . | 52 | 57 | 51.5 | 53 | . | 60 | . | 55 |
| Co | 15 | 18 | 17 | 22 | 13 | 17 | 17 | 14 | 13 | 14 | 13 | 16 | 12 | 12 | 11 | 13 | 15 | 13 | 15 | 13 |
| Cr | 42 | 122 | 103 | 104 | 74 | 100 | 106 | 81 | 79 | 50 | 74 | 93 | 75 | 76 | 90 | 73 | 98 | 74 | 102 | 76 |
| Cs | 29.6 | . | . | . | 8.9 | . | . | 10.7 | 3.1 | 57.8 | 5.8 | . | 6.8 | 10.8 | 8 | 9.9 | . | 6.6 | . | 3.8 |
| Cu | 2.5 | 28 | 14 | 16 | 5 | 8 | 10 | 14 | 2 | 55 | 3.5 | 10 | 10 | 22 | 22 | 4.5 | 21 | 33 | 16 | 28 |
| Dy | . | . | . | . | . | . | . | . | . | . | . | . | . | . | 2.3 | . | . | . | . | . |
| Er | . | . | . | . | . | . | . | . | . | . | . | . | . | . | 1.3 | . | . | . | . | . |
| Eu | 0.73 | . | . | . | 0.88 | . | . | 0.74 | 0.56 | 1.09 | 0.91 | . | 0.53 | 0.55 | 2.13 | 0.48 | . | 0.48 | . | 0.56 |
| Gd | . | . | . | . | . | . | . | . | . | . | . | . | . | . | 3.7 | . | . | . | . | . |
| Hf | 3.9 | . | . | . | 3.7 | . | . | 4.4 | 4.2 | 3.5 | 2.5 | . | 3.6 | 3.6 | 2 | 3.9 | . | 4.1 | . | 4.3 |
| Ho | . | . | . | . | . | . | . | . | . | . | . | . | . | . | 0.33 | . | . | . | . | . |
| La | 33.3 | . | . | . | 33.9 | . | . | 36.1 | 35.8 | 29.2 | 28.4 | . | 32.2 | 35.9 | 26 | 32.2 | . | 38.8 | . | 34.7 |
| Li | 30 | 40 | 58 | 36 | 46 | 40 | 35 | 62 | 22 | 100 | 54 | 50 | 48 | 44 | 42 | 40 | 22 | 36 | 32 | 34 |
| Lu | 0.28 | . | . | . | 0.16 | . | . | 0.21 | 0.23 | 0.26 | 0.19 | . | 0.17 | 0.21 | 0.3 | 0.17 | . | 0.17 | . | 0.16 |
| Nb | 20 | 16 | 11 | 32 | 10 | 12 | 5 | 10 | 5 | 10 | 10 | 5 | 20 | 5 | 5 | 10 | 5 | 10 | 5 | 20 |
| Nd | 25 | . | . | . | 25 | . | . | 24 | 25 | 23 | 18 | . | 22 | 24 | 29.2 | 24 | . | 25 | . | 24 |
| Ni | 14 | 35 | 42 | 52 | 30 | 31 | 33 | 31 | 27 | 14 | 30 | 31 | 29 | 27 | 34 | 28 | 27 | 28 | 29 | 30 |
| Pb | 16 | 9 | 12 | 10 | 20 | 10 | 9 | 24 | 28 | 40 | 24 | 13 | 24 | 20 | 12 | 32 | 12 | 24 | 9 | 28 |
| Pr | . | . | . | . | . | . | . | . | . | . | . | . | . | . | 7.2 | . | . | . | . | . |
| Rb | 130 | 122 | 98 | 112 | 130 | 108 | 118 | 150 | 90 | 160 | 110 | 99 | 130 | 130 | 110 | 140 | 112 | 120 | 119 | 130 |
| S% | 0.1 | 0.005 | 0.005 | 0.005 | 0.005 | 0.005 | 0.03 | 0.005 | 0.005 | 0.005 | 0.005 | 0.005 | 0.005 | 0.01 | 0.025 | 0.005 | 0.08 | 0.01 | 0.005 | 0.005 |
| Sc | 16.7 | . | . | . | 10.4 | . | . | 12.4 | 12.5 | 14.5 | 10.9 | . | 11.3 | 11.3 | 13 | 11.1 | . | 11.8 | . | 11.6 |
| Sm | 4.63 | . | . | . | 4.15 | . | . | 4.49 | 4.74 | 4.46 | 3.75 | . | 4.09 | 4.31 | 6.1 | 4.14 | . | 4.37 | . | 4.14 |
| Sr | 840 | 304 | 730 | 819 | 480 | 704 | 655 | 1020 | 660 | 800 | 870 | 709 | 730 | 670 | 994 | 950 | 569 | 730 | 763 | 760 |
| Ta | 0.25 | . | . | . | 0.25 | . | . | 0.25 | 0.6 | 0.25 | 0.25 | . | 0.25 | 0.5 | 0.5 | 0.25 | . | 0.25 | . | 0.25 |
| Tb | 0.6 | . | . | . | 0.4 | . | . | 0.3 | 0.6 | 0.4 | 0.4 | . | 0.4 | 0.4 | 0.4 | 0.4 | . | 0.6 | . | 0.4 |
| Th | 7.3 | . | . | . | 6.7 | . | . | 7.3 | 7 | 8.7 | 6.1 | . | 6.5 | 7.6 | 5.7 | 8.1 | . | 7.9 | . | 8.2 |
| U | 2.3 | . | . | . | 1.9 | . | . | 2.7 | 2.8 | 2.6 | 1.6 | . | 1.5 | 3.1 | 1.5 | 1.6 | . | 1.9 | . | 1.8 |
| V | 130 | . | . | . | 74 | . | . | 92 | 94 | 120 | 90 | . | 96 | 88 | 92 | 88 | . | 92 | . | 92 |
| Y | 5 | 19 | 17 | 17 | 10 | 19 | 30 | 10 | 30 | 5 | 5 | 5 | 5 | 5 | 9 | 5 | 24 | 5 | 10 | 10 |
| Yb | 1.66 | . | . | . | 0.75 | . | . | 1.14 | 1.22 | 1.56 | 0.99 | . | 1.03 | 1.07 | 0.8 | 0.97 | . | 1.08 | . | 0.94 |
| Zn | 97 | 79 | 82 | 74 | 90 | 86 | 61 | 83 | 92 | 230 | 85 | 75 | 80 | 77 | 88 | 72 | 54 | 74 | 53 | 82 |
| Zr | 100 | 126 | 86 | 76 | 110 | 89 | 86 | 90 | 80 | 120 | 90 | 69 | 110 | 90 | 100 | 100 | 90 | 100 | 77 | 90 |
| X | 6984.86 | 6969.75 | 6969.738 | 6969.47 | 6967.66 | 6969.49 | 6969.765 | 6965.06 | 6965.06 | 6987.32 | 6967.66 | 6969.808 | 6967.66 | 6967.66 | 6992.26 | 6967.66 | 6964.7 | 6965.06 | 6964.7 | 6965.06 |
| Y | 563.96 | 562.995 | 562.862 | 562.78 | 563.44 | 562.704 | 563.155 | 561.14 | 562.04 | 562.1 | 561.34 | 562.924 | 563.24 | 563.64 | 562.6 | 563.74 | 561.56 | 561.44 | 561.665 | 562.24 |

Intrusives

| Sample | P542/8.6 | P546/9.6 | PAN-86-16 | P498/6.2 | PAN-86-15 | P560/7.2 | P523/10. | P540/3 | P493/13. | P496/9.7 | HJO-87-134.1 | P497/6.8 | P489/11 | P472/5.9 | HJO-87-145 | P473/9.3 | PAN-86-12 | PAN-86-13 | P561/7.2 | P449/29 |
|---|---|---|---|---|---|---|---|---|---|---|---|---|---|---|---|---|---|---|---|---|
| Rocktype | TON1 | TON1 | TON2 | TON1 | TON2 | TON1 | TON1 | TON1 | TON1 | TON1 | TON1 | TON1 | TON1 | TON1 | TON1 | TON1 | TON2 | TON2 | TON1 | TON3 |
| SiO2 | 64.7 | 65.0 | 63.0 | 63.0 | 63.4 | 64.4 | 64.2 | 66.4 | 65.8 | 64.5 | 67.6 | 62.6 | 66.4 | 66.0 | 64.8 | 66.7 | 63.7 | 64.6 | 66.7 | 67.2 |
| TiO2 | 0.43 | 0.44 | 0.47 | 0.45 | 0.46 | 0.42 | 0.45 | 0.41 | 0.46 | 0.45 | 0.42 | 0.47 | 0.4 | 0.4 | 0.42 | 0.39 | 0.43 | 0.41 | 0.33 | 0.36 |
| Al2O3 | 15.5 | 15.8 | 16.6 | 16.7 | 16.1 | 15.8 | 16.2 | 15 | 16 | 16.1 | 15.5 | 17.4 | 15.7 | 15.4 | 15.9 | 15.4 | 15.9 | 15.6 | 15.8 | 16.2 |
| Fe2O3 | 4.3 | 4.11 | 5.16 | 4.09 | 5.04 | 4.13 | 4.58 | 4.17 | 4.68 | 4.18 | 4.2 | 4.12 | 4.05 | 4 | 4.53 | 3.9 | 4.61 | 4.43 | 3.16 | 3.13 |
| MnO | 0.07 | 0.07 | 0.08 | 0.07 | 0.1 | 0.07 | 0.08 | 0.06 | 0.06 | 0.07 | 0.05 | 0.06 | 0.05 | 0.08 | 0.08 | 0.07 | 0.08 | 0.08 | 0.06 | 0.06 |
| MgO | 2.29 | 2.29 | 2.28 | 2.24 | 2.24 | 2.23 | 2.22 | 2.21 | 2.21 | 2.20 | 2.18 | 2.17 | 2.16 | 2.15 | 2.11 | 2.06 | 2.01 | 1.95 | 1.73 | 1.51 |
| CaO | 3.33 | 3.72 | 3.69 | 4.42 | 4.34 | 3.92 | 3.45 | 2.98 | 1.74 | 3.79 | 2.84 | 4.08 | 2.4 | 3.04 | 3.77 | 2.92 | 4.03 | 3.95 | 2.58 | 3 |
| Na2O | 4.07 | 4.23 | 4.10 | 4.54 | 3.50 | 4.12 | 3.41 | 3.68 | 3.63 | 4.48 | 4.32 | 4.53 | 4.28 | 3.82 | 4.51 | 3.91 | 3.57 | 3.68 | 4.64 | 5.28 |
| K2O | 2.98 | 2.88 | 2.82 | 2.37 | 2.72 | 2.68 | 3.79 | 3.03 | 3.41 | 2.23 | 1.90 | 2.72 | 2.74 | 3.15 | 2.74 | 3.40 | 3.70 | 3.34 | 3.30 | 2.33 |
| P2O5 | 0.14 | 0.14 | 0.14 | 0.14 | 0.14 | 0.14 | 0.15 | 0.14 | 0.16 | 0.14 | 0.13 | 0.15 | 0.14 | 0.13 | 0.14 | 0.13 | 0.13 | 0.12 | 0.11 | 0.14 |
| LOI | 1.3 | 1.2 | 1.0 | 2.0 | 1.3 | 2.0 | 1.4 | 1.3 | 1.5 | 1.4 | 0.5 | 1.8 | 1.0 | 1.2 | 1.1 | 1.3 | 1.9 | 1.5 | 1.9 | 0.8 |
| Total | 99.12 | 99.91 | 99.34 | 100.02 | 99.35 | 99.91 | 99.92 | 99.39 | 99.62 | 99.53 | 99.68 | 100.07 | 99.32 | 99.40 | 100.08 | 100.19 | 100.09 | 99.70 | 100.26 | 99.98 |
| CO2 | 1.00 | 0.89 | 0.22 | 1.17 | 0.93 | 1.58 | 0.65 | 0.66 | 0.03 | 0.64 | 0.01 | 1.01 | 0.01 | 0.46 | 0.66 | 0.58 | 1.27 | 1.24 | 1.08 | 0.26 |
| B (ppm) | 20 | 10 | 5 | 5 | 5 | 5 | 5 | 40 | 5 | 5 | 5 | 5 | 5 | 60 | 5 | 20 | 5 | 5 | 5 | 5 |
| Ba | 820 | 1070 | 790 | 820 | 990 | 870 | 1700 | 910 | 1120 | 870 | 693 | 1260 | 880 | 840 | 961 | 910 | 1230 | 990 | 950 | 800 |
| Ce | 55 | 56 | 79 | 46 | 59 | 51 | 55 | 56 | 52 | 47 | . | 48 | 38 | 53 | . | 53 | 48 | 47 | 44 | 65 |
| Co | 12 | 12 | 16 | 12 | 13 | 12 | 14 | 12 | 12 | 13 | 16 | 11 | 12 | 11 | 16 | 11 | 12 | 12 | 12 | 14 |
| Cr | 73 | 77 | 48 | 64 | 37 | 67 | 80 | 76 | 76 | 66 | 113 | 69 | 68 | 71 | 95 | 66 | 37 | 38 | 60 | 33 |
| Cs | 3.6 | 6.2 | 11.3 | 2.9 | 12.7 | 6.6 | 8.8 | 4.8 | 8.2 | 3.1 | . | 7.3 | 9 | 5.5 | . | 3.9 | 5.1 | 5.5 | 7.4 | 7 |
| Cu | 6 | 10 | 25 | 2.5 | 1 | 16 | 38 | 27 | 4 | 10 | 11 | 29 | 16 | 46 | 11 | 13 | 2 | 26 | 1 | 3 |
| Dy | . | . | . | . | . | . | . | . | . | . | . | . | . | . | . | . | . | . | . | . |
| Er | . | . | . | . | . | . | . | . | . | . | . | . | . | . | . | . | . | . | . | . |
| Eu | 0.83 | 0.63 | 1.2 | 0.99 | 0.83 | 0.48 | 0.71 | 0.91 | 0.54 | 0.87 | . | 0.4 | 0.47 | 0.95 | . | 0.77 | 1.03 | 1.07 | 0.78 | 1.03 |
| Gd | . | . | . | . | . | . | . | . | . | . | . | . | . | . | . | . | . | . | . | . |
| Hf | 2.7 | 4.1 | 3.8 | 2.5 | 4.9 | 3.5 | 4.4 | 2.6 | 4.4 | 2.7 | . | 3.8 | 3.6 | 2.6 | . | 2.5 | 3.8 | 3.8 | 2.4 | 6.4 |
| Ho | . | . | . | . | . | . | . | . | . | . | . | . | . | . | . | . | . | . | . | . |
| La | 28.1 | 35.3 | 39.9 | 21.7 | 35.7 | 32.5 | 35 | 27.8 | 35.1 | 22.1 | . | 29.8 | 22 | 28.2 | . | 26.5 | 34.8 | 32.5 | 19.3 | 30.6 |
| Li | 46 | 32 | 28 | 44 | 26 | 34 | 36 | 44 | 44 | 36 | 46 | 42 | 52 | 48 | 36 | 50 | 28 | 24 | 39 | 36 |
| Lu | 0.17 | 0.21 | 0.24 | 0.15 | 0.27 | 0.17 | 0.18 | 0.16 | 0.17 | 0.16 | . | 0.15 | 0.18 | 0.17 | . | 0.16 | 0.26 | 0.26 | 0.18 | 0.12 |
| Nb | 5 | 20 | 20 | 20 | 20 | 20 | 10 | 10 | 10 | 20 | 5 | 10 | 5 | 10 | 5 | 30 | 10 | 20 | 5 | 10 |
| Nd | 20 | 23 | 30 | 18 | 24 | 24 | 26 | 19 | 24 | 19 | . | 22 | 17 | 19 | . | 19 | 23 | 23 | 13 | 24 |
| Ni | 27 | 29 | 13 | 25 | 11 | 28 | 31 | 28 | 30 | 26 | 33 | 26 | 27 | 27 | 28 | 25 | 12 | 10 | 22 | 22 |
| Pb | 8 | 22 | 20 | 8 | 16 | 24 | 20 | 1 | 28 | 16 | 9 | 24 | 24 | 20 | 12 | 20 | 16 | 20 | 14 | 16 |
| Pr | . | . | . | . | . | . | . | . | . | . | . | . | . | . | . | . | . | . | . | . |
| Rb | 130 | 130 | 140 | 110 | 110 | 120 | 120 | 140 | 130 | 90 | 93 | 120 | 150 | 140 | 89 | 120 | 150 | 120 | 120 | 80 |
| S% | 0.005 | 0.005 | 0.05 | 0.005 | 0.005 | 0.005 | 0.09 | 0.04 | 0.005 | 0.07 | 0.03 | 0.05 | 0.005 | 0.005 | 0.005 | 0.005 | 0.005 | 0.005 | 0.005 | 0.005 |
| Sc | 10.5 | 11.4 | 14.2 | 10 | 12.9 | 10.8 | 12.1 | 10.8 | 11.5 | 10.1 | . | 11.2 | 10.6 | 9.4 | . | 9.3 | 12.2 | 12 | 9.1 | 6.9 |
| Sm | 3.76 | 4.37 | 5.38 | 3.41 | 4.47 | 4.01 | 4.36 | 3.96 | 4.43 | 3.45 | . | 3.99 | 3.25 | 3.6 | . | 3.64 | 4.42 | 4.38 | 2.93 | 3.49 |
| Sr | 870 | 860 | 840 | 990 | 800 | 930 | 660 | 790 | 710 | 790 | 543 | 820 | 830 | 710 | 784 | 760 | 760 | 680 | 780 | 1000 |
| Ta | 0.25 | 0.25 | 0.25 | 0.25 | 0.25 | 0.5 | 0.25 | 0.25 | 0.5 | 0.25 | . | 0.6 | 0.25 | 0.25 | . | 0.25 | 0.25 | 0.25 | 0.25 | 0.25 |
| Tb | 0.4 | 0.4 | 0.5 | 0.3 | 0.5 | 0.3 | 0.5 | 0.3 | 0.4 | 0.4 | . | 0.3 | 0.4 | 0.4 | . | 0.3 | 0.3 | 0.5 | 0.6 | 0.9 |
| Th | 7.6 | 7 | 9.2 | 3.6 | 7.9 | 6.7 | 8 | 7.9 | 7.8 | 4.5 | . | 4.2 | 7.9 | 8 | . | 8.6 | 11 | 9.4 | 5.2 | 6.9 |
| U | 2 | 2.7 | 2.7 | 1.5 | 2.4 | 2.7 | 2.8 | 1.6 | 2.3 | 1.5 | . | 2.3 | 1.9 | 1.9 | . | 1.9 | 1.6 | 1.7 | 2.2 | 1.6 |
| V | 92 | 86 | 100 | 86 | 110 | 88 | 100 | 88 | 84 | 78 | . | 82 | 88 | 78 | . | 76 | 100 | 90 | 72 | 48 |
| Y | 20 | 5 | 5 | 20 | 10 | 10 | 10 | 20 | 20 | 5 | 15 | 10 | 10 | 10 | 5 | 10 | 20 | 20 | 5 | 5 |
| Yb | 1.03 | 1.06 | 1.33 | 0.78 | 1.41 | 1.01 | 1.08 | 1.03 | 1.08 | 0.89 | . | 0.99 | 0.87 | 0.97 | . | 0.88 | 1.45 | 1.62 | 0.94 | 0.67 |
| Zn | 73 | 70 | 90 | 72 | 110 | 70 | 71 | 71 | 69 | 74 | 63 | 71 | 72 | 76 | 50 | 75 | 84 | 79 | 73 | 87 |
| Zr | 100 | 120 | 120 | 100 | 110 | 80 | 100 | 80 | 110 | 80 | 78 | 80 | 80 | 90 | 84 | 80 | 120 | 100 | 70 | 110 |
| X | 6965.06 | 6965.06 | 6983.83 | 6967.66 | 6983.72 | 6964.7 | 6965.06 | 6965.06 | 6967.66 | 6967.66 | 6969.544 | 6967.66 | 6967.66 | 6967.66 | 6969.67 | 6967.66 | 6982.85 | 6982.3 | 6964.78 | 6984.16 |
| Y | 561.29 | 561.64 | 563.76 | 564.04 | 563.82 | 562.4 | 559.94 | 561.19 | 563.54 | 563.84 | 562.688 | 563.94 | 563.14 | 561.44 | 563.235 | 561.54 | 563.66 | 563.86 | 562.16 | 565.8 |

Appen. Cont.

| | Intrusives | | | | | | | | | | | | | | | | | Metasediments | |
|---|---|---|---|---|---|---|---|---|---|---|---|---|---|---|---|---|---|---|---|
| Sample | P474/9.5 | P475/4.2 | HJO-86-122 | P476/2.6 | P477/3.6 | HJO-86-10 | KJP-87-98 | P524/10. | P478/5.3 | P485/11. | P479/9.9 | P482/9.5 | P483/5.9 | P484/3.8 | P480/7.4 | P481/9.2 | P486/12.5 | HJO-86-118 | HJO-87-155.2 |
| Rocktype | TON1 | TON1 | TON3 | TON1 | TON1 | GRDR3 | GRDR | GRDR1 | TRPF1 | TRPF1 | TRPF1 | TRPF1 | TRPF1 | TRPF1 | TRPF1 | TRPF1 | TRPF1 | GRV | GRV |
| SiO2 | 67.9 | 68.2 | 67.5 | 70.5 | 69.7 | 67.7 | 66.6 | 69.0 | 67.8 | 70.8 | 69.4 | 71.5 | 71.2 | 69.3 | 71.0 | 70.8 | 71.5 | 52.9 | 57.0 |
| TiO2 | 0.28 | 0.28 | 0.31 | 0.24 | 0.23 | 0.32 | 0.31 | 0.37 | 0.33 | 0.23 | 0.19 | 0.18 | 0.17 | 0.19 | 0.17 | 0.16 | 0.16 | 0.61 | 0.9 |
| Al2O3 | 15.2 | 15.2 | 15.9 | 14.8 | 15.6 | 15.9 | 15.2 | 15.8 | 15.5 | 15.8 | 15.9 | 15.5 | 15.4 | 16.3 | 15.8 | 15.4 | 15.7 | 9.89 | 15.8 |
| Fe2O3 | 2.72 | 2.86 | 2.62 | 2.47 | 2.2 | 2.77 | 2.9 | 2.9 | 3.45 | 1.96 | 1.6 | 1.63 | 1.42 | 1.53 | 1.5 | 1.48 | 1.26 | 10.1 | 7.91 |
| MnO | 0.05 | 0.06 | 0.05 | 0.06 | 0.05 | 0.05 | 0.048 | 0.04 | 0.07 | 0.04 | 0.03 | 0.04 | 0.04 | 0.04 | 0.03 | 0.03 | 0.02 | 0.17 | 0.09 |
| MgO | 1.41 | 1.41 | 1.31 | 1.16 | 1.12 | 1.44 | 1.26 | 1.10 | 1.75 | 0.87 | 0.78 | 0.74 | 0.72 | 0.71 | 0.66 | 0.65 | 0.60 | 13.00 | 6.77 |
| CaO | 2.71 | 2.32 | 3.18 | 1.91 | 1.89 | 2.88 | 3.17 | 3.29 | 2.89 | 2.05 | 1.83 | 1.8 | 1.52 | 1.98 | 1.72 | 1.73 | 1.37 | 7.01 | 2.77 |
| Na2O | 4.52 | 4.21 | 5.55 | 3.58 | 4.76 | 5.69 | 5.58 | 4.79 | 4.05 | 5.03 | 5.57 | 4.89 | 4.92 | 5.18 | 5.21 | 5.01 | 5.27 | 1.89 | 1.83 |
| K2O | 2.75 | 3.32 | 2.32 | 3.83 | 3.31 | 2.26 | 2.18 | 1.85 | 3.17 | 2.39 | 2.52 | 3.24 | 3.17 | 2.98 | 2.95 | 3.04 | 3.25 | 1.15 | 3.82 |
| P2O5 | 0.09 | 0.09 | 0.12 | 0.09 | 0.08 | 0.12 | 0.12 | 0.10 | 0.11 | 0.07 | 0.06 | 0.05 | 0.05 | 0.06 | 0.06 | 0.05 | 0.05 | 0.15 | 0.35 |
| LOI | 1.6 | 1.1 | 1.2 | 0.8 | 1.1 | 0.7 | 1.2 | 0.9 | 1.1 | 1.1 | 1.2 | 0.6 | 1.0 | 1.7 | 0.8 | 1.0 | 0.7 | 2.4 | 2.5 |
| Total | 99.25 | 99.03 | 100.02 | 99.41 | 100.02 | 99.83 | 98.60 | 100.09 | 100.20 | 100.32 | 99.11 | 100.19 | 99.61 | 99.97 | 99.87 | 99.35 | 99.88 | 99.26 | 99.78 |
| CO2 | 0.81 | 0.49 | 0.48 | 0.19 | 0.50 | 0.01 | 0.30 | 0.31 | 0.19 | 0.13 | 0.27 | 0.08 | 0.48 | 0.58 | 0.04 | 0.16 | 0.01 | 0.01 | 0.01 |
| B (ppm) | 5 | 70 | 5 | 50 | 5 | 5 | 20 | 5 | 5 | 5 | 5 | 20 | 10 | 170 | 10 | 10 | 20 | 10 | 210 |
| Ba | 950 | 920 | 630 | 970 | 960 | 680 | 708 | 550 | 870 | 970 | 980 | 1080 | 1080 | 1150 | 1110 | 1070 | 1160 | 320 | 1390 |
| Ce | 32 | 34 | 50 | 32 | 23 | 38 | 43.7 | 38 | 47 | 18 | 13 | 18 | 15 | 12 | 15 | 16 | 13 | 17 | . |
| Co | 8.2 | 7.9 | 7.8 | 7 | 5.9 | 9.3 | 6 | 6.1 | 8.7 | 5 | 3.9 | 3.9 | 3.5 | 3.7 | 3.5 | 3.5 | 3.3 | 53 | 22 |
| Cr | 47 | 51 | 30 | 47 | 41 | 34 | 26 | 24 | 56 | 20 | 24 | 24 | 21 | 23 | 21 | 19 | 21 | 1230 | 517 |
| Cs | 5.5 | 11.1 | 7.9 | 14.7 | 5.2 | 4.7 | 2 | 2 | 8 | 6.6 | 6.8 | 8.5 | 5.5 | 8.3 | 7.2 | 7.2 | 3.7 | 6.1 | . |
| Cu | 11 | 20 | 21 | 61 | 5.5 | 15 | 9.5 | 2 | 11 | 7 | 17 | 55 | 50 | 17 | 53 | 23 | 5 | 71 | 61 |
| Dy | . | . | . | . | . | . | 1.3 | . | . | . | . | . | . | . | . | . | . | . | . |
| Er | . | . | . | . | . | . | 0.6 | . | . | . | . | . | . | . | . | . | . | . | . |
| Eu | 0.42 | 0.36 | 0.91 | 0.3 | 0.52 | 0.99 | 1.06 | 0.47 | 0.44 | 0.31 | 0.3 | 0.32 | 0.35 | 0.26 | 0.34 | 0.2 | 0.3 | 0.86 | . |
| Gd | . | . | . | . | . | . | 2.2 | . | . | . | . | . | . | . | . | . | . | . | . |
| Hf | 1.8 | 3.3 | 3 | 3.2 | 2 | 4.1 | 2 | 4.7 | 3.8 | 2.5 | 2.3 | 2.8 | 2.1 | 2 | 2.5 | 2.1 | 2.2 | 1.8 | . |
| Ho | . | . | . | . | . | . | 0.21 | . | . | . | . | . | . | . | . | . | . | . | . |
| La | 15.4 | 20.7 | 25.7 | 18.9 | 11.3 | 21.6 | 21.6 | 25.8 | 30 | 11.2 | 7.7 | 10.9 | 8.8 | 7.6 | 8.5 | 9.9 | 8 | 6.6 | . |
| Li | 42 | 48 | 36 | 58 | 50 | 20 | 12 | 20 | 72 | 44 | 44 | 34 | 34 | 44 | 44 | 44 | 34 | 28 | 80 |
| Lu | 0.11 | 0.16 | 0.09 | 0.2 | 0.18 | 0.15 | 0.06 | 0.06 | 0.18 | 0.09 | 0.07 | 0.12 | 0.08 | 0.05 | 0.1 | 0.09 | 0.09 | 0.3 | . |
| Nb | 20 | 20 | 10 | 10 | 10 | 10 | 4 | 20 | 10 | 5 | 5 | 5 | 5 | 10 | 10 | 10 | 10 | 10 | 5 |
| Nd | 11 | 14 | 22 | 13 | 9 | 15 | 20.3 | 14 | 19 | 7 | 6 | 8 | 6 | 5 | 6 | 7 | 5 | 11 | . |
| Ni | 19 | 20 | 15 | 20 | 20 | 18 | 22 | 18 | 23 | 10 | 11 | 11 | 10 | 10 | 10 | 10 | 9 | 430 | 88 |
| Pb | 24 | 28 | 12 | 32 | 16 | 12 | 1 | 12 | 28 | 24 | 24 | 32 | 20 | 28 | 32 | 32 | 24 | 1 | 12 |
| Pr | . | . | . | . | . | . | 5.6 | . | . | . | . | . | . | . | . | . | . | . | . |
| Rb | 120 | 170 | 130 | 160 | 150 | 100 | 79 | 90 | 190 | 140 | 110 | 150 | 120 | 160 | 120 | 150 | 130 | 70 | 173 |
| S% | 0.005 | 0.005 | 0.005 | 0.005 | 0.005 | 0.02 | 0.025 | 0.005 | 0.005 | 0.005 | 0.005 | 0.005 | 0.005 | 0.005 | 0.005 | 0.005 | 0.005 | 0.21 | 0.08 |
| Sc | 6.5 | 7.2 | 4.8 | 7.1 | 5.8 | 5.3 | 4 | 4.4 | 8.1 | 4.2 | 3.5 | 4.4 | 3.9 | 3.3 | 3.9 | 3.6 | 3.7 | 33 | . |
| Sm | 2.04 | 2.76 | 3.64 | 2.8 | 1.91 | 3.01 | 3.3 | 2.47 | 3.5 | 1.5 | 1.28 | 1.74 | 1.25 | 1.06 | 1.46 | 1.39 | 1.18 | 2.73 | . |
| Sr | 910 | 710 | 1010 | 510 | 720 | 960 | 935 | 440 | 710 | 820 | 1190 | 760 | 720 | 950 | 910 | 840 | 800 | 280 | 415 |
| Ta | 0.25 | 0.25 | 0.25 | 0.6 | 0.25 | 0.25 | 0.5 | 0.5 | 0.6 | 0.25 | 0.25 | 0.7 | 0.5 | 0.25 | 0.5 | 0.25 | 0.25 | 0.25 | . |
| Tb | 0.2 | 0.2 | 0.3 | 0.3 | 0.3 | 0.3 | 0.2 | 0.2 | 0.4 | 0.2 | 0.2 | 0.3 | 0.2 | 0.1 | 0.2 | 0.2 | 0.2 | 0.2 | . |
| Th | 2.9 | 6.6 | 4.9 | 8.1 | 5.1 | 4.3 | 4 | 4.1 | 8.9 | 3 | 2.7 | 3.4 | 2.1 | 1.2 | 2.4 | 2.3 | 2 | 1.7 | . |
| U | 0.8 | 2.9 | 1.2 | 2.7 | 3.1 | 1.6 | 1.1 | 0.4 | 2.3 | 0.9 | 1 | 1.8 | 1.2 | 0.8 | 1.5 | 1.2 | 1 | 0.6 | . |
| V | 52 | 54 | 48 | 48 | 38 | 52 | 50 | 40 | 64 | 34 | 30 | 30 | 26 | 30 | 28 | 28 | 28 | 200 | . |
| Y | 10 | 10 | 5 | 10 | 10 | 20 | 6 | 10 | 5 | 5 | 5 | 10 | 5 | 5 | 5 | 5 | 10 | 20 | 14 |
| Yb | 0.5 | 0.92 | 0.61 | 1.04 | 0.87 | 0.59 | 0.4 | 0.41 | 1.05 | 0.51 | 0.46 | 0.65 | 0.45 | 0.39 | 0.5 | 0.48 | 0.46 | 1.86 | . |
| Zn | 58 | 60 | 66 | 54 | 70 | 75 | 51 | 65 | 65 | 51 | 50 | 47 | 43 | 46 | 52 | 47 | 25 | 96 | 120 |
| Zr | 60 | 60 | 80 | 50 | 50 | 90 | 68 | 120 | 70 | 50 | 10 | 20 | 40 | 30 | 40 | 20 | 30 | 30 | 210 |
| X | 6967.66 | 6967.66 | 6982.7 | 6967.66 | 6967.66 | 6985.9 | 6986 | 6965.06 | 6967.66 | 6967.66 | 6967.66 | 6967.66 | 6967.66 | 6967.66 | 6967.66 | 6967.66 | 6967.66 | 6983.16 | 6970.352 |
| Y | 561.64 | 561.74 | 565.65 | 561.84 | 561.94 | 566.25 | 566.25 | 560.04 | 562.04 | 562.74 | 562.14 | 562.44 | 562.54 | 562.64 | 562.24 | 562.34 | 562.84 | 565.48 | 562.96 |

Metasediments

| Sample | HJO-86-111 | HJO-87-142.4 | HJO-86-112 | P463/5.5 | P467/7.2 | HJO-86-113 | HJO-87-142.5 | HJO-86-115 | P408/5.9 | P507/4.7 | HJO-86-109 | P453/7.3 | P469/5.3 | HJO-87-158 | P499/6.0 | HJO-87-147 | HJO-87-160.3 | PAN-86-24.1 | P529/11. | P467/31. |
|---|---|---|---|---|---|---|---|---|---|---|---|---|---|---|---|---|---|---|---|---|
| Rocktype | GRV | GRV | GRV | GRV | GRV | GRV | GRV | GRV | GRV | GRV | GRV | GRV | GRV | LOL | GRV | GRV | FY | GRV | GRV | GRV |
| SiO2 | 56.4 | 62.7 | 59.2 | 55.3 | 56.7 | 63.1 | 63.9 | 56.1 | 57.5 | 59.9 | 59.0 | 61.4 | 59.0 | 57.4 | 61.5 | 62.0 | 60.0 | 63.5 | 62.4 | 61.6 |
| TiO2 | 0.92 | 0.72 | 0.68 | 0.66 | 0.84 | 0.65 | 0.68 | 0.9 | 0.83 | 0.82 | 0.91 | 0.73 | 0.87 | 0.83 | 0.83 | 0.77 | 0.79 | 0.76 | 0.76 | 0.78 |
| Al2O3 | 13.9 | 14.3 | 13.6 | 16.7 | 16.1 | 13.2 | 14.5 | 17.2 | 17.2 | 16.6 | 16.7 | 16.4 | 17.4 | 20.5 | 17.3 | 17 | 18.2 | 15.4 | 16.4 | 17.1 |
| Fe2O3 | 12.5 | 7.2 | 10.8 | 7.77 | 11.4 | 9.18 | 6.85 | 11.9 | 9.15 | 9.2 | 10.4 | 8.02 | 9.65 | 7.4 | 7.25 | 7.71 | 7.89 | 8.31 | 7.62 | 7.25 |
| MnO | 0.17 | 0.09 | 0.17 | 0.14 | 0.14 | 0.15 | 0.08 | 0.1 | 0.1 | 0.12 | 0.09 | 0.09 | 0.11 | 0.07 | 0.09 | 0.08 | 0.07 | 0.07 | 0.07 | 0.09 |
| MgO | 5.78 | 5.38 | 5.34 | 5.19 | 4.72 | 4.61 | 4.58 | 4.47 | 4.29 | 3.87 | 3.85 | 3.82 | 3.79 | 3.76 | 3.62 | 3.54 | 3.50 | 3.49 | 3.49 | 3.49 |
| CaO | 3.24 | 3.19 | 3.5 | 6.25 | 3.22 | 3.74 | 2.57 | 2.06 | 2.14 | 2.07 | 1.65 | 2.41 | 1.44 | 0.92 | 1.59 | 1.49 | 1.35 | 1.93 | 2.08 | 1.51 |
| Na2O | 2.63 | 1.85 | 2.68 | 3.31 | 2.36 | 2.84 | 2.43 | 2.12 | 3.27 | 2.56 | 1.78 | 2.17 | 1.57 | 1.69 | 1.61 | 2.70 | 1.74 | 2.25 | 2.61 | 2.40 |
| K2O | 2.29 | 2.07 | 1.54 | 2.02 | 1.91 | 1.12 | 2.15 | 2.15 | 1.69 | 1.85 | 2.58 | 2.39 | 3.37 | 3.19 | 2.64 | 2.50 | 2.97 | 1.98 | 2.14 | 2.49 |
| P2O5 | 0.15 | 0.15 | 0.13 | 0.21 | 0.10 | 0.12 | 0.15 | 0.12 | 0.11 | 0.10 | 0.10 | 0.13 | 0.11 | 0.11 | 0.11 | 0.13 | 0.25 | 0.09 | 0.09 | 0.10 |
| LOI | 1.9 | 2.2 | 1.6 | 1.2 | 2.3 | 1.3 | 1.9 | 2.8 | 2.7 | 2.5 | 2.8 | 2.2 | 2.5 | 4.5 | 2.9 | 2.4 | 3.2 | 2.2 | 1.9 | 2.8 |
| Total | 99.91 | 99.88 | 99.26 | 98.78 | 99.80 | 100.02 | 99.82 | 99.89 | 98.98 | 99.63 | 99.83 | 99.79 | 99.78 | 100.34 | 99.39 | 100.31 | 99.99 | 100.01 | 99.59 | 99.58 |
| CO2 | 0.01 | 0.01 | 0.01 | 0.07 | 0.01 | 0.01 | 0.01 | 0.01 | 0.02 | 0.02 | 0.01 | 0.02 | 0.01 | 0.01 | 0.01 | 0.04 | 0.01 | 0.01 | 0.01 | 0.01 |
| B (ppm) | 30 | 48 | 220 | 5 | 110 | 10 | 21 | 70 | 30 | 50 | 120 | 70 | 160 | 96 | 40 | 25 | 59 | 10 | 40 | 220 |
| Ba | 670 | 686 | 450 | 820 | 310 | 400 | 1180 | 420 | 410 | 390 | 710 | 640 | 820 | 643 | 640 | 949 | 696 | 430 | 540 | 440 |
| Ce | 35 | . | 24 | 81 | 46 | 32 | . | 16 | 26 | 31 | 19 | 40 | 41 | . | 41 | . | . | 27 | 30 | 47 |
| Co | 39 | 37 | 34 | 30 | 47 | 31 | 25 | 40 | 36 | 39 | 39 | 39 | 37 | 16 | 36 | 35 | 55 | 33 | 29 | 35 |
| Cr | 490 | 383 | 470 | 130 | 410 | 530 | 337 | 280 | 240 | 280 | 290 | 280 | 280 | 273 | 300 | 284 | 256 | 260 | 220 | 320 |
| Cs | 13.3 | . | 5.2 | 10 | 17.1 | 3.7 | . | 6.4 | 12.2 | 22.2 | 6.4 | 27.7 | 10.2 | . | 1.7 | . | . | 11.2 | 14.4 | 5.7 |
| Cu | 100 | 69 | 32 | 54 | 110 | 49 | 53 | 90 | 75 | 59 | 67 | 81 | 74 | 54 | 57 | 57 | 68 | 64 | 53 | 57 |
| Dy | . | . | . | . | . | . | . | . | . | . | . | . | . | . | . | . | . | . | . | . |
| Er | . | . | . | . | . | . | . | . | . | . | . | . | . | . | . | . | . | . | . | . |
| Eu | 0.89 | . | 0.74 | 1.66 | 0.88 | 0.89 | . | 0.71 | 0.72 | 1.21 | 0.72 | 1.27 | 1.14 | . | 1.05 | . | . | 0.99 | 1.06 | 1.1 |
| Gd | . | . | . | . | . | . | . | . | . | . | . | . | . | . | . | . | . | . | . | . |
| Hf | 2.6 | . | 2.7 | 2.6 | 3.4 | 2.6 | . | 2.8 | 2.8 | 3.2 | 3.1 | 3.3 | 2.7 | . | 3.6 | . | . | 4.2 | 3.5 | 3.4 |
| Ho | . | . | . | . | . | . | . | . | . | . | . | . | . | . | . | . | . | . | . | . |
| La | 15.7 | . | 11 | 35.8 | 21.6 | 16.6 | . | 7.5 | 12.1 | 12.5 | 7.8 | 23.9 | 16.5 | . | 19.8 | . | . | 14.1 | 17.5 | 23.3 |
| Li | 68 | 40 | 44 | 64 | 48 | 32 | 30 | 58 | 57 | 48 | 76 | 38 | 56 | 27 | 44 | 52 | 32 | 66 | 56 | 44 |
| Lu | 0.36 | . | 0.28 | 0.26 | 0.34 | 0.28 | . | 0.28 | 0.29 | 0.3 | 0.32 | 0.33 | 0.29 | . | 0.31 | . | . | 0.29 | 0.27 | 0.36 |
| Nb | 20 | 5 | 20 | 10 | 20 | 10 | 5 | 30 | 20 | 20 | 20 | 30 | 30 | 16 | 20 | 5 | 20 | 20 | 5 | 10 |
| Nd | 15 | . | 9 | 32 | 19 | 14 | . | 9 | 12 | 14 | 8 | 18 | 11 | . | 14 | . | . | 11 | 13 | 21 |
| Ni | 160 | 150 | 150 | 55 | 260 | 160 | 91 | 110 | 130 | 140 | 120 | 150 | 140 | 49 | 150 | 110 | 190 | 99 | 110 | 140 |
| Pb | 1 | 9 | 8 | 16 | 12 | 1 | 9 | 12 | 6 | 88 | 4 | 8 | 24 | 10 | 1 | 11 | 8 | 4 | 12 | 16 |
| Pr | . | . | . | . | . | . | . | . | . | . | . | . | . | . | . | . | . | . | . | . |
| Rb | 100 | 78 | 80 | 110 | 130 | 50 | 91 | 100 | 80 | 120 | 120 | 120 | 160 | 119 | 110 | 85 | 124 | 110 | 100 | 120 |
| S% | 0.38 | 0.19 | 0.08 | 0.18 | 0.82 | 0.22 | 0.33 | 0.15 | 0.24 | 0.24 | 0.34 | 0.72 | 0.63 | 0.07 | 0.57 | 0.64 | 0.56 | 0.23 | 0.29 | 0.47 |
| Sc | 32.6 | . | 25.6 | 23 | 28 | 24.9 | . | 37.1 | 28.4 | 29 | 32.2 | 24.1 | 28.3 | . | 24.6 | . | . | 23.3 | 23.5 | 25.4 |
| Sm | 3.22 | . | 2.22 | 5.91 | 4.01 | 2.82 | . | 1.8 | 2.35 | 3.31 | 2.01 | 4.01 | 3.08 | . | 3.44 | . | . | 2.06 | 3.02 | 4.16 |
| Sr | 260 | 277 | 320 | 880 | 180 | 330 | 370 | 210 | 270 | 230 | 150 | 230 | 210 | 159 | 210 | 309 | 198 | 220 | 280 | 210 |
| Ta | 0.25 | . | 0.25 | 0.25 | 0.25 | 0.25 | . | 0.25 | 0.5 | 0.25 | 0.25 | 0.25 | 0.25 | . | 0.25 | . | . | 0.25 | 0.25 | 0.25 |
| Tb | 0.6 | . | 0.5 | 0.7 | 0.5 | 0.6 | . | 0.5 | 0.3 | 0.5 | 0.3 | 0.5 | 0.7 | . | 0.4 | . | . | 0.3 | 0.5 | 0.5 |
| Th | 2.3 | . | 3.4 | 7 | 5.5 | 3.1 | . | 4 | 3.6 | 4.2 | 4.2 | 5 | 3.8 | . | 5 | . | . | 4.3 | 4.5 | 6 |
| U | 1 | . | 1 | 1.1 | 1.8 | 0.9 | . | 1.1 | 1.3 | 1.2 | 1.4 | 1.2 | 1.2 | . | 1.8 | . | . | 1.6 | 1.5 | 1.9 |
| V | 200 | . | 180 | 170 | 200 | 180 | . | 260 | 220 | 200 | 220 | 180 | 190 | . | 170 | . | . | 170 | 160 | 170 |
| Y | 20 | 5 | 10 | 20 | 10 | 10 | 5 | 5 | 10 | 5 | 10 | 30 | 10 | 25 | 20 | 16 | 11 | 20 | 5 | 5 |
| Yb | 2.08 | . | 1.73 | 1.38 | 2.16 | 1.65 | . | 1.77 | 1.69 | 1.95 | 1.88 | 1.92 | 1.66 | . | 1.98 | . | . | 1.44 | 1.62 | 2.29 |
| Zn | 120 | 74 | 110 | 130 | 150 | 98 | 76 | 140 | 160 | 640 | 140 | 130 | 210 | 100 | 130 | 120 | 110 | 140 | 120 | 130 |
| Zr | 90 | 106 | 70 | 100 | 120 | 90 | 112 | 120 | 110 | 120 | 120 | 130 | 130 | 135 | 140 | 113 | 128 | 130 | 110 | 140 |
| X | 6984.04 | 6969.895 | 6983.92 | 6967.66 | 6967.66 | 6983.76 | 6969.9 | 6983.73 | 6987.566 | 6966.6 | 6984.19 | 6967.66 | 6967.66 | 6970.452 | 6967.66 | 6970.03 | 6970.452 | 6980.77 | 6965.06 | 6967.66 |
| Y | 564.91 | 562.77 | 565.03 | 560.64 | 560.9 | 565.15 | 562.764 | 565.18 | 560.832 | 560.48 | 564.78 | 559.5 | 561.14 | 562.915 | 564.14 | 563.03 | 562.028 | 564.75 | 560.54 | 560.9 |

Appen. Cont.

| | Metasediments | | | | | | | | | | | | | | | | | | | |
|---|---|---|---|---|---|---|---|---|---|---|---|---|---|---|---|---|---|---|---|---|
| Sample | P457/5.3 | P513/13. | P532/7.9 | HJO-87-141 | P464/8.2 | HJO-87-133 | P462/7.5 | P455/5.3 | P401/4.5 | HJO-87-122.1 | P509/5.9 | P521/9.7 | HJO-87-155.1 | HJO-86-108 | K-87-30 | P508/5.3 | HJO-87-134.4 | P531/9.1 | HJO-87-134.5 | HJO-87-162 |
| Rocktype | GRV | GRV | GRV | GRV | GRV | GRV | GRV | GRV | GRV | GRV | GRV | GRV | GRV | GRV | GRV | GRV | GRV | GRV | GRV | GRV |
| SiO2 | 66.5 | 63.0 | 63.7 | 63.3 | 69.1 | 60.4 | 62.6 | 64.9 | 65.1 | 66.3 | 64.6 | 67.1 | 61.6 | 64.0 | 58.0 | 66.6 | 64.3 | 68.4 | 66.4 | 60.6 |
| TiO2 | 0.76 | 0.7 | 0.74 | 0.74 | 0.62 | 0.8 | 0.77 | 0.77 | 0.77 | 0.64 | 0.63 | 0.65 | 0.78 | 0.73 | 0.75 | 0.64 | 0.72 | 0.64 | 0.65 | 0.48 |
| Al2O3 | 14.6 | 14.8 | 16.1 | 16.4 | 13.3 | 18.7 | 17.5 | 15.9 | 15 | 15 | 15.4 | 13.8 | 17.6 | 15.3 | 17.1 | 15 | 16 | 13.9 | 15.1 | 18.3 |
| Fe2O3 | 6.91 | 8.65 | 7.33 | 7.37 | 6.06 | 7.47 | 7 | 6.97 | 7.52 | 6.16 | 5.67 | 7.13 | 6.99 | 7.59 | 9.44 | 5.78 | 7.02 | 5.89 | 6.36 | 6.37 |
| MnO | 0.08 | 0.13 | 0.07 | 0.07 | 0.07 | 0.07 | 0.07 | 0.11 | 0.09 | 0.06 | 0.08 | 0.07 | 0.05 | 0.09 | 0.055 | 0.09 | 0.06 | 0.06 | 0.06 | 0.11 |
| MgO | 3.47 | 3.43 | 3.41 | 3.40 | 3.40 | 3.37 | 3.31 | 3.29 | 3.24 | 3.17 | 3.16 | 3.16 | 3.15 | 3.13 | 3.08 | 3.06 | 3.04 | 3.01 | 2.92 | 2.90 |
| CaO | 1.81 | 3.64 | 2.17 | 1.01 | 1.12 | 1.39 | 1.39 | 2.09 | 2.06 | 1.7 | 1.86 | 1.63 | 1.53 | 2.35 | 1.3 | 2.52 | 1.17 | 2.03 | 1.27 | 3.96 |
| Na2O | 2.16 | 2.06 | 2.69 | 2.07 | 1.75 | 2.31 | 2.04 | 1.86 | 2.80 | 2.89 | 3.50 | 1.70 | 3.23 | 2.88 | 4.84 | 3.57 | 2.42 | 2.97 | 2.60 | 4.11 |
| K2O | 2.06 | 2.10 | 1.97 | 2.72 | 1.64 | 2.55 | 2.73 | 2.22 | 1.59 | 1.90 | 1.90 | 2.11 | 3.01 | 1.72 | 2.56 | 1.33 | 2.47 | 1.86 | 2.12 | 1.90 |
| P2O5 | 0.07 | 0.12 | 0.08 | 0.13 | 0.09 | 0.12 | 0.13 | 0.10 | 0.09 | 0.11 | 0.09 | 0.10 | 0.12 | 0.10 | 0.12 | 0.10 | 0.12 | 0.08 | 0.11 | 0.23 |
| LOI | 1.7 | 1.3 | 1.9 | 2.5 | 2.7 | 3.1 | 2.5 | 2.1 | 2.0 | 2.0 | 2.2 | 2.2 | 2.0 | 1.7 | 1.4 | 1.5 | 2.6 | 1.2 | 2.4 | 0.9 |
| Total | 100.12 | 99.94 | 100.11 | 99.75 | 99.85 | 100.26 | 100.08 | 100.29 | 100.26 | 99.93 | 99.05 | 99.68 | 100.06 | 99.59 | 98.64 | 100.23 | 99.94 | 100.00 | 99.98 | 99.89 |
| CO2 | 0.02 | 0.01 | 0.01 | 0.01 | 0.01 | 0.01 | 0.01 | 0.01 | 0.02 | 0.02 | 0.01 | 0.03 | 0.01 | 0.01 | 0.01 | 0.04 | 0.01 | 0.01 | 0.01 | 0.01 |
| B (ppm) | 20 | 1100 | 5 | 46 | 20 | 55 | 520 | 30 | 20 | 16 | 10 | 130 | 140 | 180 | 390 | 20 | 40 | 5 | 34 | 5 |
| Ba | 410 | 640 | 570 | 758 | 330 | 659 | 640 | 430 | 370 | 564 | 900 | 360 | 672 | 460 | 352 | 350 | 751 | 390 | 671 | 509 |
| Ce | 53 | 39 | 28 | . | 39 | . | 61 | 33 | 31 | . | 44 | 32 | . | 35 | 35.4 | 45 | . | 33 | . | . |
| Co | 34 | 35 | 30 | 27 | 19 | 21 | 32 | 32 | 29 | 13 | 26 | 32 | 36 | 31 | 22 | 24 | 23 | 24 | 19 | 19 |
| Cr | 290 | 290 | 190 | 288 | 180 | 263 | 240 | 280 | 250 | 266 | 210 | 370 | 287 | 240 | 180 | 190 | 277 | 210 | 259 | 50 |
| Cs | 5.5 | 13.9 | 6.4 | . | 8.5 | . | 19.6 | 2.2 | 5.5 | . | 3.6 | 6.8 | . | 6.6 | 89 | 7.2 | . | 8.7 | . | . |
| Cu | 12 | 65 | 76 | 58 | 55 | 56 | 57 | 49 | 69 | 27 | 57 | 89 | 73 | 55 | 29 | 54 | 49 | 28 | 42 | 12 |
| Dy | . | . | . | . | . | . | . | . | . | . | . | . | . | . | 1.5 | . | . | . | . | . |
| Er | . | . | . | . | . | . | . | . | . | . | . | . | . | . | 0.5 | . | . | . | . | . |
| Eu | 1.1 | 0.95 | 0.62 | . | 0.72 | . | 1.31 | 0.99 | 0.89 | . | 0.87 | 0.39 | . | 0.36 | 1.27 | 0.96 | . | 0.5 | . | . |
| Gd | . | . | . | . | . | . | . | . | . | . | . | . | . | . | 2.1 | . | . | . | . | . |
| Hf | 3.4 | 2.8 | 3.5 | . | 2.4 | . | 3.3 | 3 | 3 | . | 3.4 | 4.8 | . | 4.2 | 3 | 3.3 | . | 3.4 | . | . |
| Ho | . | . | . | . | . | . | . | . | . | . | . | . | . | . | 0.23 | . | . | . | . | . |
| La | 21.7 | 15.1 | 16.3 | . | 18.2 | . | 27 | 19.4 | 13.7 | . | 22.5 | 19.3 | . | 20.4 | 17.5 | 23.5 | . | 20.2 | . | . |
| Li | 50 | 46 | 48 | 43 | 52 | 42 | 62 | 26 | 48 | 48 | 50 | 28 | 56 | 64 | 210 | 44 | 41 | 62 | 39 | 58 |
| Lu | 0.36 | 0.25 | 0.24 | . | 0.24 | . | 0.26 | 0.34 | 0.26 | . | 0.27 | 0.3 | . | 0.27 | 0.025 | 0.24 | . | 0.25 | . | . |
| Nb | 10 | 5 | 20 | 15 | 20 | 17 | 20 | 10 | 10 | 5 | 10 | 10 | 16 | 10 | 5 | 5 | 13 | 20 | 15 | 15 |
| Nd | 16 | 9 | 12 | . | 11 | . | 19 | 15 | 14 | . | 18 | 13 | . | 16 | 18.3 | 18 | . | 15 | . | . |
| Ni | 130 | 100 | 99 | 82 | 130 | 62 | 120 | 150 | 120 | 29 | 81 | 140 | 110 | 90 | 89 | 95 | 71 | 92 | 51 | 17 |
| Pb | 24 | 20 | 8 | 10 | 16 | 6 | 20 | 16 | 20 | 6 | 24 | 40 | 9 | 8 | 1 | 20 | 6 | 8 | 6 | 7 |
| Pr | . | . | . | . | . | . | . | . | . | . | . | . | . | . | 4.5 | . | . | . | . | . |
| Rb | 110 | 100 | 110 | 85 | 100 | 87 | 110 | 90 | 70 | 74 | 80 | 90 | 126 | 90 | 192 | 60 | 62 | 130 | 131 | 116 |
| S% | 0.1 | 0.52 | 0.33 | 0.31 | 0.34 | 0.09 | 0.48 | 0.24 | 0.43 | 0.02 | 0.28 | 0.74 | 0.45 | 0.33 | 0.3 | 0.34 | 0.17 | 0.21 | 0.11 | 0.2 |
| Sc | 23.8 | 27.7 | 22.8 | . | 10.4 | . | 21.8 | 21.5 | 19.9 | . | 19.1 | 18.2 | . | 23.9 | 20 | 18.4 | . | 18.6 | . | . |
| Sm | 3.84 | 2.67 | 2.77 | . | 2.64 | . | 4.17 | 3.41 | 2.8 | . | 3.56 | 2.98 | . | 3.24 | 3.5 | 3.51 | . | 2.87 | . | . |
| Sr | 190 | 450 | 340 | 185 | 120 | 231 | 300 | 170 | 210 | 257 | 450 | 90 | 414 | 300 | 224 | 340 | 244 | 290 | 254 | 520 |
| Ta | 0.25 | 0.25 | 0.5 | . | 0.25 | . | 0.25 | 0.25 | 0.5 | . | 0.25 | 0.6 | . | 0.9 | 1 | 0.25 | . | 0.25 | . | . |
| Tb | 0.6 | 0.5 | 0.3 | . | 0.4 | . | 0.5 | 0.4 | 0.6 | . | 0.4 | 0.5 | . | 0.4 | 0.3 | 0.4 | . | 0.5 | . | . |
| Th | 5.1 | 3.9 | 3.1 | . | 4.7 | . | 6.3 | 4.8 | 4 | . | 5.3 | 5.5 | . | 4.4 | 4.8 | 4.8 | . | 3.6 | . | . |
| U | 1.6 | 0.7 | 1 | . | 1.7 | . | 1.9 | 1.6 | 1.6 | . | 1.7 | 1.7 | . | 1.3 | 1.3 | 1.3 | . | 1.2 | . | . |
| V | 150 | 190 | 170 | . | 110 | . | 160 | 150 | 150 | . | 130 | 120 | . | 170 | 180 | 140 | . | 140 | . | . |
| Y | 5 | 10 | 10 | 33 | 30 | 34 | 10 | 30 | 20 | 17 | 10 | 20 | 12 | 10 | 5 | 30 | 29 | 10 | 5 | 5 |
| Yb | 2.17 | 1.64 | 1.45 | . | 1.47 | . | 1.75 | 2.07 | 1.67 | . | 1.65 | 1.78 | . | 1.63 | 0.3 | 1.69 | . | 1.39 | . | . |
| Zn | 130 | 120 | 98 | 95 | 140 | 80 | 150 | 150 | 140 | 94 | 110 | 230 | 110 | 120 | 90 | 120 | 100 | 96 | 94 | 110 |
| Zr | 130 | 90 | 90 | 120 | 120 | 120 | 160 | 120 | 110 | 110 | 100 | 130 | 148 | 120 | 107 | 110 | 119 | 90 | 109 | 110 |
| X | 6967.66 | 6984.365 | 6965.06 | 6969.87 | 6967.66 | 6969.595 | 6967.66 | 6967.66 | 6987.76 | 6969.555 | 6966.6 | 6965.06 | 6970.348 | 6984.5 | 6991.8 | 6966.6 | 6969.548 | 6965.06 | 6969.655 | 6970.445 |
| Y | 559.94 | 564.42 | 560.84 | 562.83 | 560.74 | 562.61 | 560.54 | 559.74 | 560.364 | 562.63 | 560.38 | 559.74 | 562.964 | 564.64 | 562.1 | 560.43 | 562.674 | 560.74 | 562.67 | 563.04 |

Metasediments

| Sample | HJO-87-140.3 | P535/13. | HJO-87-136.1 | P454/5.7 | HJO-87-140.4 | HJO-87-121 | HJO-87-160.1 | HJO-87-148 | HJO-87-134.2 | P459/8.0 | HJO-87-140.1 | HJO-87-165 | HJO-87-142.2 | P456/3.9 | HJO-87-126.1 | HJO-86-110 | HJO-87-142.1 | HJO-87-142.3 | P413/3.7 | HJO-87-139.2 |
|---|---|---|---|---|---|---|---|---|---|---|---|---|---|---|---|---|---|---|---|---|
| Rocktype | GRV | GRV | GRV | GRV | GRV | GRV | GRV | GRV | GRV | GRV | GRV | GRV | GRV | GRV | GRV | GRV | GRV | GRV | GRV | GRV |
| SiO2 | 65.7 | 67.7 | 65.5 | 66.4 | 66.3 | 65.3 | 59.2 | 67.1 | 66.7 | 63.2 | 67.7 | 69.6 | 67.9 | 67.4 | 66.2 | 64.0 | 69.0 | 69.0 | 63.1 | 64.0 |
| TiO2 | 0.65 | 0.64 | 0.68 | 0.7 | 0.67 | 0.72 | 0.67 | 0.63 | 0.64 | 0.71 | 0.6 | 0.6 | 0.62 | 0.65 | 0.65 | 0.65 | 0.59 | 0.6 | 0.58 | 0.44 |
| Al2O3 | 14.8 | 13.1 | 15.6 | 14.1 | 15.4 | 15.4 | 20 | 14.8 | 15.1 | 17.3 | 14.6 | 13.5 | 14.8 | 14.6 | 15.6 | 15.6 | 14.2 | 14.3 | 15.9 | 15.6 |
| Fe2O3 | 6.5 | 6.92 | 6.44 | 6.95 | 6.22 | 6.3 | 5.74 | 5.94 | 6.43 | 5.81 | 6.12 | 5.93 | 5.92 | 5.64 | 5.91 | 7.24 | 5.69 | 5.85 | 5.35 | 4.83 |
| MnO | 0.06 | 0.06 | 0.07 | 0.09 | 0.06 | 0.06 | 0.1 | 0.05 | 0.06 | 0.06 | 0.06 | 0.04 | 0.05 | 0.15 | 0.05 | 0.09 | 0.05 | 0.05 | 0.09 | 0.09 |
| MgO | 2.89 | 2.86 | 2.85 | 2.84 | 2.83 | 2.78 | 2.78 | 2.76 | 2.75 | 2.73 | 2.69 | 2.69 | 2.64 | 2.62 | 2.61 | 2.61 | 2.57 | 2.54 | 2.52 | 2.52 |
| CaO | 1.4 | 2.08 | 1.43 | 2.71 | 1.53 | 1.87 | 4.83 | 1.75 | 1.29 | 2.83 | 1.41 | 1.08 | 1.33 | 3.42 | 1.55 | 2.29 | 1.36 | 1.46 | 3.9 | 3.7 |
| Na2O | 2.57 | 2.68 | 2.44 | 2.52 | 2.69 | 2.90 | 3.15 | 2.88 | 2.26 | 3.10 | 2.79 | 2.66 | 2.73 | 2.16 | 3.17 | 3.39 | 2.73 | 2.63 | 4.55 | 4.18 |
| K2O | 2.05 | 1.90 | 2.90 | 1.61 | 1.99 | 2.30 | 1.65 | 2.27 | 2.83 | 2.86 | 2.02 | 1.81 | 2.10 | 0.97 | 2.23 | 2.62 | 1.83 | 2.02 | 1.90 | 2.88 |
| P2O5 | 0.11 | 0.08 | 0.12 | 0.10 | 0.11 | 0.14 | 0.18 | 0.11 | 0.11 | 0.15 | 0.12 | 0.08 | 0.11 | 0.16 | 0.11 | 0.15 | 0.10 | 0.11 | 0.16 | 0.15 |
| LOI | 2.1 | 1.5 | 2.1 | 1.6 | 2.2 | 2.5 | 1.6 | 1.5 | 1.9 | 1.5 | 2.2 | 1.9 | 1.9 | 2.2 | 2.2 | 1.2 | 1.9 | 1.8 | 0.9 | 1.2 |
| Total | 98.81 | 99.49 | 100.11 | 99.64 | 100.03 | 100.24 | 99.92 | 99.83 | 100.10 | 100.22 | 100.27 | 99.92 | 100.13 | 99.93 | 100.31 | 99.80 | 99.97 | 100.33 | 98.98 | 99.55 |
| CO2 | 0.01 | 0.01 | 0.01 | 0.01 | 0.01 | 0.27 | 0.01 | 0.01 | 0.01 | 0.01 | 0.01 | 0.01 | 0.01 | 0.01 | 0.01 | 0.01 | 0.01 | 0.01 | 0.01 | 0.83 |
| B (ppm) | 16 | 60 | 48 | 5 | 20 | 30 | 66 | 40 | 21 | 20 | 43 | 28 | 25 | 5 | 49 | 70 | 22 | 24 | 5 | 5 |
| Ba | 563 | 300 | 678 | 230 | 608 | 727 | 312 | 598 | 826 | 660 | 586 | 527 | 659 | 220 | 762 | 760 | 543 | 611 | 690 | 901 |
| Ce | . | 35 | . | 30 | . | . | . | . | . | 51 | . | . | . | 49 | . | 46 | . | . | 43 | . |
| Co | 29 | 25 | 26 | 29 | 20 | 13 | 26 | 26 | 23 | 27 | 21 | 22 | 30 | 34 | 18 | 23 | 26 | 21 | 17 | 17 |
| Cr | 266 | 220 | 259 | 300 | 259 | 250 | 166 | 218 | 243 | 190 | 229 | 246 | 233 | 250 | 232 | 140 | 240 | 244 | 100 | 99 |
| Cs | . | 5.1 | . | 1.6 | . | . | . | . | . | 7.4 | . | . | . | 4.4 | . | 6.8 | . | . | 28.7 | . |
| Cu | 51 | 160 | 44 | 76 | 40 | 30 | 31 | 48 | 50 | 53 | 43 | 49 | 48 | 72 | 46 | 46 | 45 | 39 | 23 | 16 |
| Dy | . | . | . | . | . | . | . | . | . | . | . | . | . | . | . | . | . | . | . | . |
| Er | . | . | . | . | . | . | . | . | . | . | . | . | . | . | . | . | . | . | . | . |
| Eu | . | 0.61 | . | 0.66 | . | . | . | . | . | 1.14 | . | . | . | 1.31 | . | 1.07 | . | . | 0.98 | . |
| Gd | . | . | . | . | . | . | . | . | . | . | . | . | . | . | . | . | . | . | . | . |
| Hf | . | 2.6 | . | 3.9 | . | . | . | . | . | 3.8 | . | . | . | 4 | . | 3.4 | . | . | 3.1 | . |
| Ho | . | . | . | . | . | . | . | . | . | . | . | . | . | . | . | . | . | . | . | . |
| La | . | 16.6 | . | 19.5 | . | . | . | . | . | 22.5 | . | . | . | 24.3 | . | 23.1 | . | . | 22.3 | . |
| Li | 41 | 58 | 31 | 24 | 47 | 38 | 34 | 41 | 45 | 44 | 37 | 35 | 35 | 32 | 34 | 60 | 33 | 38 | 34 | 43 |
| Lu | . | 0.26 | . | 0.29 | . | . | . | . | . | 0.27 | . | . | . | 0.32 | . | 0.26 | . | . | 0.19 | . |
| Nb | 5 | 20 | 20 | 20 | 5 | 5 | 16 | 14 | 14 | 5 | 5 | 16 | 5 | 20 | 19 | 10 | 23 | 15 | 20 | 23 |
| Nd | . | 12 | . | 16 | . | . | . | . | . | 14 | . | . | . | 22 | . | 19 | . | . | 19 | . |
| Ni | 88 | 94 | 75 | 110 | 63 | 26 | 64 | 75 | 62 | 84 | 55 | 59 | 93 | 170 | 52 | 50 | 80 | 61 | 48 | 32 |
| Pb | 7 | 8 | 21 | 16 | 7 | 10 | 8 | 11 | 7 | 28 | 6 | 6 | 9 | 24 | 7 | 16 | 9 | 8 | 24 | 11 |
| Pr | . | . | . | . | . | . | . | . | . | . | . | . | . | . | . | . | . | . | . | . |
| Rb | 86 | 140 | 106 | 110 | 70 | 69 | 95 | 86 | 96 | 130 | 86 | 75 | 83 | 60 | 89 | 120 | 63 | 81 | 70 | 90 |
| S% | 0.39 | 0.55 | 0.32 | 1.02 | 0.43 | 0.13 | 0.38 | 0.39 | 0.18 | 0.39 | 0.24 | 0.18 | 0.36 | 0.63 | 0.3 | 0.29 | 0.33 | 0.3 | 0.5 | 0.005 |
| Sc | . | 16.3 | . | 14.8 | . | . | . | . | . | 17.4 | . | . | . | 18.3 | . | 18.2 | . | . | 11.8 | . |
| Sm | . | 2.67 | . | 3.07 | . | . | . | . | . | 3.79 | . | . | . | 3.46 | . | 3.78 | . | . | 3.73 | . |
| Sr | 268 | 280 | 232 | 210 | 291 | 314 | 442 | 503 | 265 | 460 | 290 | 238 | 313 | 210 | 351 | 540 | 307 | 302 | 710 | 712 |
| Ta | . | 0.25 | . | 0.25 | . | . | . | . | . | 0.25 | . | . | . | 0.25 | . | 0.25 | . | . | 0.25 | . |
| Tb | . | 0.5 | . | 0.5 | . | . | . | . | . | 0.5 | . | . | . | 0.4 | . | 0.6 | . | . | 0.3 | . |
| Th | . | 3.7 | . | 5.6 | . | . | . | . | . | 7.4 | . | . | . | 5 | . | 6.5 | . | . | 5.9 | . |
| U | . | 0.9 | . | 2.5 | . | . | . | . | . | 2.6 | . | . | . | 0.05 | . | 2 | . | . | 1.8 | . |
| V | . | 140 | . | 120 | . | . | . | . | . | 130 | . | . | . | 120 | . | 140 | . | . | 110 | . |
| Y | 5 | 5 | 11 | 50 | 23 | 18 | 17 | 25 | 13 | 10 | 5 | 5 | 5 | 10 | 28 | 10 | 14 | 17 | 10 | 20 |
| Yb | . | 1.34 | . | 1.5 | . | . | . | . | . | 1.37 | . | . | . | 2.12 | . | 1.66 | . | . | 1.09 | . |
| Zn | 86 | 77 | 220 | 140 | 65 | 92 | 72 | 92 | 94 | 110 | 110 | 86 | 96 | 96 | 110 | 110 | 93 | 91 | 100 | 74 |
| Zr | 100 | 100 | 113 | 180 | 144 | 124 | 121 | 119 | 107 | 150 | 98 | 103 | 113 | 130 | 137 | 110 | 113 | 127 | 110 | 94 |
| X | 6969.812 | 6965.06 | 6969.508 | 6967.66 | 6969.816 | 6969.635 | 6970.46 | 6970.055 | 6969.548 | 6967.66 | 6969.808 | 6970.388 | 6969.886 | 6967.66 | 6969.774 | 6984.12 | 6969.882 | 6969.89 | 6987.42 | 6969.812 |
| Y | 562.856 | 561.05 | 562.742 | 559.64 | 562.85 | 562.76 | 562.03 | 562.944 | 562.686 | 560.14 | 562.872 | 563.065 | 562.775 | 559.84 | 562.84 | 564.83 | 562.776 | 562.772 | 561.184 | 562.92 |

Appen. Cont.

Metasediments

| Sample | HJO-86-120 | HJO-87-142.6 | HJO-87-125.3 | P461/3.7 | HJO-87-134.3 | HJO-87-161 | HJO-87-140.6 | PAN-86-31 | HJO-87-140.5 | HJO-86-119 | HJO-87-125.2 | HJO-87-151 | P512/20. | P460/8.2 | HJO-86-106 | P571/30. | P458/6.7 | P419/6.5 | HJO-86-103 | PAN-86-18 |
|---|---|---|---|---|---|---|---|---|---|---|---|---|---|---|---|---|---|---|---|---|
| Rocktype | GRV | GRV | GRV | GRV | GRV | GRV | GRV | GRV | GRV | GRV | GRV | GRV | GRV | GRV | GRV | GRV | GRV | GRV | GRV | GRV |
| SiO2 | 65.6 | 68.6 | 69.1 | 60.0 | 68.4 | 62.3 | 69.7 | 60.7 | 68.3 | 63.4 | 65.4 | 63.4 | 65.9 | 66.6 | 55.5 | 66.8 | 66.1 | 64.9 | 67.2 | 67.0 |
| TiO2 | 0.6 | 0.61 | 0.58 | 0.54 | 0.61 | 0.53 | 0.55 | 0.87 | 0.59 | 0.62 | 0.42 | 0.65 | 0.57 | 0.48 | 0.62 | 0.46 | 0.43 | 0.42 | 0.53 | 0.48 |
| Al2O3 | 13.5 | 14.4 | 13.8 | 18.3 | 14.5 | 18.8 | 14.1 | 20 | 14.5 | 15.2 | 15.1 | 16.4 | 16.1 | 15.3 | 19.4 | 15.6 | 15.4 | 14.7 | 15.8 | 16.3 |
| Fe2O3 | 9.19 | 5.55 | 5.81 | 6.43 | 5.72 | 5.44 | 5.35 | 6.3 | 5.74 | 8.78 | 4.65 | 6.52 | 5.69 | 4.55 | 7.93 | 4.58 | 4.9 | 7.28 | 5.34 | 4.79 |
| MnO | 0.15 | 0.05 | 0.05 | 0.11 | 0.05 | 0.09 | 0.05 | 0.07 | 0.05 | 0.12 | 0.09 | 0.09 | 0.08 | 0.07 | 0.21 | 0.1 | 0.1 | 0.12 | 0.06 | 0.04 |
| MgO | 2.51 | 2.50 | 2.50 | 2.49 | 2.49 | 2.49 | 2.47 | 2.38 | 2.34 | 2.31 | 2.30 | 2.18 | 2.15 | 2.12 | 1.98 | 1.94 | 1.77 | 1.61 | 1.61 | 1.48 |
| CaO | 2.4 | 1.55 | 1.62 | 5.1 | 1.61 | 2.42 | 1.54 | 1.4 | 1.52 | 2.85 | 3.78 | 2.8 | 2.92 | 2.72 | 4.33 | 4.2 | 2.68 | 1.76 | 1.7 | 2.81 |
| Na2O | 2.91 | 2.82 | 2.77 | 3.15 | 2.99 | 3.07 | 2.98 | 1.79 | 3.01 | 3.59 | 3.47 | 4.76 | 3.99 | 3.74 | 1.57 | 2.96 | 3.93 | 3.22 | 3.14 | 3.54 |
| K2O | 1.75 | 1.92 | 2.08 | 2.14 | 1.97 | 2.58 | 1.70 | 3.43 | 1.89 | 2.17 | 2.95 | 2.37 | 1.99 | 2.51 | 3.69 | 1.77 | 2.95 | 4.12 | 2.85 | 2.25 |
| P2O5 | 0.12 | 0.10 | 0.11 | 0.22 | 0.11 | 0.24 | 0.10 | 0.19 | 0.10 | 0.17 | 0.15 | 0.24 | 0.13 | 0.16 | 0.39 | 0.15 | 0.14 | 0.16 | 0.15 | 0.10 |
| LOI | 1.3 | 1.9 | 1.9 | 1.0 | 1.7 | 2.0 | 1.5 | 3.1 | 1.9 | 0.9 | 1.7 | 0.6 | 0.8 | 1.0 | 3.1 | 1.1 | 0.9 | 1.3 | 1.6 | 1.1 |
| Total | 100.04 | 99.95 | 100.35 | 99.48 | 100.15 | 99.96 | 100.08 | 100.21 | 99.97 | 100.06 | 100.01 | 100.03 | 100.29 | 99.25 | 98.70 | 99.64 | 99.33 | 99.60 | 100.00 | 99.87 |
| CO2 | 0.01 | 0.01 | 0.02 | 0.01 | 0.01 | 0.01 | 0.01 | 0.01 | 0.01 | 0.01 | 1.08 | 0.01 | 0.01 | 0.01 | 0.01 | 0.03 | 0.44 | 0.02 | 0.01 | 0.01 |
| B (ppm) | 60 | 20 | 21 | 5 | 25 | 13 | 27 | 80 | 24 | 5 | 5 | 5 | 210 | 5 | 1900 | 20 | 5 | 5 | 100 | 5 |
| Ba | 560 | 561 | 500 | 730 | 561 | 839 | 504 | 780 | 571 | 690 | 970 | 707 | 710 | 920 | 1710 | 1100 | 1160 | 1380 | 990 | 780 |
| Ce | 43 | . | . | 59 | . | . | . | 36 | . | 51 | . | . | 64 | 50 | 111 | 58 | 60 | 48 | 55 | 47 |
| Co | 26 | 29 | 28 | 13 | 25 | 16 | 26 | 26 | 25 | 21 | 17 | 20 | 22 | 20 | 13 | 17 | 14 | 9.5 | 17 | 16 |
| Cr | 190 | 237 | 236 | 49 | 240 | 59 | 219 | 140 | 215 | 97 | 93 | 63 | 100 | 100 | 32 | 94 | 72 | 24 | 67 | 67 |
| Cs | 6.3 | . | . | 6.8 | . | . | . | 8.1 | . | 6.9 | . | . | 3.4 | 3.9 | 9.6 | 8.7 | 4.9 | 6.5 | 11.8 | 7.6 |
| Cu | 54 | 57 | 58 | 30 | 52 | 12 | 45 | 38 | 49 | 46 | 20 | 45 | 45 | 38 | 29 | 79 | 41 | 56 | 36 | 31 |
| Dy | . | . | . | . | . | . | . | . | . | . | . | . | . | . | . | . | . | . | . | . |
| Er | . | . | . | . | . | . | . | . | . | . | . | . | . | . | . | . | . | . | . | . |
| Eu | 0.88 | . | . | 1.01 | . | . | . | 0.83 | . | 1.3 | . | . | 1.26 | 1 | 1.13 | 1.17 | 0.64 | 0.74 | 0.79 | 0.66 |
| Gd | . | . | . | . | . | . | . | . | . | . | . | . | . | . | . | . | . | . | . | . |
| Hf | 3.1 | . | . | 2.9 | . | . | . | 4.1 | . | 3.2 | . | . | 3.1 | 3.6 | 7.8 | 3.5 | 2.9 | 3.6 | 5 | 4.4 |
| Ho | . | . | . | . | . | . | . | . | . | . | . | . | . | . | . | . | . | . | . | . |
| La | 21.8 | . | . | 26.7 | . | . | . | 20.4 | . | 26.2 | . | . | 29.2 | 23.9 | 61 | 37.3 | 27.9 | 26.1 | 33.6 | 26.8 |
| Li | 42 | 38 | 27 | 52 | 41 | 37 | 36 | 100 | 35 | 44 | 60 | 31 | 36 | 34 | 40 | 26 | 46 | 22 | 44 | 36 |
| Lu | 0.25 | . | . | 0.28 | . | . | . | 0.31 | . | 0.28 | . | . | 0.28 | 0.18 | 0.36 | 0.19 | 0.17 | 0.18 | 0.25 | 0.19 |
| Nb | 10 | 15 | 5 | 40 | 5 | 20 | 28 | 20 | 12 | 10 | 5 | 5 | 20 | 20 | 20 | 10 | 10 | 10 | 20 | 10 |
| Nd | 18 | . | . | 20 | . | . | . | 19 | . | 22 | . | . | 19 | 16 | 44 | 24 | 16 | 20 | 24 | 21 |
| Ni | 65 | 79 | 67 | 21 | 75 | 19 | 74 | 55 | 73 | 39 | 33 | 21 | 44 | 63 | 21 | 52 | 47 | 20 | 29 | 31 |
| Pb | 16 | 9 | 8 | 16 | 6 | 6 | 8 | 12 | 8 | 12 | 9 | 11 | 24 | 14 | 16 | 20 | 20 | 24 | 20 | 20 |
| Pr | . | . | . | . | . | . | . | . | . | . | . | . | . | . | . | . | . | . | . | . |
| Rb | 90 | 77 | 75 | 100 | 82 | 96 | 73 | 130 | 72 | 90 | 99 | 79 | 90 | 100 | 160 | 70 | 120 | 180 | 130 | 100 |
| S% | 0.38 | 0.43 | 0.26 | 0.25 | 0.32 | 0.16 | 0.4 | 0.19 | 0.39 | 0.39 | 0.005 | 0.14 | 0.47 | 0.3 | 0.005 | 0.79 | 0.31 | 0.59 | 0.26 | 0.28 |
| Sc | 18.4 | . | . | 11.7 | . | . | . | 26.3 | . | 16.9 | . | . | 15.9 | 10.8 | 8 | 11.1 | 11.9 | 8.2 | 12 | 11.4 |
| Sm | 3.39 | . | . | 3.97 | . | . | . | 3.2 | . | 4.19 | . | . | 4.28 | 3.52 | 8.55 | 5.52 | 3.73 | 3.54 | 4.52 | 3.97 |
| Sr | 410 | 331 | 311 | 600 | 323 | 344 | 354 | 400 | 341 | 570 | 598 | 670 | 580 | 720 | 1120 | 690 | 880 | 310 | 720 | 770 |
| Ta | 0.5 | . | . | 0.25 | . | . | . | 0.25 | . | 0.25 | . | . | 0.25 | 0.25 | 0.8 | 0.25 | 0.25 | 0.25 | 0.25 | 0.25 |
| Tb | 0.6 | . | . | 0.8 | . | . | . | 0.4 | . | 0.5 | . | . | 0.5 | 0.3 | 0.9 | 0.7 | 0.4 | 0.4 | 0.7 | 0.2 |
| Th | 4.5 | . | . | 5.5 | . | . | . | 7.5 | . | 5.7 | . | . | 6.5 | 7.4 | 19 | 9.8 | 8 | 8.2 | 7.8 | 6.3 |
| U | 1.5 | . | . | 1.7 | . | . | . | 2.2 | . | 1.9 | . | . | 1.5 | 1.9 | 2.7 | 2.9 | 2.6 | 2.6 | 2.6 | 2.2 |
| V | 140 | . | . | 110 | . | . | . | 190 | . | 140 | . | . | 120 | 90 | 120 | 94 | 84 | 78 | 100 | 100 |
| Y | 10 | 5 | 25 | 5 | 5 | 21 | 5 | 10 | 13 | 20 | 5 | 16 | 5 | 5 | 20 | 5 | 10 | 5 | 5 | 5 |
| Yb | 1.64 | . | . | 1.46 | . | . | . | 1.71 | . | 1.68 | . | . | 1.45 | 1.17 | 2 | 1.02 | 0.85 | 1.09 | 1.43 | 1.12 |
| Zn | 110 | 85 | 98 | 130 | 96 | 83 | 88 | 170 | 87 | 100 | 72 | 70 | 100 | 100 | 120 | 97 | 160 | 120 | 100 | 120 |
| Zr | 100 | 112 | 121 | 130 | 116 | 100 | 106 | 110 | 111 | 110 | 84 | 112 | 140 | 110 | 250 | 120 | 90 | 130 | 130 | 110 |
| X | 6983.01 | 6969.902 | 6969.496 | 6967.66 | 6969.544 | 6970.468 | 6969.818 | 6981 | 6969.817 | 6983.12 | 6969.492 | 6970.23 | 6984.325 | 6967.66 | 6984.89 | 6967.66 | 6967.66 | 6987.34 | 6984.86 | 6984.1 |
| Y | 565.47 | 562.758 | 562.7 | 560.44 | 562.678 | 563.024 | 562.844 | 564.98 | 562.847 | 565.49 | 562.702 | 563.02 | 564.425 | 560.34 | 564.34 | 559.355 | 560.04 | 561.6 | 564.08 | 565.14 |

Metasediments

| Sample | P420/2.8 | PAN-86-10 | KJP-87-77 | P429/5.3 | HJO-86-104 | P428/5.9 | P430/4.5 | HJO-86-35 | P410/15. | P411/12. | PAN-86-32 | HJO-86-114 | HJO-86-34 | HJO-86-36 | PAN-86-19 |
|---|---|---|---|---|---|---|---|---|---|---|---|---|---|---|---|
| Rocktype | GRV | GRV | GRAKL | GRV | GRV | GRV | GRV | FEMUO | FEMUO | FEMUO | FEMUO | FEMUO | FEMUO | FEMUO | FEMUO |
| SiO2 | 66.3 | 67.1 | 55.3 | 67.8 | 72.4 | 66.3 | 67.5 | 44.6 | 51.8 | 59.7 | 66.9 | 50.7 | 49.4 | 49.3 | 53.1 |
| TiO2 | 0.37 | 0.56 | 0.92 | 0.35 | 0.34 | 0.38 | 0.35 | 0.32 | 0.47 | 0.58 | 0.21 | 0.23 | 0.19 | 0.12 | 0.34 |
| Al2O3 | 15.4 | 16.2 | 18.7 | 15.7 | 15 | 16.1 | 15.5 | 8.65 | 12.2 | 15.3 | 5.86 | 5.76 | 4.2 | 3.05 | 8.69 |
| Fe2O3 | 4.56 | 3.52 | 8.68 | 3.23 | 3.81 | 3.54 | 4.29 | 33.8 | 25.4 | 11.1 | 19 | 39.3 | 39.6 | 43.5 | 29 |
| MnO | 0.13 | 0.05 | 0.18 | 0.14 | 0.04 | 0.49 | 0.58 | 0.23 | 0.29 | 0.21 | 0.14 | 0.56 | 0.17 | 0.25 | 0.21 |
| MgO | 1.41 | 1.28 | 1.08 | 1.03 | 0.79 | 0.76 | 0.68 | 3.65 | 3.03 | 2.91 | 2.77 | 2.50 | 2.03 | 1.81 | 1.67 |
| CaO | 2.98 | 2.7 | 2.49 | 3.94 | 0.99 | 3.9 | 2.48 | 4.93 | 3.11 | 3.37 | 3.19 | 2.34 | 2.77 | 3.05 | 3.7 |
| Na2O | 3.87 | 5.55 | 2.69 | 2.37 | 1.79 | 2.60 | 1.44 | 0.35 | 0.01 | 1.03 | 0.01 | 0.05 | 0.14 | 0.18 | 0.30 |
| K2O | 3.26 | 1.78 | 6.12 | 4.35 | 3.10 | 4.45 | 4.79 | 0.51 | 1.95 | 2.96 | 0.40 | 0.13 | 0.10 | 0.16 | 0.13 |
| P2O5 | 0.15 | 0.13 | 0.41 | 0.14 | 0.11 | 0.16 | 0.13 | 0.18 | 0.28 | 0.11 | 0.19 | 0.30 | 0.18 | 0.25 | 0.26 |
| LOI | 0.7 | 0.6 | 1.5 | 0.9 | 1.8 | 0.3 | 1.4 | 3.2 | 1.8 | 2.4 | 2.2 | 0.0 | 1.4 | 0.0 | 2.2 |
| Total | 99.13 | 99.49 | 98.04 | 99.98 | 100.14 | 98.99 | 99.13 | 100.38 | 100.31 | 99.66 | 100.83 | 101.88 | 100.17 | 101.68 | 99.56 |
| CO2 | 0.03 | 0.01 | 0.01 | 0.01 | 0.01 | 0.03 | 0.01 | 0.01 | 0.01 | 0.05 | 0.15 | 0.01 | 0.53 | 0.09 | 0.68 |
| B (ppm) | 5 | 5 | 70 | 50 | 220 | 30 | 60 | 5 | 5 | 30 | 5 | 5 | 5 | 5 | 80 |
| Ba | 1010 | 1030 | 2630 | 1190 | 840 | 1450 | 1420 | 120 | 530 | 630 | 170 | 140 | 80 | 110 | 80 |
| Ce | 49 | 34 | 269 | 56 | 35 | 61 | 62 | 27 | 37 | 32 | 25 | 12 | 16 | 12 | 28 |
| Co | 6.6 | 13 | 14 | 6.7 | 5.2 | 7.4 | 11 | 14 | 16 | 34 | 16 | 7.7 | 11 | 5.4 | 28 |
| Cr | 24 | 81 | 1 | 17 | 68 | 18 | 25 | 91 | 110 | 170 | 52 | 66 | 66 | 30 | 53 |
| Cs | 15 | 6.5 | 17 | 29.5 | 9.1 | 14.6 | 147 | 5.9 | 9.7 | 3.4 | 4.3 | 1.5 | 0.1 | 0.1 | 1.1 |
| Cu | 2.5 | 36 | 42 | 14 | 4 | 24 | 19 | 120 | 70 | 89 | 76 | 0.25 | 67 | 2 | 250 |
| Dy | . | . | 8.5 | . | . | . | . | . | . | . | . | . | . | . | . |
| Er | . | . | 3.5 | . | . | . | . | . | . | . | . | . | . | . | . |
| Eu | 0.88 | 1.14 | 7.35 | 1.06 | 0.56 | 1.05 | 1.26 | 0.59 | 1 | 1.14 | 0.7 | 0.52 | 0.65 | 0.76 | 1.16 |
| Gd | . | . | 16 | . | . | . | . | . | . | . | . | . | . | . | . |
| Hf | 3.8 | 3.1 | 9 | 3.6 | 3.6 | 3.5 | 3.9 | 2.5 | 1.8 | 2.9 | 1.2 | 1.1 | 1 | 0.9 | 3.4 |
| Ho | . | . | 1.51 | . | . | . | . | . | . | . | . | . | . | . | . |
| La | 26.5 | 22.9 | 138 | 30.2 | 21.9 | 32.3 | 35.1 | 15.6 | 16.7 | 20.9 | 11.9 | 4.3 | 10.6 | 6.3 | 16.4 |
| Li | 36 | 34 | 54 | 92 | 24 | 46 | 140 | 22 | 46 | 46 | 14 | 14 | 10 | 18 | 16 |
| Lu | 0.16 | 0.17 | 0.4 | 0.19 | 0.17 | 0.17 | 0.21 | 0.26 | 0.28 | 0.33 | 0.27 | 0.35 | 0.25 | 0.26 | 0.2 |
| Nb | 10 | 20 | 22 | 20 | 10 | 10 | 5 | 40 | 30 | 20 | 10 | 20 | 30 | 10 | 30 |
| Nd | 19 | 16 | 144 | 21 | 13 | 24 | 23 | 13 | 13 | 16 | 9 | 4 | 7 | 5 | 14 |
| Ni | 14 | 27 | 8 | 12 | 10 | 14 | 19 | 40 | 61 | 110 | 36 | 32 | 34 | 14 | 75 |
| Pb | 28 | 20 | 28 | 32 | 20 | 170 | 220 | 1 | 1 | 1 | 1 | 12 | 1 | 1 | 1 |
| Pr | . | . | 35.3 | . | . | . | . | . | . | . | . | . | . | . | . |
| Rb | 150 | 80 | 214 | 190 | 120 | 180 | 440 | 40 | 150 | 160 | 50 | 10 | 30 | 20 | 20 |
| S% | 0.08 | 0.21 | 0.025 | 0.29 | 0.03 | 0.25 | 0.92 | 3.34 | 1.36 | 2.57 | 1.76 | 0.005 | 1.38 | 0.04 | 2.95 |
| Sc | 7.4 | 11.4 | 8 | 7.1 | 6.6 | 7 | 7.6 | 13 | 16.6 | 24.8 | 8 | 9.3 | 8.1 | 4.2 | 7.3 |
| Sm | 3.6 | 3.46 | 25.1 | 4.07 | 2.56 | 4.29 | 4.26 | 2.68 | 2.86 | 2.48 | 2.13 | 1.14 | 1.71 | 1.3 | 2.92 |
| Sr | 580 | 740 | 3320 | 500 | 530 | 400 | 360 | 5 | 40 | 250 | 5 | 5 | 5 | 5 | 10 |
| Ta | 0.25 | 0.25 | 1 | 0.25 | 0.5 | 0.25 | 0.25 | 0.5 | 0.25 | 0.25 | 0.25 | 0.25 | 0.25 | 0.25 | 0.25 |
| Tb | 0.5 | 0.4 | 1.9 | 0.3 | 0.4 | 0.4 | 0.4 | 0.4 | 0.4 | 0.3 | 0.3 | 0.4 | 0.2 | 0.1 | 0.3 |
| Th | 9.3 | 5.9 | 23.1 | 9.2 | 7.5 | 8.5 | 9.7 | 4.1 | 4 | 5.4 | 3 | 2.2 | 2.1 | 1.4 | 2.1 |
| U | 2.4 | 1.4 | 1.2 | 2.9 | 2.1 | 2.8 | 3.7 | 1 | 1.2 | 3.7 | 0.8 | 0.7 | 0.7 | 0.6 | 0.4 |
| V | 68 | 100 | 170 | 62 | 60 | 72 | 74 | 76 | 120 | 150 | 50 | 60 | 52 | 32 | 46 |
| Y | 5 | 10 | 36 | 20 | 10 | 10 | 10 | 5 | 5 | 10 | 20 | 5 | 5 | 5 | 5 |
| Yb | 0.96 | 1.11 | 2 | 1.13 | 0.78 | 1.01 | 1.22 | 1.53 | 1.67 | 1.96 | 1.61 | 2.17 | 1.21 | 1.43 | 1.06 |
| Zn | 100 | 88 | 140 | 110 | 58 | 510 | 1400 | 150 | 90 | 100 | 140 | 55 | 51 | 38 | 260 |
| Zr | 110 | 100 | 246 | 130 | 100 | 110 | 130 | 70 | 50 | 90 | 40 | 5 | 5 | 5 | 90 |
| X | 6987.332 | 6987.47 | 6997.55 | 6987.26 | 6984.94 | 6987.288 | 6987.23 | 6971.5 | 6987.5 | 6987.5 | 6964.88 | 6983.73 | 6971.76 | 6971.95 | 6985.1 |
| Y | 561.7 | 561.24 | 560.82 | 562.8 | 564.34 | 562.6 | 563 | 565.3 | 560.926 | 560.99 | 565.84 | 565.18 | 565.2 | 565.15 | 565.78 |

Key for abbreviations:

UM = Ultramafic rock
MAF = Mafic volcanic rock
ITUF = Intermediate tuff
PLITUF = Intermediate plagioclase-phyric flow
IAGL = Intermediate agglomerate
IVULK = Intermediate volcanic rock
PLITUF = Intermediate crystal tuff
PLPF = Felsic plagioclase porphyry dike
HLTUF = Felsic lapilli tuff
PLHTUF = Felsic crystal tuff
PLHVUL = Felsic plagioclase-phyric volcanic rock
HVUL = Felsic volcanic rock
HAGL = Felsic agglomerate
KVAFB = Quartz-bearing amphibolite
QPLPF = Quartz-plagioclase porphyry dike
TON = Tonalite
GRDR = Granodiorite
TRPF = Trondhjemite porphyry
GRV = Graywacke - mica schist
LOL = Chlorite schist
FY = Phyllite
GRAKL = Garnet-bearing mica schist
FEMUO = Banded iron formation